

NASA Contractor Report 4396, Vol. II

Effects of Rotation on Coolant Passage Heat Transfer

*Volume II—Coolant Passages With Trips
Normal and Skewed to the Flow*

B. V. Johnson, J. H. Wagner,
and G. D. Steuber
*Pratt & Whitney
East Hartford, Connecticut*

N94-15991

Unclass

H1/34 0191155

Prepared for
Lewis Research Center
under Contract NAS3-23691

NASA

National Aeronautics and
Space Administration

Office of Management

Scientific and Technical
Information Program

1993

(NASA-CR-4396-Vol-2) EFFECTS OF
ROTATION ON COOLANT PASSAGE HEAT
TRANSFER. VOLUME 2: COOLANT
PASSAGES WITH TRIPS NORMAL AND
SKEWED TO THE FLOW Final Report
(PWA) 123 P

PAGE _____ INTENTIONALLY BLANK

PAGE _____ INTENTIONALLY BLANK

FOREWORD

This report covers work performed under NASA Contract NAS3-23691 to investigate heat transfer characteristics of rotating multipass passages for configurations and dimensions typical of modern gas turbine blades under the Hot Section Technology (HOST) program. The NASA Program Manager is Mr. Frederick Yeh, Hot Section Technology (HOST), NASA Lewis Research Center. Dr. S. Tanrikut served as Program Manager at Pratt & Whitney. Acknowledgements are given to L. D. Aceto, R. A. Graziani, T. J. Hajek, F. C. Kopper, I. Linask, S. Orr and the assistance of their colleagues at Pratt & Whitney and UTRC for their contributions to the program.

Effects of Rotation on Coolant Passage Heat Transfer – Final Report

Volume II – Coolant Passages with Trips Normal and Skewed to the Flow

TABLE OF CONTENTS

	<u>Page</u>
1.0 SUMMARY	1
2.0 INTRODUCTION	2
2.1 Background	2
2.2 Previous and Concurrent Studies	2
2.3 Objectives	5
3.0 EXPERIMENTAL APPARATUS AND PROCEDURES	6
3.1 Heat Transfer Model	6
3.2 Rotating Heat Transfer Facility	12
3.3 Experimental Procedures	17
4.0 EXPERIMENTAL PARAMETERS AND TEST MATRIX	20
4.1 Overview	20
4.2 Flow Parameters	20
4.3 Geometric Parameters	21
4.4 Test Conditions	22
4.5 Outline for Presentation of Results	23
5.0 HEAT TRANSFER RESULTS FOR BASELINE FLOW CONDITIONS .	30
5.1 Stationary Baseline Flow Condition	30
5.2 Rotating Baseline Flow Condition	32
5.3 Comparison of Stationary and Rotating Results	32
5.4 Concluding Comments for Baseline Flow Conditions	34
6.0 HEAT TRANSFER RESULTS FOR VARIATION OF PARAMETERS ABOUT BASELINE FLOW CONDITIONS	36
6.1 Effect of Reynolds Number	36
6.2 Effect of Rotation	37
6.3 Effect of Density Ratio	45
6.4 Effect of Model Orientation	48

PRECEDING PAGE BLANK NOT FILMED

	<u>Page</u>
7.0 HEAT TRANSFER RESULTS FOR LEADING AND TRAILING SURFACES	50
7.1 Variation with Rotation Number	50
7.2 Variation with Density Ratio	51
7.3 Variation with Buoyancy Parameter	64
7.4 Variation with Flow Direction	76
7.5 Concluding Discussion for Leading and Trailing Surfaces	77
8.0 HEAT TRANSFER RESULTS FOR SIDE WALLS	79
9.0 HEAT TRANSFER RESULTS FOR TURN REGIONS	85
9.1 Tip Turn	85
9.2 Root Turn	94
10.0 COMPARISON WITH OTHER RESULTS	95
10.1 Stationary Experimental Results	95
10.2 Rotating Analytical Results	95
10.3 Rotating Experimental Results	95
11.0 CORRELATING PARAMETERS FOR ROTATING COOLANT PASSAGES	98
12.0 SUMMARY OF RESULTS AND CONCLUSIONS	100
13.0 APPENDIX	102
13.1 Error Analysis	102
13.2 Pressure Loss Measurements	103
13.3 Model Geometry Information	106
LIST OF SYMBOLS	109
REFERENCES	112

LIST OF TABLES

<u>Table</u>	<u>Page</u>
4.0 EXPERIMENTAL PARAMETERS AND TEST MATRIX	
4.1 Test Matrix for Rotating Heat Transfer Experiments With Normal Trips	24
4.2 Test Matrix for Rotating Heat Transfer Experiments With Skewed Trips	26
11.0 CORRELATING PARAMETERS FOR ROTATING COOLANT PASSAGES	
11.1 Recommended Correlation Parameters for Rotating Coolant Passages	99
13.0 APPENDIX	
13.1 Model Heat Transfer Geometry Information	107
13.2 Model Pressure Tap Geometry Information	108

LIST OF FIGURES

<u>Figure</u>	<u>Page</u>
2.0 INTRODUCTION	
2.1 Typical Coolant Passage Configurations for Aircraft Gas Turbine Rotating Airfoils.	3
3.0 EXPERIMENTAL APPARATUS AND PROCEDURES	
3.1 Cross Sectional View of Coolant Passage Heat Transfer Model Assembly.	7
3.2 Details of Test Section Elements (Normal Trips).	8
3.3 Photograph of Uninstrumented Coolant Passage Heat Transfer Model With Leading Edge (+ Ω) Plane Test Sections Removed.	9
3.4 Cross Sectional View of Coolant Passage Heat Transfer Model Assembly With Normal Trip Model.	10
3.5 Cross Sectional View of Coolant Passage Heat Transfer Model Assembly With Skewed Trip Rough Walls.	11
3.6 Instrumentation Plan for Coolant Passage Heat Transfer Model.	13
3.7 Test Surface Identification Plan for Coolant Passage Heat Transfer. ...	14
3.8 Photograph of Instrumented Coolant Passage Heat Transfer Model With Trailing Edge (+ Ω) Plane Test Section Removed	15
3.9 Photograph of Assembled Model Mounted on Base With Pressure Shell Removed.	15

<u>Figure</u>		<u>Page</u>
3.10	Photograph of Model Mounted in Rotating Heat Transfer Facility . . .	16
3.11	Schematic Sketch of Rotating Heat Transfer Facility.	16
4.0 EXPERIMENTAL PARAMETERS AND TEST MATRIX		
4.1	Test Conditions for Parametric Rotating Heat Transfer Study With Normal Trips.	29
4.2	Test Conditions for Parametric Rotating Heat Transfer Study With Skewed Trips.	29
5.0 HEAT TRANSFER RESULTS FOR BASELINE FLOW CONDITIONS		
5.1	Effect of Trip Configuration on Heat Transfer for Stationary Baseline Flow Conditions.	31
5.2	Effect of Trip Configuration on Heat Transfer for Rotating Baseline Flow Conditions.	33
5.3	Comparison of Heat Transfer for Stationary and Rotating Baseline Flow Conditions.	35
6.0 HEAT TRANSFER RESULTS FOR VARIATION OF PARAMETERS ABOUT BASELINE FLOW CONDITIONS		
6.1	Effect of Reynolds Number on Heat Transfer Ratio for Normal Trips and No Rotation.	38
6.2	Effect of Reynolds Number on Heat Transfer Ratio for Skewed Trips and No Rotation.	39
6.3	Effect of Reynolds Number on Heat Transfer Ratio for Normal Trips and a Rotation Number of 0.12.	40
6.4	Effect of Reynolds Number on Heat Transfer Ratio for Skewed Trips and a Rotation Number of 0.12.	41
6.5	Effect of Rotation Number on Heat Transfer Ratio for Normal Trips. .	42
6.6	Effect of Rotation Number on Heat Transfer Ratio for Skewed Trips. .	43
6.7	Effect of Density Ratio on Heat Transfer Rotation for Normal Trips . .	46
6.8	Effect of Density Ratio on Heat Transfer Ratio for Skewed Trips	47
6.9	Effect of Model Orientation on Heat Transfer Ratio for Skewed Trips .	49
7.0 HEAT TRANSFER RESULTS FOR LEADING AND TRAILING SURFACES		
7.1	Effect of Rotation Number on Heat Transfer Ratios in the First Passage.	52
7.2	Effect of Rotation Number on Heat Transfer Ratios in the Second Passage.	54
7.3	Effect of Rotation Number on Heat Transfer Ratios in the Third Passage.	56
7.4	Effect of Density Ratio on Heat Transfer Ratios in the First Passage. .	58
7.5	Effect of Density Ratio on Heat Transfer Ratios in the Second Passage. .	60
7.6	Effect of Density Ratio on Heat Transfer Ratios in the Third Passage. .	62
7.7	Effect of Buoyancy Parameter on Heat Transfer Ratios in the First Passage.	66

<u>Figure</u>		<u>Page</u>
7.8	Effect of Buoyancy Parameter on Heat Transfer Ratios in the Second Passage.	68
7.9	Effect of Buoyancy Parameter on Heat Transfer Ratios in the Third Passage.	70
7.10	Comparison of Effects of Rotation and Flow Direction on Heat Transfer Ratios	72
7.11	Comparison of Effects of Buoyancy Parameter and Flow Direction on Heat Transfer Ratios	74
8.0 HEAT TRANSFER RESULTS FOR SIDE WALLS		
8.1	Effect of Buoyancy Parameter on Heat Transfer Ratios in the First Passage.	80
8.2	Effect of Buoyancy Parameter on Heat Transfer Ratios in the Second Passage.	82
9.0 HEAT TRANSFER RESULTS FOR TURN REGIONS		
9.1	Effect of Buoyancy Term on Heat Transfer Ratios in the First Turn. ...	86
9.2	Effect of Buoyancy Parameter on Heat Transfer Ratios in the First Turn.	88
9.3	Effect of Buoyancy Term on Heat Transfer Ratios in the Second Turn.	90
9.4	Effect of Buoyancy Parameter on Heat Transfer Ratios in the Second Turn.	92
10.0 COMPARISON WITH OTHER RESULTS		
10.1	Comparison of Stationary Heat Transfer Results From Leading and Trailing Surfaces With Boyle and Han et al.	96
13.0 APPENDIX		
13.1	Effect of Reynolds Number on Pressure Drop in Model.	104
13.2	Effect of Rotation on Pressure Drop in Model.	105

1.0 SUMMARY

Experiments were conducted to determine the effects of buoyancy and Coriolis forces on heat transfer in turbine blade internal coolant passages. The experiments were conducted with a large scale, multi-pass, heat transfer model with both radially inward and outward flow. Normal and skewed trip strips on the leading and trailing surfaces of the radial coolant passages were used to produce the rough walls. An analysis of the governing flow equations showed that four parameters influence the heat transfer in rotating passages: coolant-to-wall temperature ratio, Rossby number, Reynolds number and radius-to-passage hydraulic diameter ratio. The first three of these four parameters were varied over ranges which are typical of advanced gas turbine engine operating conditions. Results were correlated and compared to previous results from stationary and rotating similar models with trip strips. The heat transfer coefficients on surfaces, where the heat transfer increased with rotation and buoyancy, varied by as much as a factor of two. Maximum values of the heat transfer coefficients with high rotation were only slightly above the highest levels obtained with the smooth wall model. The heat transfer coefficients on surfaces, where the heat transfer decreased with rotation, varied by as much as a factor of three due to rotation and buoyancy. Heat transfer coefficients from the test surfaces with skewed trip strips were less sensitive to the effects of buoyancy than were the surfaces with normal trip strips. It was concluded that both Coriolis and buoyancy effects must be considered in turbine blade cooling designs with trip strips and that the effects of rotation were markedly different depending upon the flow direction.

The major portion of the test program for this work was supported by the NASA/Lewis Research Center under the Hot Section Technology (HOST) initiative, Contract No. NAS3-23691 to Pratt & Whitney, Commercial Engineering. The work was performed under the direction of Mr. F. Yeh, NASA Project Manager. The design, fabrication and instrumentation of all of the models, additional experiments to enhance the benchmark data base and the development of physical models for heat transfer phenomena occurring in the coolant passages were conducted under the United Technologies Corporation independent research program. Data from these experiments and information from technical papers and reports, produced outside the scope of Contract NAS3-23691 are also included in this report. Tabulated data and results for each test element and flow condition of the entire data base are available on magnetic tape through Mr. F. Yeh (NASA Lewis Research Center).

2.0 INTRODUCTION

2.1 Background

Current and future high performance gas turbine engines exploit internal convection cooling schemes to maintain acceptable airfoil metal temperatures. This approach requires complex coolant passage configurations within the rotating blades as illustrated in Figure 2.1. Most coolant passage designs enhance heat transfer coefficients above smooth channel levels by utilizing turbulence promoters. Summaries of the technical problems and needs of the current gas turbine blade designer are presented by Suo (1978) and Taylor (1980).

Advanced gas turbine airfoils are subjected to high heat loads that require escalating cooling requirements to satisfy airfoil life goals. The efficient management of cooling air dictates detailed knowledge of local heat load and cooling air flow distribution for temperature and life predictions. However, predictions of heat transfer and pressure loss in airfoil coolant passages currently rely primarily on correlations derived from the results of stationary experiments. Adjustment factors are usually applied to these correlations to bring them into nominal correspondence with engine experience. This is unsatisfactory when blade cooling conditions for new designs lie outside the range of previous experience.

Knowledge of the local heat transfer in the cooling passages is extremely important in the prediction of blade metal temperatures, i.e. blade life. Rotation of turbine blade cooling passages gives rise to Coriolis and buoyancy forces which can significantly alter the local heat transfer in the internal coolant passages due to the development of cross stream (Coriolis), as well as, radial (buoyant) secondary flows. Buoyancy forces in gas turbine blades are substantial because of the high rotational speeds and coolant temperature gradients. Earlier investigations with single pass co- and counter-flowing stationary coolant passages indicated that there can also be substantial differences in the heat transfer when the buoyancy forces are aligned with or counter to the forced convection direction. A better understanding of Coriolis and buoyancy effects and the capability to predict the heat transfer response to these effects will allow the turbine blade designer to achieve cooling configurations which utilize less flow and which reduce thermal stresses in the airfoil.

An extensive analytical and experimental program was originated and sponsored by NASA at the Lewis Research Center, Cleveland, Ohio, as part of the Hot Section Technology (HOST) program. The objectives of this program were (1) to gain insight on the effect of rotation on heat transfer in turbine blade passages, (2) to develop a broad data base for heat transfer and pressure drop in rotating coolant passages, and (3) to improve computational techniques and develop correlations that can be useful to the gas turbine industry for turbine blade design. The attainment of these objectives become even more critical with the advent of the Integrated High Performance Turbine Engine Technology (IHPTET) initiative. As part of the IHPTET goal, the turbine would operate at near stoichiometric (3500-4000F) inlet temperatures, maintain efficiencies in the 88-94% range, and require total coolant flows of only 4 to 6 percent of the engine air flow rate. To attain these ambitious goals, a thorough understanding on the rotational effects of heat transfer and flow in turbine blade passages is mandatory.

2.2 Previous and Concurrent Studies

Heat transfer experiments in multiple-pass coolant passages with normal trips have been conducted in stationary models by several investigators to obtain a data base for the thermal design of gas turbine airfoils, e.g., Webb et al. (1971), Boyle (1984), Han et al.

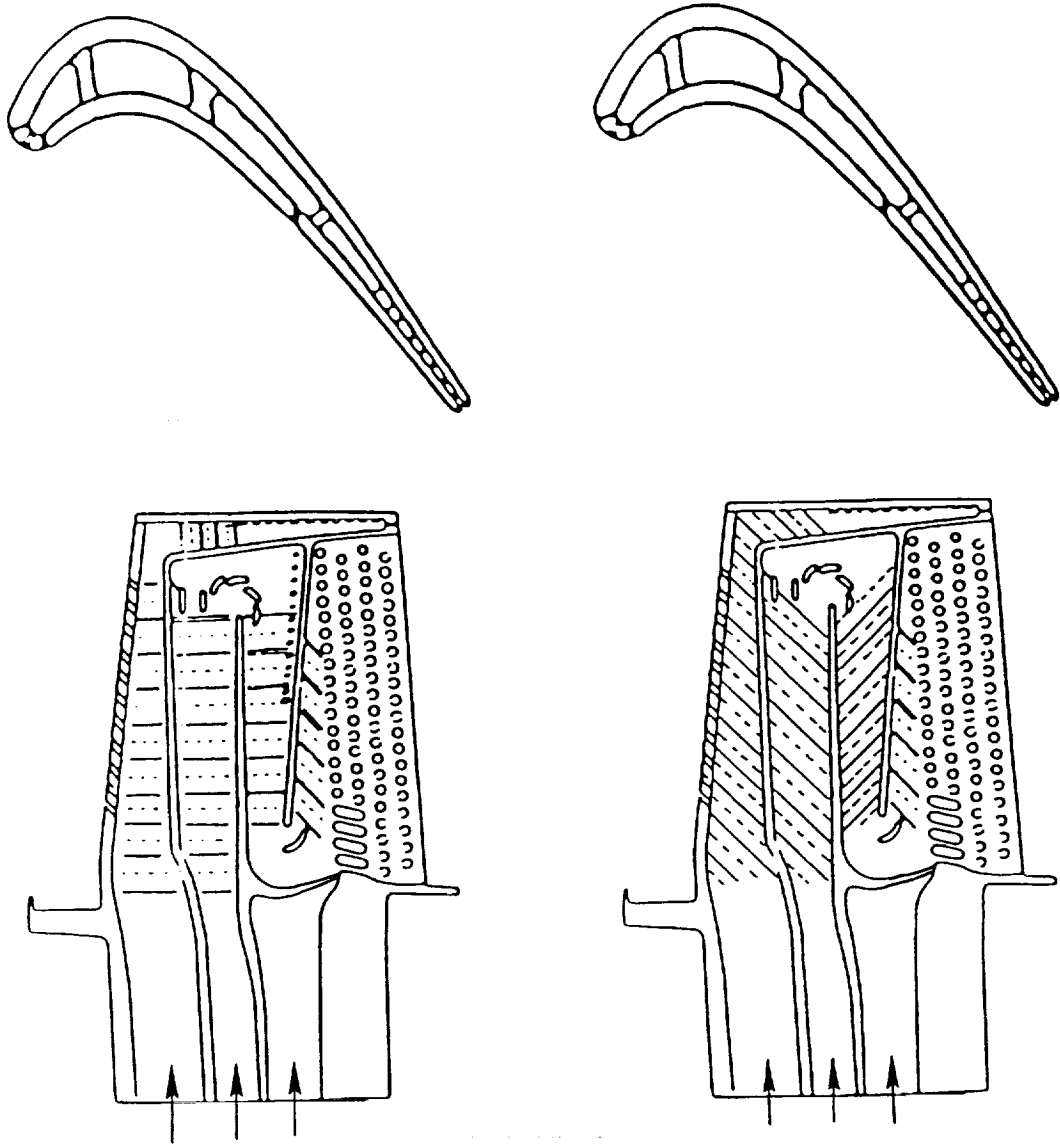


Figure 2.1- Typical Coolant Passage Configurations for Aircraft Gas Turbine Rotating Airfoils.

(1986), Metzger et al. (1988). These data bases are directly applicable to the cooling designs of stationary vanes. However, the effects of Coriolis forces and buoyancy, due to the large rotational gravity forces (up to 50,000 g), are not accounted for.

The complex coupling of the Coriolis and viscous forces has prompted many investigators to study the flow field generated in unheated, rotating circular and rectangular passages without the added complexity of buoyancy, i.e., Hart (1971), Wagner and Velkoff (1972), Moore (1967) and Johnston et al. (1972). The effects of rotation on various processes in rotating components was also summarized by Johnston (1970). The effects of rotation on the location of flow reattachment after a backward facing step presented by Rothe and Johnston (1979) is especially helpful in understanding the effects of rotation on heat transfer in passages with trips. These investigators have documented strong secondary flows and have identified aspects of flow stability which produce streamwise oriented, vortex-like structures in the flow of rotating radial passages.

Concurrent with the present program, flow and heat transfer inside rotating radial ducts has been predicted by Iacovides and Launder (1990) for a constant density turbulent fluid (i.e. with Coriolis effects but without buoyancy) and by Sturgess and Datta (1987). Results from these numerical studies have also shown strong secondary flows and a variation in the heat transfer around the perimeter of the duct.

The generation of secondary flows by Coriolis forces produces a complicated three-dimensional flow that greatly alters the circumferential heat transfer distribution in rotating duct flows. The secondary flows produced in these configurations will influence the distribution of heat transfer according to the movement or migration of fluid from one surface to another and the mixing of the near-wall fluid with the mainstream or core flow. Thus, the circumferential distribution of heat transfer will be vastly different in each of these geometries, as it will be in the wide variety of cooling channel geometries found in advanced aircraft gas turbine blades.

The effects of buoyancy on heat transfer without the complicating effects of Coriolis-generated secondary flow have been studied in vertical stationary ducts. Effects of buoyancy on heat transfer were reported by Eckert et al. (1953 and 1954), Metais and Eckert (1964) and Brundrett and Burroughs (1967). Flow criteria for forced-, mixed- and free-convection heat transfer was developed for parallel flow and counter flow configurations by Eckert et al. (1953) and Metais and Eckert (1964). Based on these experimental results, buoyancy forces would be expected to cause significant changes in the heat transfer in turbine blade coolant passages and to be strongly dependent on flow direction (radially inward vs. radially outward).

The combined effects of Coriolis and buoyancy forces on heat transfer has been studied by a number of investigators. Prior to the present study, experiments were conducted by Iskakov and Trushin (1983), Morris (1981), Morris and Ayhan (1979), Lokai and Gunchenko (1979), Johnson (1978) and Mori et al. (1971). Concurrent with the present study (1983 to 1988), experiments were conducted by Taslem et al. (1989), Guidez (1988), and Clifford (1985). The smooth wall experiments conducted under the present NASA and UTC program were reported in Volume 1 of this report and by Wagner et al. (1989 and 1990). With the exception of Taslim and Clifford, all of the aforementioned work was conducted with smooth-wall models. Large increases and decreases in local heat transfer were found to occur by some previous investigators under certain conditions of rotation while other investigators showed lesser effects. Analysis of these results did not show consistent trends. The inconsistency of the previous results is attributed to differences in the measurement techniques, models and test conditions.

Most of the published work on rotating duct flows has been on experiments conducted with long, straight ducts with flow traveling either radially outward or radially inward with

respect to the axis of rotation and with smooth walls. As depicted in Figure 2.1, modern gas turbine airfoils employ complicated serpentine shaped coolant passages that utilize coolant flowing both radially inward and radially outward. The walls of the coolant passages usually have trip strips to increase the heat transfer coefficient. During the rotation of blades, the centrifugal forces of rotation will influence the heat transfer in each of these cases differently. Also, the upstream and downstream influence of the turns will affect the heat transfer in these passages and becomes very complicated during rotation.

2.3 Objectives

Currently, the analysis of airfoil internal passage heat transfer and pressure loss relies mainly on correlations derived from testing models in a static (nonrotating) environment. Executing tests with rotation is difficult and costly. As a consequence, there is limited data that can be used to account for the effects of rotation on internal heat transfer and pressure loss in typical turbine blade designs. Some data are available for smooth tubes over a limited range of relevant parameters, but application of these data to complicated flow passages of a turbine airfoil would not be appropriate. Presently, adjustment factors are applied to the static test derived correlations to bring them into nominal correspondence with engine experience. This, in practice, accounts for rotation effects.

Under the NASA HOST program, a comprehensive experimental project was formulated in 1982 to identify and separate effects of Coriolis and buoyancy forces for the range dimensionless flow parameters encountered in axial flow, aircraft gas turbines. The specific objective of this experimental project was to acquire and correlate benchmark-quality heat transfer data for a multi-pass, coolant passage under conditions similar to those experienced in the blades of advanced aircraft gas turbines. A comprehensive test matrix was formulated, encompassing the range of Reynolds numbers, rotation numbers, and heating rates expected in a modern gas turbine engine.

The results presented in this report are from the second phase of a two phase program directed at studying the effects of rotation on a multi-pass model with smooth and rough wall configurations. The first phase utilized the smooth wall configuration. The results from the smooth wall phase are reported in Volume 1 of the final report on this contract. Initial results for outward flow in the first passage were also previously presented by Wagner, Johnson and Hajek (1989). The effects of flow direction and buoyancy with smooth walls were presented by Wagner, Johnson and Kopper (1990). The present report covers the rough wall phase with trips (surface roughness elements) oriented at 90 and 45 degrees (normal and skewed trips) to the flow direction. Initial results for the model with normal trips were previously presented by Wagner, Johnson, Graziani and Yeh (1991). Summaries of the results for the model with skew trips and with selected model orientations were presented by Johnson, Wagner, Steuber and Yeh (1992 and 1993, respectively). Comparisons will be made with the results of Volume 1 for smooth walls in the same model and with previous rotating and stationary experiments employing trips 90 degrees to the flow direction and trips oriented 45 degrees to the flow direction.

3.0 EXPERIMENTAL APPARATUS AND PROCEDURES

3.1 Heat Transfer Model

A four legged heat transfer model, used for the NASA-sponsored heat transfer and pressure drop experiments, was designed, fabricated and instrumented under UTC sponsorship. The model consists of three heated straight sections, one unheated straight section, and three turn sections as shown in Figure 3.1. The streamwise location of each test surface is identified by a letter A to R. The orientations of the test surface at each streamwise location are denoted "leading" and "trailing" for the surfaces in the plane of Figure 3.1 and "side walls" for the surfaces (crosshatched) perpendicular to the plane of Figure 3.1. Cross sections of the straight sections are shown in Figure 3.2. The model was designed for constant temperature, steady-state heat balance measurements and for wall static pressure measurements. A photograph of the uninstrumented coolant passage heat transfer model is shown in Figure 3.3.

Model Design

Each streamwise location in the straight heated sections has the cross-sectional shape and features shown in Figure 3.2. All four copper walls were heated on the side opposite the test surface with thin film electric resistance heaters. The heaters were designed to produce a maximum heat flux of 4.6 to 6.2 watts per square centimeter (30 to 40 watts per square inch). The heaters were fastened to the copper test surfaces using standard strain gage adhesives. The temperatures of the copper test surfaces were measured with two chromel-alumel thermocouples which were inserted into drilled holes of each test surface and fastened with epoxy. The copper test surfaces were separated from each other in both the streamwise direction and around the coolant passage cross section with 1.52mm (0.060 in.) thick sections of G-10 or G-11 laminated fiberglass material. Details on the heat balance and the calculation of the effective heat transfer area for each test section will be discussed in a subsequent section.

Trip strips were machined in a staggered pattern on the leading and trailing surfaces of the 6 inch (152.4 mm) straight length of each passage of the normal trip (Fig. 3.4) and the skewed trip (Fig. 3.5) configurations. No trips were on the guard elements ($X/d < 3$) in the first passage. The trip height, ($e/d = 0.1$), shape (circular) and spacing ($P/e = 10$) of the trips are shown in Figure 3.2. These geometrical parameters and trip shape are typical of the trips cast on the coolant passage walls of turbine blades.

The turn sections had smooth walls with three sides of the wall surfaces heated and the fourth side unheated. The unheated surface was the inner-radius, curved surface shown in Figure 3.1. Two heated test surface (leading and trailing wall surfaces) cover the coolant passage in the plane shown in Figure 3.1 for streamwise locations E, F, J, K, P and R. For example, at streamwise location E, the leading and trailing test elements are 37 and 53, respectively (Figure 3.6). Two heated test surfaces cover the outer radius curved surfaces (side walls surfaces). At streamwise location E, these are test surfaces 5 and 6.

The radial location of the center of each heat test surface is defined by the relationship, $R = RADH + RBASE$. $RBASE$ was equal to 466.73 mm (18.375 in.) for all the tests reported in Volume II. The model geometric information for each heat transfer section is tabulated in TABLE 13.1. The tabulated information includes: d , local hydraulic diameter; A_c , local cross-sectional area; CA , area of heat transfer segment; $RADH$, distance from center of heat transfer segment to $RBASE$; S , streamwise distance from model inlet; and X , streamwise distance from start of each straight section.

STREAMWISE LOCATION OF TEST SECTIONS IDENTIFIED BY A TO R. ALL FOUR TEST SECTION SURFACES FOR STREAMWISE LOCATIONS A THROUGH R ARE HEATED

Cross-sectional of coolant passages Z-Z is shown in Fig. 3.7

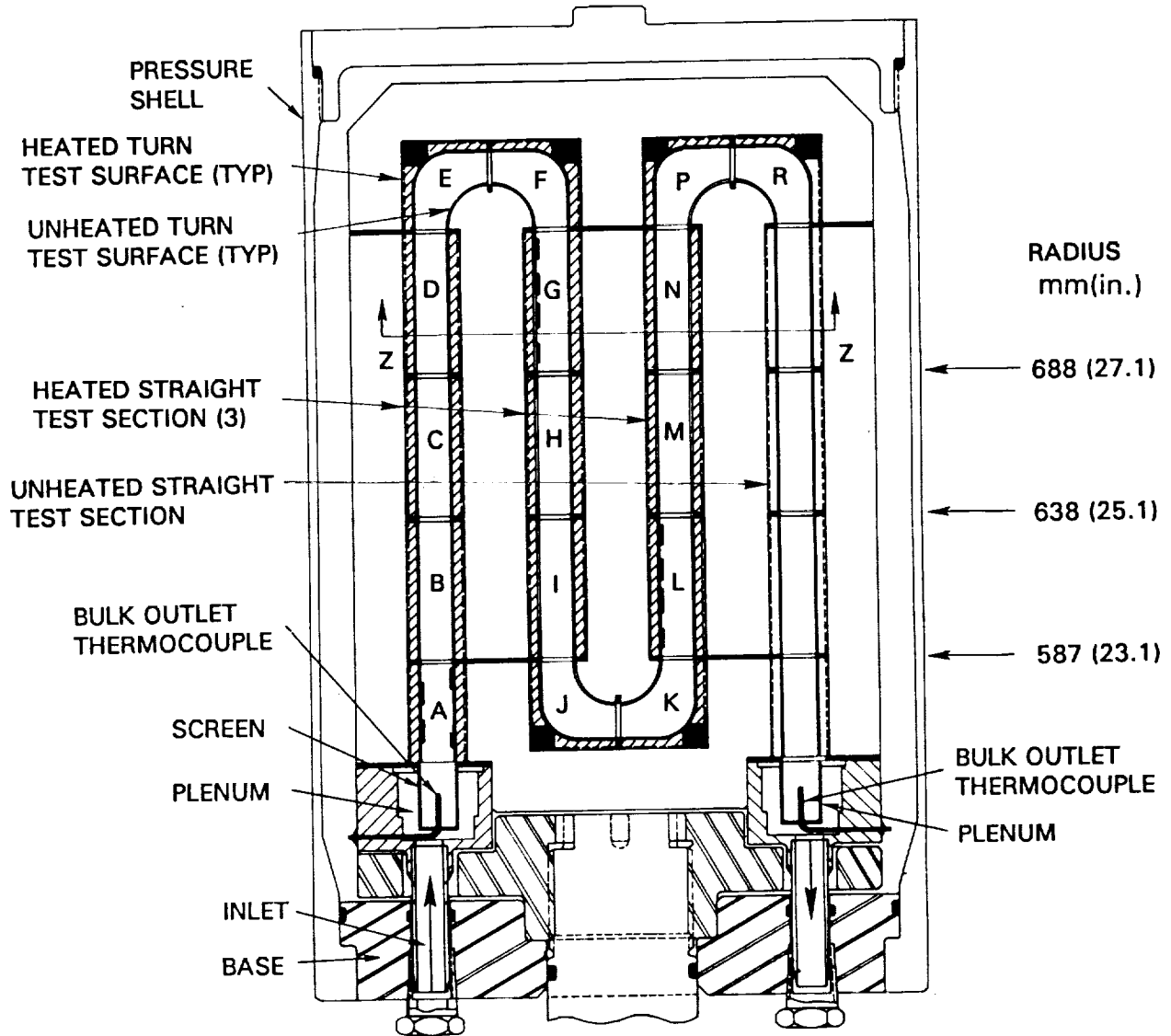


Figure 3.1- Cross Sectional View of Coolant Passage Heat Transfer Model Assembly.

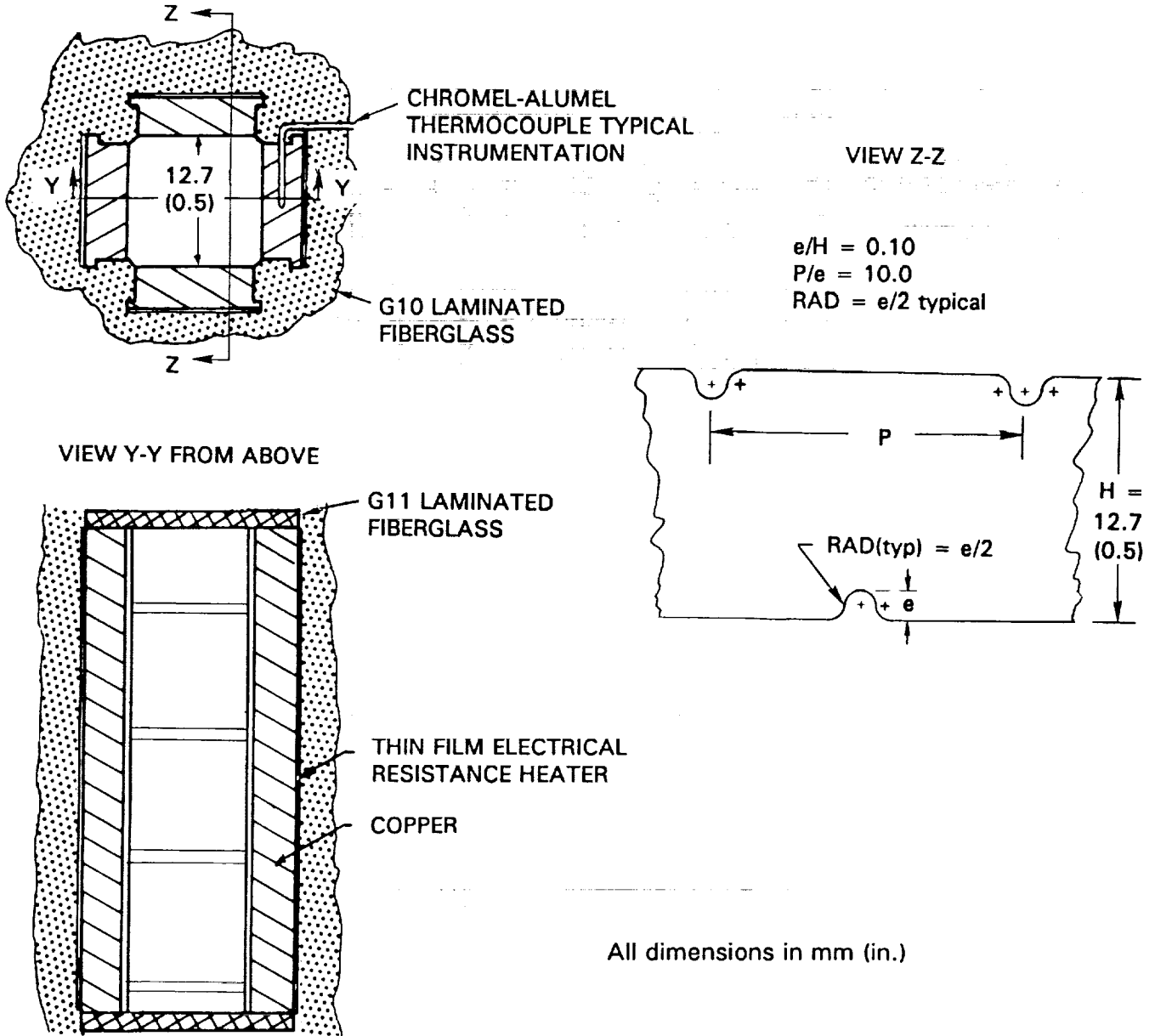


Figure 3.2- Details of Test Section Elements (Normal trips).

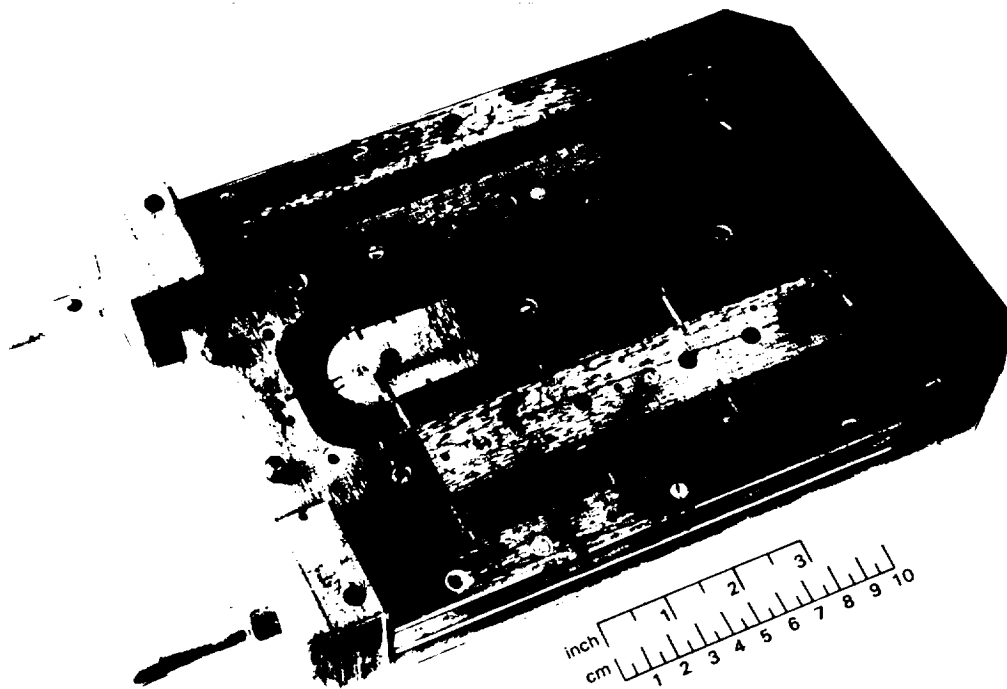


Figure 3.3- Photograph of Uninstrumented Coolant Passage Heat Transfer Model With Leading Edge ($+\Omega$) Plane Test Sections Removed.

STREAMWISE LOCATION OF TEST SECTIONS IDENTIFIED BY A TO R. ALL FOUR TEST SECTION SURFACES FOR STREAMWISE LOCATION A THROUGH R ARE HEATED.

TRIP LOCATIONS:
LOCATIONS:

----- LEADING TEST SECTION SURFACES

———— TRAILING TEST SECTION SURFACES

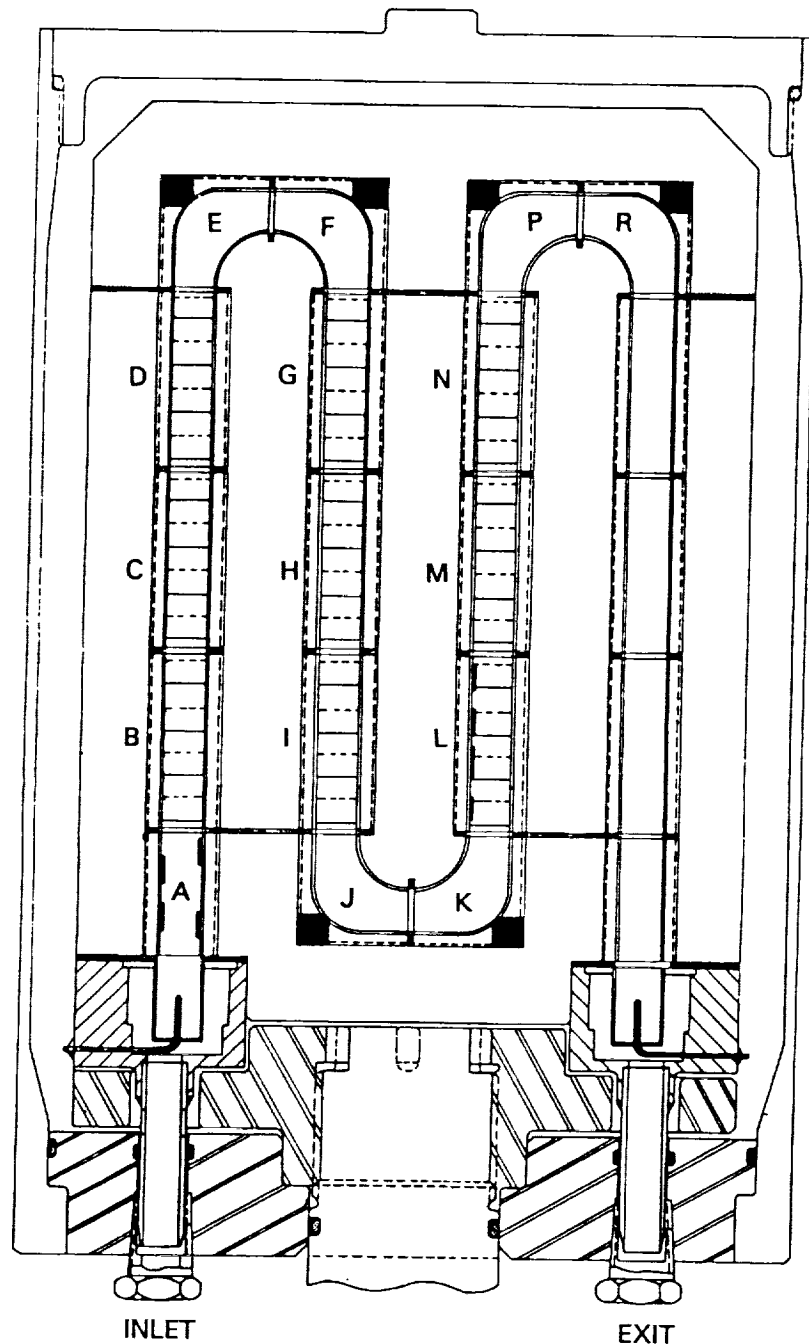


Figure 3.4- Cross Sectional View of Coolant Passage Heat Transfer Model Assembly With Normal Trip Model.

STREAMWISE LOCATION OF TEST SECTIONS IDENTIFIED BY A TO R. ALL FOUR TEST SECTION SURFACES FOR STREAMWISE LOCATION A THROUGH R ARE HEATED.

TRIP LOCATIONS: - - - - - LEADING TEST SECTION SURFACES ——— TRAILING TEST SECTION SURFACES

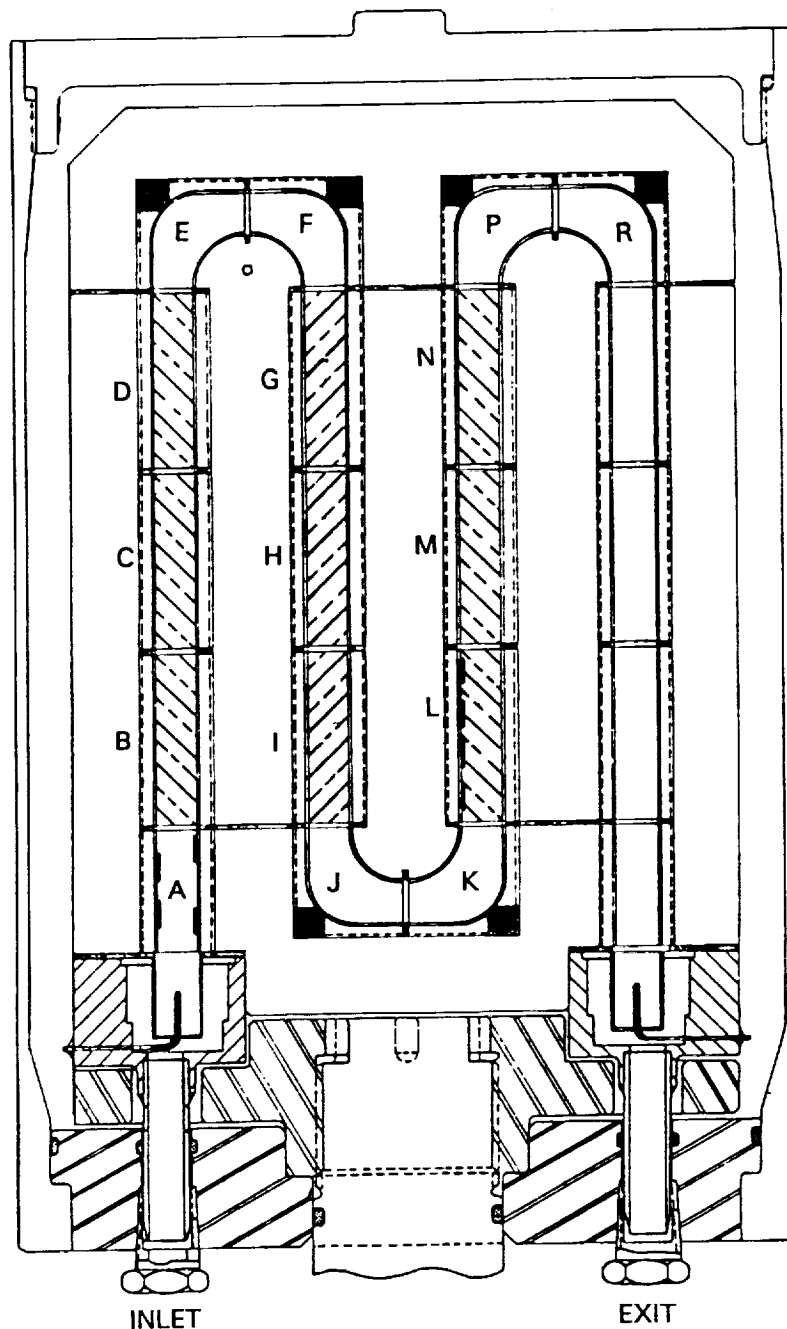


Figure 3.5- Cross Sectional View of Coolant Passage Heat Transfer Model Assembly With Skewed Trip Rough Walls.

Model Instrumentation

The instrumentation plan and the test surface identification plan for the coolant passage heat transfer model are shown in Figures 3.6 and 3.7, respectively. The streamwise locations (A through R) were previously identified in Figure 3.1. Each heat transfer test surface is identified by a number (1 through 64) as shown in Figure 3.6. Note that test surfaces 2, 20, 34 and 50 are located at streamwise location B (Figure 3.6). Test surfaces 34 and 50 are the leading and trailing surfaces respectively when the model is in the $\alpha = 0$ orientation. Test surfaces 2 and 20 are at sidewall locations for $\alpha = 0$.

Pressure measurement locations are shown at 16 places on Figure 3.6. The locations are on the side walls as shown and were chosen to separate the turn pressure losses from the straight section losses. The pressure tap is a 0.51 mm (0.020 in.) diameter hole drilled perpendicular to the test section surface midway across the passage.

The test section surface locations for $\alpha = 0$ and $\alpha = 45$ deg orientations are shown in Figure 3.7. Note that for $\alpha = 0$, the plane passing through the four coolant passages centerline of the straight test sections also passes through the axis of rotation and the straight sections are also radial sections. For $\alpha = 45$ deg, the plane passing through the centerline of the four coolant passages is skewed from the axis of rotation as shown in Figure 3.7. The radial positions of several locations are shown on Figure 3.1 for reference.

A photograph of a partially-assembled, instrumentated, coolant passage heat transfer model is shown in Figure 3.8. Each of the 64 test surfaces has two chromel-alumel thermocouples imbedded and has a thin film heater attached (Figure 3.2). The six leads from each test surface multiplied by sixty four test surfaces result in 384 leads for this portion of the model. Additional thermocouples are positioned at the air inlet and exhaust locations and on the steel backing plates. A photograph of the assembled model mounted on the base is shown in Figure 3.9. A photograph of the model mounted in the Rotating Heat Transfer Facility is shown in Figure 3.10.

3.2 Rotating Heat Transfer Facility

Rotating Components

The Rotating Heat Transfer Facility (RHTF) (Figures 3.10 & 3.11) consists of the containment vessel with the integral arm assembly and motor with associated controller. The containment vessel is 1.83 m (6.0 ft.) in diameter and was designed to withstand a destructive failure of the rotating assembly. The vessel was designed for operation at a pressure of 5 to 13 mm of Hg absolute to reduce the power required to rotate the arm. The rotating arm assembly is driven by a 11KW (15 Hp) DC motor via a toothed belt. Shaft rpm is controlled by an adjustable feedback electronic controller. Maximum shaft speed is approximately 3,500 rpm producing body forces on the model of approximately 14,000 g's at the tip of the model and approximately 10,000 g's at the root. The maximum shaft speed for the present program was 1100 rpm. A safety shutdown interlock circuit is used to turn off the drive motor and model heater power supplies, turn on a magnetic brake and open the containment vessel vacuum chamber vent. The safety shutdown system prevents damage to the model or the facility in the event of a leak in the model or an imbalance in the rotating assembly.

The shaft assembly comprises a main outer shaft with two shorter inner shafts. This shaft arrangement was designed for dual fluid paths from each rotary union mounted on the ends of the shaft to the rotating assembly. Grooves located on the exterior surface of the outer shaft allow instrumentation and power leads to extend from the rotating arm to

TEST SECTION ELEMENT IDENTIFICATION
 SIDE WALL TEST SECTION SURFACES 1-32 ARE IN PLANE
 PERPENDICULAR TO VIEW SHOWN

TEST SECTION SURFACES 33-48 ARE ON " + Ω " LEADING PLANE

TEST SECTION SURFACES (49)-(64) ARE ON " + Ω " TRAILING PLANE

PRESSURE MEASUREMENT LOCATIONS \square 1 - \square 16 Smooth and Skewed Trips
 \circ 1 - \circ 16 Normal Trips

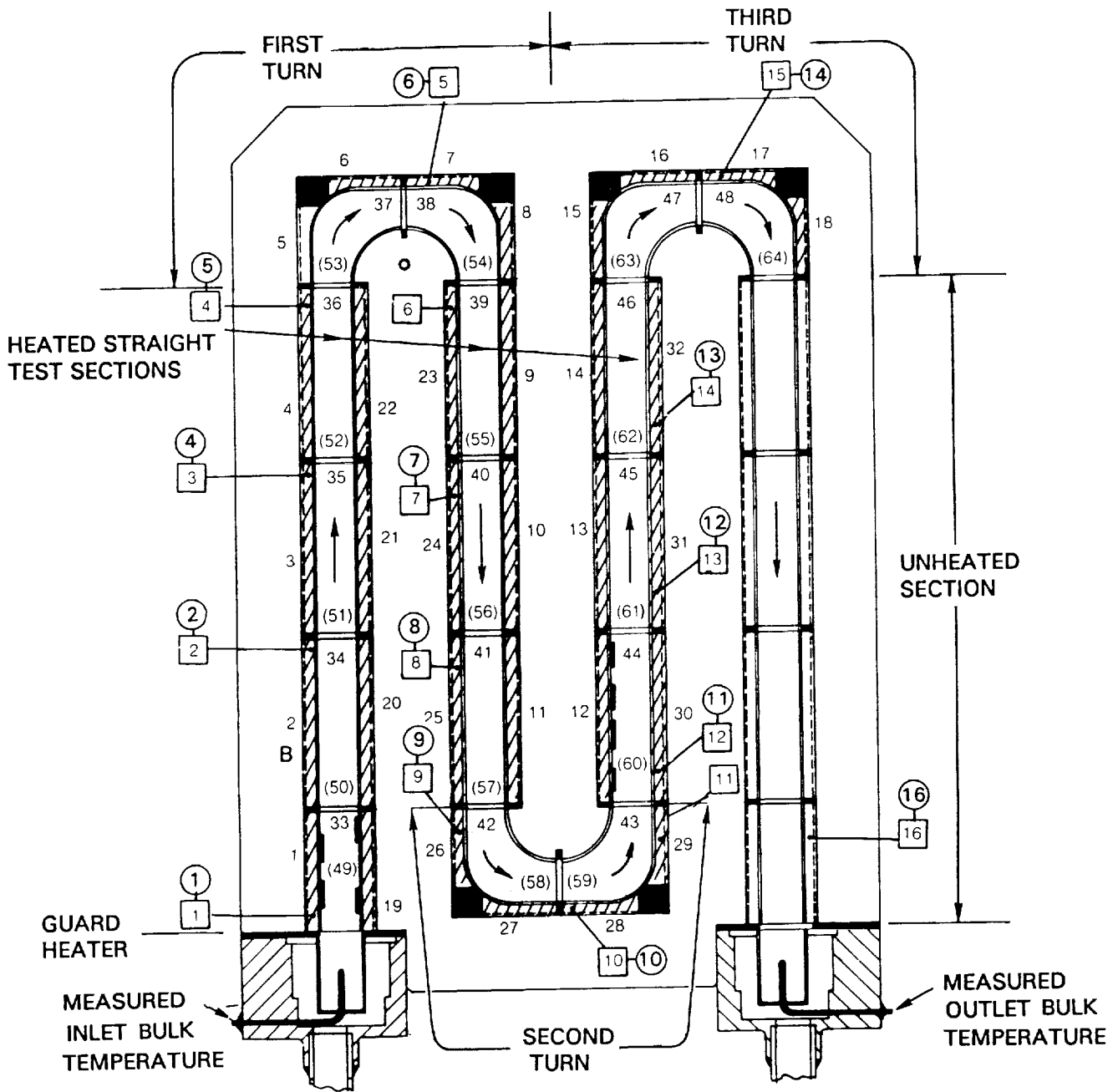
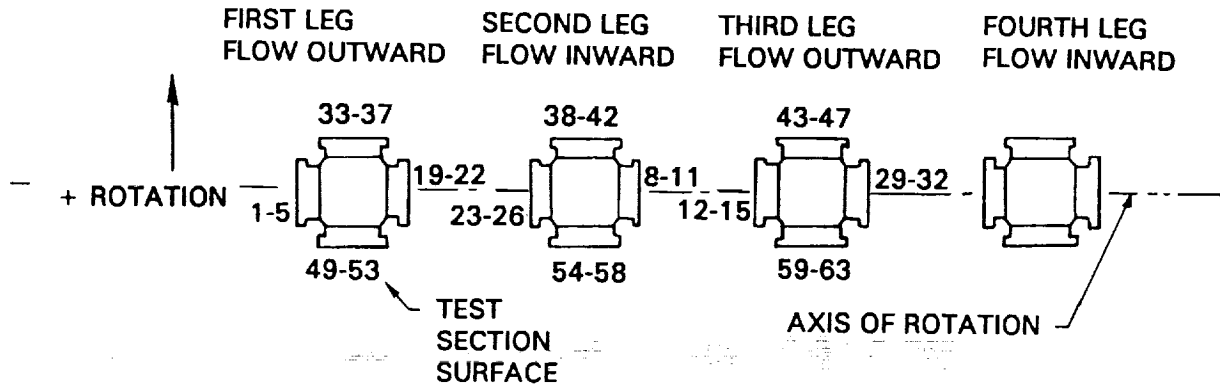
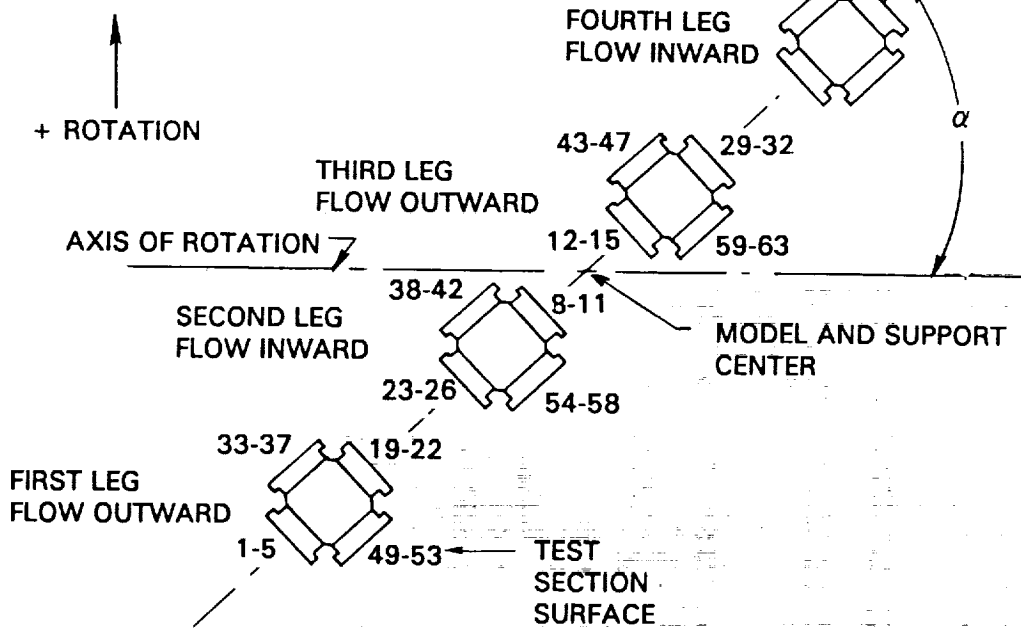


Figure 3.6- Instrumentation Plan for Coolant Passage Heat Transfer Model.

$\alpha = 0$ DEG. ORIENTATION



$\alpha = 45$ DEG. ORIENTATION



Note: View from the axis of rotation looking radially outward to the model

Figure 3.7- Test Surface Identification Plan for Coolant Passage Heat Transfer.

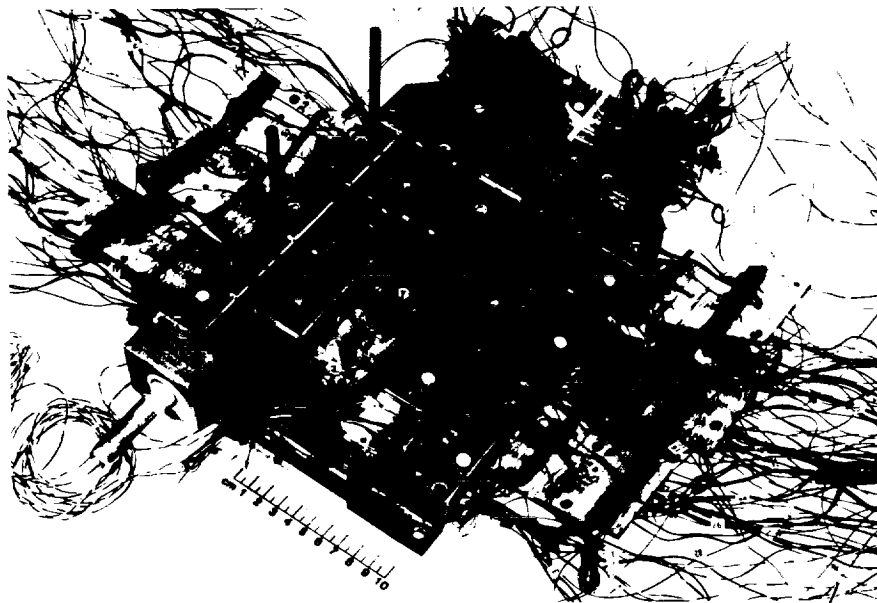


Figure 3.8- Photograph of Instrumented Coolant Passage Heat Transfer Model With Trailing Edge ($+\Omega$) Plane Test Section Removed (Two thermocouples and thin film heaters mounted on each test section).

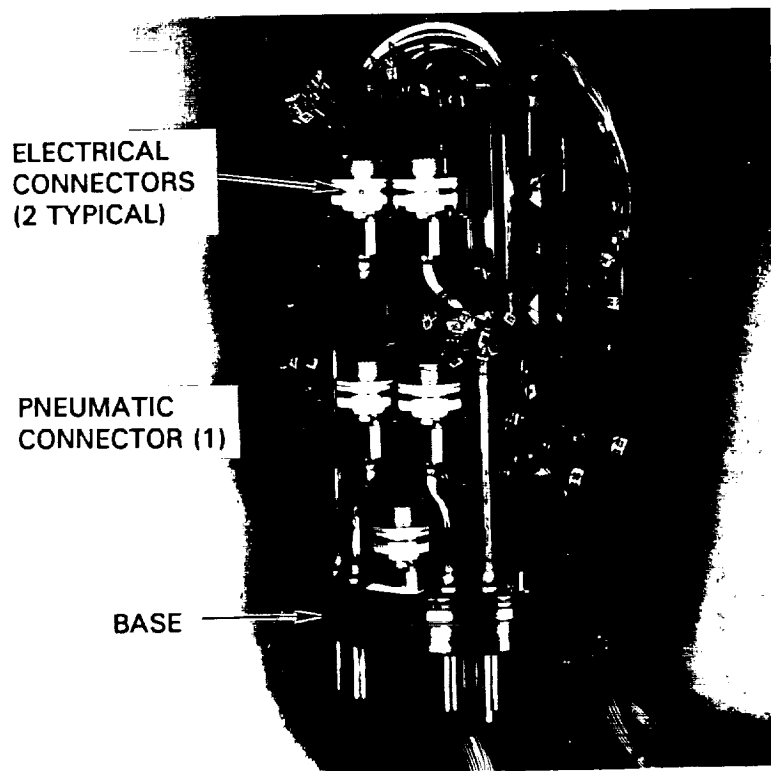


Figure 3.9- Photograph of Assembled Model Mounted on Base With Pressure Shell Removed.

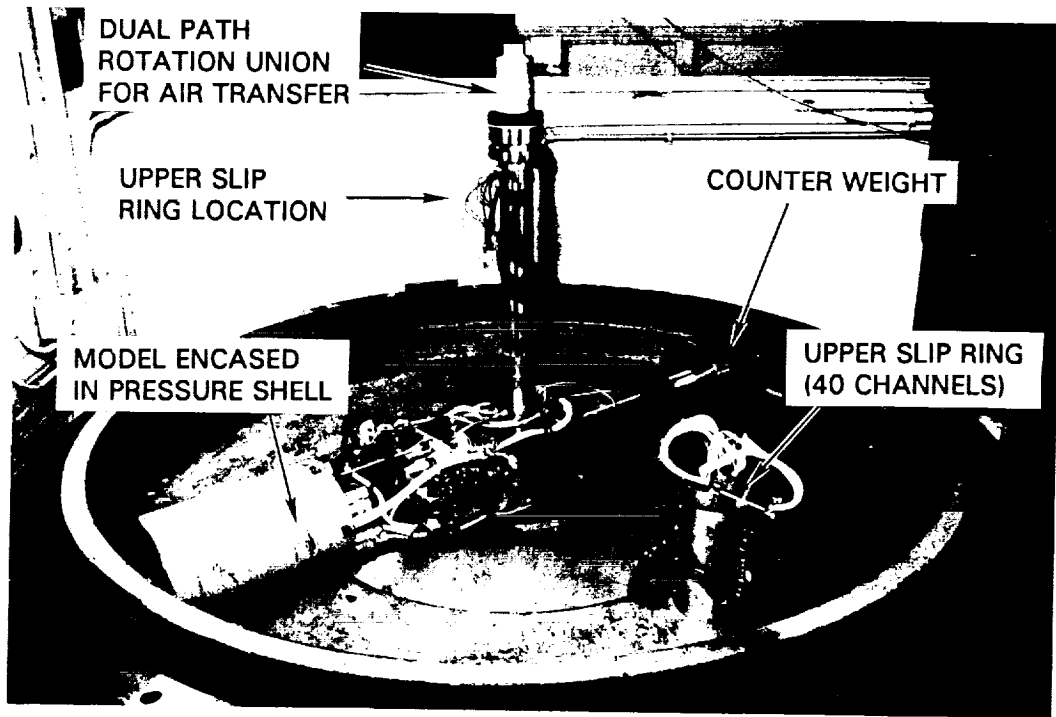


Figure 3.10- Photograph of Model Mounted in Rotating Heat Transfer Facility (Rotating heat transfer facility with cover removed).

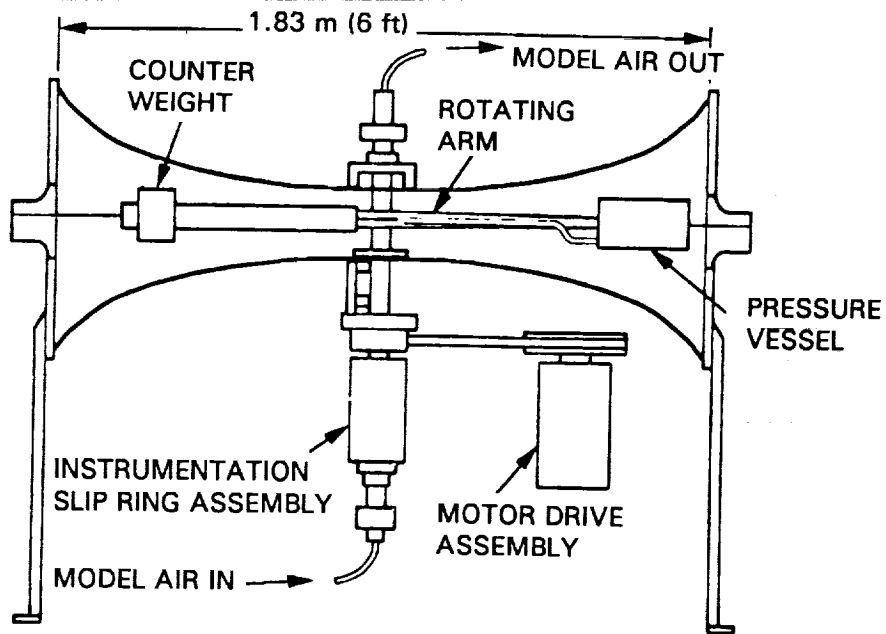


Figure 3.11- Schematic Sketch of Rotating Heat Transfer Facility.

the rotating portion of the instrumentation slipping. Two slipping assemblies (a 40 channel unit located on the upper end of the shaft and a 200 channel unit located on the lower end of the shaft) are used to transfer heater power and instrumentation leads between the stationary and rotating frames of reference.

Data Acquisition System

The data acquisition system contains two major components; the computer and the data acquisition control unit. The computer consisted of a processor unit with 128k memory, two 20cm (8 in.) floppy disk drives and a DECWRITER III terminal. The Hewlett Packard 3497A data acquisition system can be controlled from the front panel or through the interface connected to the computer. The model heater voltages for the 64 heat transfer test sections are set manually and adjusted until the required wall surface temperatures are obtained. Upon completion of the acquisition of voltage data through the acquisition control unit and the computer, results are calculated and printed in engineering units. Flow parameter and raw data are stored on disk for future reduction.

Heater Power Source

The power supply system provides DC power for the thin film foil resistance heaters used to heat the model test section elements. There are 72 individually controlled power supplies which are rated for 50 watts of power with a maximum current draw of one amp. Individual units can be arranged in parallel as needed to supply additional power. Heater supply voltage and the voltage across precision current measurement resistors are measured by the data acquisition unit.

Flow Monitoring System

Model coolant air is supplied by the UTRC 27 atm (400 psig) air system which is regulated to approximately 10 atm (150 psig) at the RHTF. The air flow rate is measured with variable area flow meters. The model coolant return air flows through an additional flow meter to determine a mass flow balance on the system. The mass flow, inlet and exit, were balanced to approximately 3 percent, which was also the total uncertainty in the flow measurements. Model pressure is controlled by back pressuring the model air flow system with the return air control valve. The maximum mass flow rate available is dependent on the model operating pressure and the total pressure loss of the system including the heat transfer model. For typical models, the maximum air flow rate is approximately 0.02 kg/sec (0.044 lbm/sec).

3.3 Experimental Procedures

Data Acquisition

Testing was conducted with air at dimensionless flow conditions typical of advanced gas turbine designs. The required dimensionless rotation numbers were obtained with rotation rates of 1100 RPM or less by operating the model at a pressure of approximately 10 atmospheres. The model inlet air temperature was typically 27C (80F) and the copper elements were held at 49C, 71C, 93C and 116C (120F, 160F, 200F and 240F) for inlet coolant-to-wall temperature differences of 22C, 44C, 67C and 89C (40F, 80F, 120F and 160F). Temperatures of the copper elements were measured with two chromel-alumel thermocouples inserted in drilled holes of each element.

Data Reduction

Heat transfer characteristics were determined from a heat balance on each heated test surface. The heat added to the coolant by convection was determined from the electrical power used to heat each test surface and the heat conducted from the test surface to the support structure. Heater supply power for individual model segments was determined by multiplying the calculated voltage across each of the microfoil heater leads and the current determined from the voltage measured across precision 0.1 ohm resistors. The voltage across the microfoil heater leads was determined by accounting for the voltage drop across the heater supply leads. The net heat flux (convected heat flux), assuming negligible radiation energy transfer, was determined by subtracting the conducted backloss from the heater power input. The heat transfer coefficients were based on the projected area rather than the total heat transfer surface area due to trip geometry. Note that the total heat transfer surface area was 1.11 times the projected area for the normal trip model and 1.15 times the projected area for the skewed trip model.

The conduction loss parameter for each heated segment was determined by heating the model segments with no coolant flow to a steady state temperature condition and measuring the voltage and current required to calculate heater power necessary to maintain all the model temperatures. For this condition, the convected heat flux is zero and the total heater power is due to the backloss conduction. The conduction backloss parameter is calculated by dividing this heater power by the temperature difference of the heated segments and the support frame. The bulk temperature used to calculate heat transfer coefficients was determined with a thermodynamic energy balance through each discrete system of heated segments.

Nusselt numbers and Reynolds numbers were calculated for each element. The fluid properties in the Nusselt and Reynolds numbers were evaluated at the film temperature, i.e., $T_f = (T_w + T_b)/2$. The heat transfer results presented herein have also been normalized with a correlation for fully developed, turbulent flow in a smooth tube. The constant heat flux Colburn equation, adjusted for constant wall temperature was used to obtain the Nusselt number for fully developed, turbulent flow in a smooth tube (Kays and Perkins (1973)). The resulting equation for the constant wall temperature condition with a Prandtl number equal to 0.72 is as follows.

$$Nu_{\infty} = 0.0176 * (Re)^{0.8}$$

Data Repeatability and Uncertainty

Electronic noise in the data signals of the RHTF was present only when the shaft was rotating. The probable sources for this electronic noise were (1) rotating instrumentation leads through magnetic flux lines generated by the DC motor, (2) motor power controller noise and (3) induced alternating currents through the lead and slipping instrumentation system generating fluctuating voltages. The voltage data used in the data reduction program was obtained by averaging ten successive voltage measurements of each data channel. Repeatability of the measurements indicated the calculated mean temperature was consistently within 0.2 C (0.4 F) of the mean temperature.

An uncertainty analysis (Section 13.1) of the data reduction equations using the methods of Kline and McClintock (1953) showed that approximately 3/4 of the estimated uncertainty in calculating heat transfer coefficient was due to the measurement of temperatures in the model. The uncertainty of the heat transfer coefficient is influenced mainly by the wall-to-coolant temperature difference and the net heat flux from each element. Uncertainty in the heat transfer coefficient increases when either the temperature difference or the net heat flux decreases. As X/d increases, the uncertainty in the heat transfer coefficients increase because the wall-to-coolant temperature difference

decreases. For low heat fluxes (i.e. low Reynolds numbers and on leading surfaces with rotation) the uncertainty in the heat transfer also increased. Estimates of the error in calculating heat transfer coefficient typically varied from approximately ± 6 percent at the inlet to ± 30 percent at the exit of the heat transfer model for the baseline stationary test conditions. The uncertainty in the lowest heat transfer coefficient on the leading side of the third passage with rotation is estimated to be 40 percent, primarily due to the uncertainty in the calculated bulk temperature. Although the uncertainty analysis was useful in quantifying the maximum possible uncertainty in calculating heat transfer coefficient, multiple experiments at the same test condition were repeatable within ranges approximately half those suggested by the analysis.

4.0 EXPERIMENTAL PARAMETERS AND TEST MATRIX

4.1 Overview

The present study of heat transfer from a serpentine, square-passage model was conducted with two wall trip geometries at dimensionless flow parameters representative of those used in axial flow aircraft gas turbines. The serpentine path in the model produced the flow and geometric conditions encountered in the internal coolant passages of gas turbines: (a) flow radially outward from a radial inle, (b) flow radially outward and from downstream of a turn, (c) flow radially inward from downstream of a turn (d) flow in a turn at the blade tip and (e) flow in a turn at the blade root. Heat transfer was obtained on all four sides of these coolant passages.

This study was comprised of experiments conducted under the contract and supplemental experiments and analyses and interpretation of results conducted under the United Technologies Corporation (P&W and UTRC) independent research program.

4.2 Flow Parameters

A dimensional analysis study performed at UTRC prior to the onset of the present study (Suo, 1980 and reprinted as Section 10 of Hajek et al., 1991), similar to that of Guidez (1988), showed that the flow patterns and hence convective heat transfer would be influenced by four nondimensional flow parameters and several geometric parameters. The nondimensional flow parameters are as follows:

Reynolds number	$\rho V d/\mu$
Rotation Number	$\Omega d/V$
Density Ratio	$(\rho_b - \rho_w)/\rho_b = (T_w - T_b)/T_w$
Buoyancy Parameter	$[(\rho_b - \rho_w)/\rho_b](\Omega R/V)(\Omega d/V)$

For flow in rotating radial coolant passages, Coriolis forces, represented by the nondimensional parameter, $\Omega d/V$, and the nondimensional streamwise velocity gradients, produce secondary flows in the plane perpendicular to the radial direction. These secondary flows are produced by the viscous force/Coriolis force interaction. Buoyancy also produces secondary flows in the radial direction. For flow in rotating radial coolant passages with walls hotter than the bulk fluid, the buoyancy effects always tend to drive the heated flow inward. Thus the buoyancy flow direction is opposite the mean velocity direction for flow radially outward and is in the same direction for flow radially inward. From previous studies, both the Coriolis and buoyancy forces can be expected to produce significant changes to the coolant passage flow field and hence heat transfer. Rotating constant-temperature flow studies by Johnston et al. (1972) have shown that the Coriolis forces can dampen turbulent fluctuations and laminarize flow in portions of a channel. Combined free and forced convection studies in stationary systems have shown that the turbulent shear structure and heat transfer is significantly altered with co-flowing or counter-flowing buoyancy effects (Eckert et al, 1953, and Metais and Eckert, 1964). The results from the present experimental study show regions where the viscous, Coriolis or buoyancy forces dominate the flow field and regions where the interactions between the forces are strong.

4.3 Geometric Parameters

The flow and heat transfer in stationary coolant passages are also strong functions of the geometric parameters. Rotation of the coolant passages adds several additional geometric parameters. The geometric parameters are as follows:

Streamwise location	S/d or X/d	variable
Passage aspect ratio	H/W	constant
Trip height	e/H	constant
Trip spacing	P/e	constant
Trip geometry	curvilinear	constant
Trip orientation	ϕ	variable
Radial location	\bar{R}/d	constant
Flow direction	inward, outward	variable
Passage orientation	α	variable
Turn location	tip, root	variable
Wall location	leading, trailing, side	variable

Although all eleven of the geometric parameters identified could be important for coolant passages in rotating turbine blades, the present study was limited in the following manner:

- The passage aspect ratio (H/W) was fixed at 1.0, the configuration employed for the study reported in Volume I - Coolant Passages with Smooth Walls.
- The radial location (\bar{R}/d) was fixed for this study at 49. In Volume 1, the dimensionless parameter, $(\Omega R/V)(\Delta\rho/\rho)$ or $(\Omega d/V)(R/d)(\Delta\rho/\rho)$, in conjunction with the rotation parameter, $(\Omega d/V)$, was shown to correlate the effects of buoyancy.
- The passage orientation was fixed at $\alpha = 0$ for the normal trip geometry. The passage orientation was 0 and 45 deg for the skewed trip model.
- The trip height (e) was fixed at 10 percent of the coolant passage height (H).
- The trip spacing, P , was fixed at the passage height, H , to obtain a value of $P/e = 10$, typical of the values employed in aircraft gas turbine blades.
- The trip geometry was curvilinear as shown in Fig. 3.2. The curvilinear shape is typical of that obtained in blade casting processes and used to avoid high stresses in sharp corners.
- The trip orientations were chosen to be $\phi = 90$ deg, normal to the radial direction, and $\phi = 45$, halfway between the normal and radial direction.
- The trip spacing was staggered on the opposite walls. The trips were located on the leading and trailing walls. The heat transfer required from the side or rib walls does not generally require augmentation devices.

The effect of flow direction and turn location are important and will be identified from the experimental results. Entrance effects (streamwise location) are expected to be significant in each of the three legs as the flow develops downstream of the inlet and downstream of the turns.

4.4 Test Conditions

The test conditions for the heat transfer experiments with the normal and skewed trip models are tabulated in Tables 4.1 and 4.2 respectively. The variations of Reynolds number, rotation numbers and inlet wall to bulk temperature differences for each configuration are shown in Figs. 4.1 and 4.2.

The standard rotating flow condition used in the study was that for tests No. 307 and 209, $Re = 25,000$, $Ro = \Omega d/V = 0.24$, and $\Delta T_{in} = 44.4^\circ C$ ($80^\circ F$). The original plan was to vary parameters only about the standard flow condition, varying only one parameter at a time. However at the completion of the original test plan for the smooth wall model, it became apparent that the heat transfer relationships were complex and that the viscous, Coriolis and buoyancy forces each would dominate the flow field for various combinations of the test conditions for each wall trip geometry (i.e. smooth wall, normal trips, skewed trips). Therefore, the test matrix was expanded to include a larger range of rotation numbers and inlet wall-to-bulk temperature differences.

The results obtained show first order effects for the following parameters:

- **Reynolds Number** – The Reynolds number was varied from 12,500 to 75,000 for the stationary experiments and from 12,500 to 75,000 for the rotating experiments.
- **Rotation Number** – The rotation number $\Omega d/V$ (the inverse of the Rossby number) and the streamwise velocity gradients are the primary nondimensional factors governing secondary flow in the plane perpendicular to the centerline of rotating radial ducts.
- **Density Ratio** – The density ratio, $[(\rho_b - \rho_w)/\rho_b]$, is one of the basic nondimensional parameters obtained from several previous dimensional analysis of flow in a rotating radial duct. The product of the density ratio and a gravitational parameter, $(\Omega d/V)^2(R/d)$, cause secondary flow in the radial direction. For this study with heated walls and for the gas turbine blades, the buoyancy effect is always radially inward whether the flow direction is radially inward or outward. Note: for small variations of pressure, $(\rho_b - \rho_w)/\rho_b = (T_w - T_b)/T_w$.
- **Streamwise Location** – The range of X/d in each passage varies from 0 to 14 and is in the developing flow region for constant wall temperature conditions.
- **Trip Orientation** – The heat transfer coefficients varied with trip orientation.
- **Wall Location** – Heat transfer coefficients varied considerably from leading to trailing surfaces and on the side or rib walls.
- **Turn Location** – The combined effects of Coriolis forces, secondary flows produced by the trips, and buoyancy forces caused the heat transfer in the turns to vary from root to tip and from smooth to trip geometry.

- **Passage Orientation** – The serpentine model was constructed such that the plane, which contains the centerlines of all four passages, could be rotated about a radial axis through the geometric centerline of all four evenly-spaced passages. For $\alpha = 0^\circ$, extensions of the centerlines of all four passages would pass through the axis of rotation as shown in Figure 9. One side of the square passage becomes the leading side, i.e. $\square\uparrow$. For $\alpha = 45^\circ$, each test section passage has two leading and two trailing sides, i.e. $\diamond\uparrow$.
- **Flow Direction** – The direction of the flow causes the buoyancy, viscous and Coriolis forces to interact in a complex manner. Previous investigators conducting free and forced convection experiments in stationary tests have attributed the differences in heat transfer between flow upward and downward to changes in the turbulent structure of the flow.

4.5 Outline for Presentation of Results

A total of forty-nine tests were conducted with the two models with normal and skewed trips as shown in Tables 4.1, and 4.2 (repeat runs were also obtained under the same test number). This report also includes discussion of phenomena in the coolant passages developed under United Technologies Corporation independent research program and in the preparation of technical papers outside the scope of the contract effort (e.g., Wagner et al. 1989, 1990, 1991). In order to make the presentation of the principle results for this program tractable and discernible to the reader, the heat transfer data is presented in several stages.

- 1) The heat transfer results for the rotating and stationary baseline flow conditions are presented in Section 5.0. The results from the experiments with normal and skewed trips are also compared with results from the baseline experiments with smooth walls.
- 2) In Section 6.0, the heat transfer results are presented as a variation of the geometric parameters, X/d and wall location about the rotating and stationary standard flow condition for both trip geometries. The variations include the Reynolds number, the rotation number and the inlet wall to bulk temperature (density ratio) difference for the models with normal and skewed trips and the model orientation angle α for the model with skewed trip.
- 3) In Section 7.0 all the results are presented as a function of two nondimensional flow parameters. This presentation will be used to discern the complex heat transfer relationships that occur on the leading and trailing surfaces in the straight passages for various streamwise locations over a wide range of flow conditions.
- 4) Heat transfer results from the side or rib walls are presented in Section 8.0. The results from the present experiments with trips are compared to previous results with smooth walls.
- 5) Heat transfer results from the turn regions are presented in Section 9.0. The results from the present experiments with trips are compared to previous results with smooth walls.
- 6) Results from the present report will be compared with results from previous or other concurrent experiments in Section 10.
- 7) Recommendations for the pertinent correlating parameters of each region for design applications are discussed in Section 11.

Table 4.1- Test Matrix For Rotating Heat Transfer Experiments With Normal Trips
Contract NAS3-23691

Test No.	UTRC Run	Dimensional Parameters					Basic Dimensionless Parameters				Secondary Dimensionless Parameters			Comments	
		P M/m ² x10 ⁻⁶ (psi)	Ω rpm	m Kg/sec (lb/sec)	ΔT ° C (° F)	R cm (in)	α deg	Re	Ro	$\frac{(\Delta T)}{T}$	$\frac{\bar{R}}{d}$	$\frac{(\Delta \rho)(\Omega R)}{(\rho)(V)}$	Gr Re ²		Grx10 ⁻⁸
301	2.10	1.024 (148.6)	0	0.0032 (0.007)	44.4 (80)	63.5 (25)	0	12,653	0.00	0.13	49	0.000	0.000	0.00	No Rotation
302	3.9	1.014 (147.0)	0	0.0059 (0.013)	44.4 (80)	63.5 (25)	0	25,176	0.00	0.13	49	0.000	0.000	0.00	
303	4.7	1.019 (147.8)	0	0.0118 (0.026)	44.4 (80)	63.5 (25)	0	49,988	0.00	0.13	49	0.000	0.000	0.00	
304	5.10	0.998 (144.7)	0	0.0177 (0.039)	44.4 (80)	63.5 (25)	0	75,270	0.00	0.13	49	0.000	0.000	0.00	
305	11.7	1.017 (147.5)	145	0.0059 (0.013)	44.4 (80)	63.5 (25)	0	25,001	0.06	0.13	49	0.320	0.020	0.12	Vary Ro
306	8.8	1.022 (148.3)	275	0.0059 (0.013)	44.4 (80)	63.5 (25)	0	24,998	0.12	0.13	49	0.604	0.071	0.44	Hold T, Re
307	16.11	1.019 (147.8)	550	0.0059 (0.013)	45.0 (81)	63.5 (25)	0	24,957	0.23	0.13	49	1.209	0.281	1.75	
308	26.12	1.021 (148.1)	825	0.0059 (0.013)	45.0 (81)	63.5 (25)	0	24,769	0.35	0.13	49	1.755	0.606	3.72	
309	12.9	1.022 (148.2)	145	0.0032 (0.007)	44.4 (80)	63.5 (25)	0	12,546	0.12	0.13	49	0.607	0.070	0.12	Vary Re
310	17.7	1.031 (149.6)	550	0.0118 (0.026)	44.4 (80)	63.5 (25)	0	49,938	0.12	0.13	49	0.652	0.079	1.97	Hold T, Ro
311	27.8	1.017 (147.5)	825	0.0177 (0.039)	45.6 (82)	63.5 (25)	0	74,756	0.12	0.13	49	0.654	0.078	4.37	
312	18.10	1.022 (148.3)	550	0.0059 (0.013)	22.8 (41)	63.5 (25)	0	24,864	0.24	0.07	49	0.694	0.170	1.05	Vary T, Ro
313	19.14	1.021 (148.1)	550	0.0064 (0.014)	89.4 (161)	63.5 (25)	0	24,758	0.23	0.23	49	2.120	0.486	2.98	Re = 25,000

Table 4.1- Test Matrix For Rotating Heat Transfer Experiments With Normal Trips (Concluded)
Contract NAS3-23691

Test No.	UTRC Run	Dimensional Parameters				Basic Dimensionless Parameters				Secondary Dimensionless Parameters			Comments	
		P N/m ² x10 ⁻⁶ (psi)	Ω rpm	m Kg/sec (lb/sec)	ΔT o C (o F)	R cm (in)	α deg	Re	Ro	$\left(\frac{\Delta T}{T}\right) \frac{R}{d}$	$\left(\frac{\Delta \rho}{\rho}\right) \left(\frac{\Omega R}{V}\right)$	Gr Re ²		Grx10 ⁻⁸
401	20.8	1.021 (148.1)	145	0.0059 (0.013)	22.2 (40)	63.5 (25)	0	25,026	0.06	0.07	49	0.180	0.012	0.07
402	22.8	1.019 (147.8)	145	0.0064 (0.014)	88.9 (160)	63.5 (25)	0	24,982	0.06	0.23	49	0.591	0.037	0.23
403	21.5	1.022 (148.2)	275	0.0059 (0.013)	22.2 (40)	63.5 (25)	0	24,942	0.12	0.07	49	0.340	0.042	0.26
404	23.7	1.019 (147.8)	275	0.0064 (0.014)	88.9 (160)	63.5 (25)	0	24,866	0.11	0.23	49	1.094	0.127	0.79
406	31.9	1.020 (148.0)	825	0.0059 (0.013)	23.3 (42)	63.5 (25)	0	25,134	0.35	0.08	49	0.998	0.355	2.25
405	30.10	1.020 (148.0)	825	0.0064 (0.014)	82.2 (148)	63.5 (25)	0	24,434	0.35	0.22	49	2.724	0.910	5.44

NOTES: Re = $\rho v d / \mu$ Gr/Re² = $(\Delta \rho / \rho) (\Omega R / V) (\Omega d / V)$
 Ro = $\Omega d / V$ Gr = $(\Delta \rho / \rho) (\Omega R / V) (\Omega d / V) (\rho v d / \mu)^2$

Table 4.2- Test Matrix For Rotating Heat Transfer Experiments With Skewed Trips
Contract NAS3-23691

Test UTRC No. Run	Dimensional Parameters				Basic Dimensionless Parameters				Secondary Dimensionless Parameters			Comments		
	P $N/m^2 \times 10^{-6}$ (psi)	Ω rpm	m Kg/sec (lb/sec)	ΔT ° C (° F)	\bar{R} cm (in)	α deg	Re	Ro	$\left(\frac{\Delta T}{T}\right)_{in}$	$\frac{\bar{R}}{d}$	$\frac{\Delta \rho}{\rho} \left(\frac{\Omega R}{V}\right)$		$\frac{Gr}{Re^2}$	$Gr \times 10^{-8}$
201 6.7	1.018 (147.7)	0	0.0059 (0.013)	45.0 (81)	63.5 (25)	0	25,337	0.000	0.13	49	0.000	0.00	0.00	No Rotation
202 9.9	1.019 (147.8)	0	0.0027 (0.006)	44.4 (80)	63.5 (25)	0	12,490	0.000	0.13	49	0.000	0.00	0.00	
203 8.8	1.031 (149.5)	0	0.0113 (0.025)	44.4 (80)	63.5 (25)	0	50,801	0.000	0.13	49	0.000	0.00	0.00	
204 10.8	1.000 (145.0)	0	0.0177 (0.039)	44.4 (80)	63.5 (25)	0	75,351	0.000	0.13	49	0.000	0.00	0.00	
205 25.9	1.015 (147.2)	15	0.0059 (0.013)	44.4 (80)	63.5 (25)	0	25,128	0.006	0.13	49	0.033	0.00	0.00	Vary Ro
206 28.10	1.018 (147.7)	145	0.0059 (0.013)	44.4 (80)	63.5 (25)	0	25,206	0.060	0.13	49	0.319	0.02	0.12	Hold T, Re
207 14.10	1.016 (147.3)	275	0.0059 (0.013)	44.4 (80)	63.5 (25)	0	24,907	0.120	0.13	49	0.590	0.08	0.42	
208 33.10	1.011 (146.7)	412	0.0059 (0.013)	44.4 (80)	63.5 (25)	0	24,981	0.180	0.13	49	0.880	0.15	0.95	
209 17.10	1.018 (147.7)	550	0.0059 (0.013)	44.4 (80)	63.5 (25)	0	24,037	0.230	0.13	49	1.181	0.17	1.72	
210 48.8	1.016 (147.4)	825	0.0059 (0.013)	45.0 (81)	63.5 (25)	0	24,582	0.340	0.13	49	1.702	0.59	3.54	
211 30.11	1.020 (147.9)	145	0.0032 (0.007)	44.4 (80)	63.5 (25)	0	12,574	0.120	0.13	49	0.591	0.07	0.11	Vary Re
212 22.9	1.037 (150.4)	550	0.0118 (0.026)	45.0 (81)	63.5 (25)	0	50,066	0.120	0.13	49	0.630	0.08	1.88	Hold T, Ro
213 42.11	1.004 (145.6)	825	0.0181 (0.040)	44.4 (80)	63.5 (25)	0	75,872	0.110	0.13	49	0.600	0.07	3.83	

Table 4.2- Test Matrix For Rotating Heat Transfer Experiments With Skewed Trips (Cont.)
 Contract NAS3-23691

Test UTRC No. Run	Dimensional Parameters				Basic Dimensionless Parameters				Secondary Dimensionless Parameters			Comments		
	P N/m ² × 10 ⁻⁶ (psf)	Ω rpm	m Kg/sec (lb/sec)	ΔT ° C (° F)	R cm (in)	α deg	Re	Ro	$\left(\frac{\Delta T}{T}\right)_{in}$	$\frac{\bar{R}}{d}$	$\frac{\left(\frac{\Delta P}{\rho}\right)\left(\frac{\Omega R}{V}\right)}{Re^2}$		Gr Re ²	Gr × 10 ⁻⁸
214 15.11	1.015 (147.2)	275	0.0064 (0.014)	89.4 (161)	63.5 (25)	0	24,849	0.110	0.23	49	1.069	0.12	0.76	High
215 23.8	1.038 (150.6)	550	0.0122 (0.027)	88.9 (160)	63.5 (25)	0	50,148	0.120	0.23	49	1.166	0.14	3.54	
216 29.8	1.015 (147.2)	145	0.0064 (0.014)	88.9 (160)	63.5 (25)	0	25,004	0.060	0.23	49	0.567	0.03	0.21	Vary T, Ro at Re=25,000
217 35.10	1.014 (147.1)	412	0.0064 (0.014)	66.7 (120)	63.5 (25)	0	24,969	0.160	0.18	49	1.172	0.19	1.21	
218 34.9	1.013 (146.9)	412	0.0059 (0.013)	22.2 (40)	63.5 (25)	0	25,143	0.180	0.07	49	0.493	0.19	0.56	
219 36.10	1.016 (147.3)	412	0.0064 (0.014)	88.9 (160)	63.5 (25)	0	25,127	0.170	0.23	49	1.548	0.26	1.65	
220 18.9	1.007 (146.1)	550	0.0059 (0.013)	22.2 (40)	63.5 (25)	0	25,088	0.240	0.07	49	0.666	0.16	1.01	
221 20.9	1.016 (147.3)	550	0.0064 (0.014)	66.7 (120)	63.5 (25)	0	25,037	0.220	0.18	49	1.436	0.33	2.08	
222 21.10	1.016 (147.4)	550	0.0064 (0.014)	89.4 (161)	63.5 (25)	0	24,960	0.220	0.23	49	2.024	0.45	2.83	
223 41.12	1.018 (147.7)	825	0.0059 (0.013)	22.8 (41)	63.5 (25)	0	24,564	0.360	0.07	49	0.970	0.35	2.10	
224 40.8	1.018 (147.6)	825	0.0064 (0.014)	66.1 (119)	63.5 (25)	0	24,919	0.360	0.18	49	2.368	0.81	5.02	

Table 4.2- Test Matrix For Rotating Heat Transfer Experiments With Skewed Trips (Concluded)
Contract NAS3-23691

Test No.	UTRC Run	Dimensional Parameters				Basic Dimensionless Parameters			Secondary Dimensionless Parameters			Comments		
		P $N/m^2 \times 10^{-6}$ (psi)	Ω rpm	ΔT ° C (° F)	\bar{R} cm (in)	α deg	Re	Ro	$\left(\frac{\Delta T}{T}\right)_{in}$	$\frac{\bar{R}}{d} \left(\frac{\Delta \rho}{\rho}\right) \left(\frac{\Omega R}{V}\right)$	Gr		Re^2	
225	59.9	1.018 (147.6)	825 (0.013)	45.0 (81)	63.5 (25)	45	24,750	0.340	0.13	49	1.698	0.58	3.56	Angle Variation = 45°
226	50.9	1.016 (147.3)	550 (0.013)	44.4 (80)	63.5 (25)	45	24,871	0.230	0.13	49	1.201	0.28	1.72	
227	49.9	1.016 (147.3)	275 (0.013)	44.4 (80)	63.5 (25)	45	24,976	0.120	0.13	49	0.598	0.07	0.43	
228	52.8	1.017 (147.5)	275 (0.014)	88.9 (160)	63.5 (25)	45	25,919	0.110	0.23	49	1.067	0.12	0.76	
229	54.9	1.022 (148.3)	550 (0.026)	44.4 (80)	63.5 (25)	45	50,160	0.120	0.13	49	0.626	0.07	1.85	
230	53.9	1.023 (148.4)	550 (0.027)	88.9 (160)	63.5 (25)	45	49,733	0.120	0.23	49	1.175	0.14	3.5	

NOTES: $Re = \rho V d / \mu$ $Gr/Re^2 = (\Delta \rho / \rho) (\Omega R / V) (\Omega d / V)$
 $Ro = \Omega R / V$ $Gr = (\Delta \rho / \rho) (\Omega R / V) (\Omega d / V) (\rho V d / \mu)^2$

$\alpha = 0$ (STD)
 $\bar{R}/d = 49$ (STD)

NOTE: STD. ROTATING BASELINE FLOW CONDITIONS

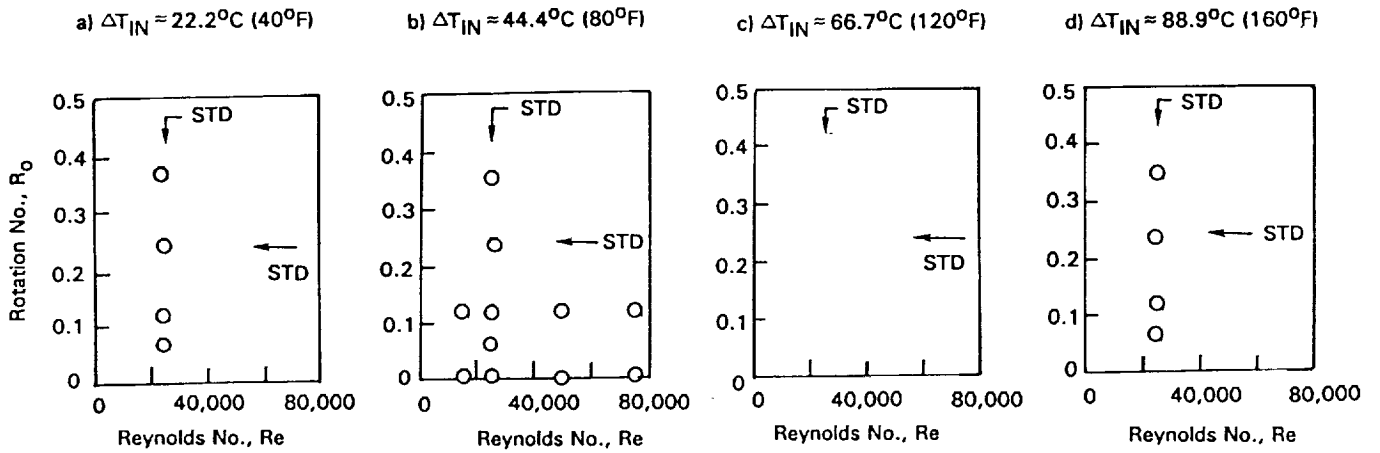


Figure 4.1- Test Conditions for Parametric Rotating Heat Transfer Study With Normal Trips.

$\alpha = 0$ (STD)
 $\bar{R}/d = 49$ (STD)

NOTE: STD. ROTATING BASELINE FLOW CONDITIONS

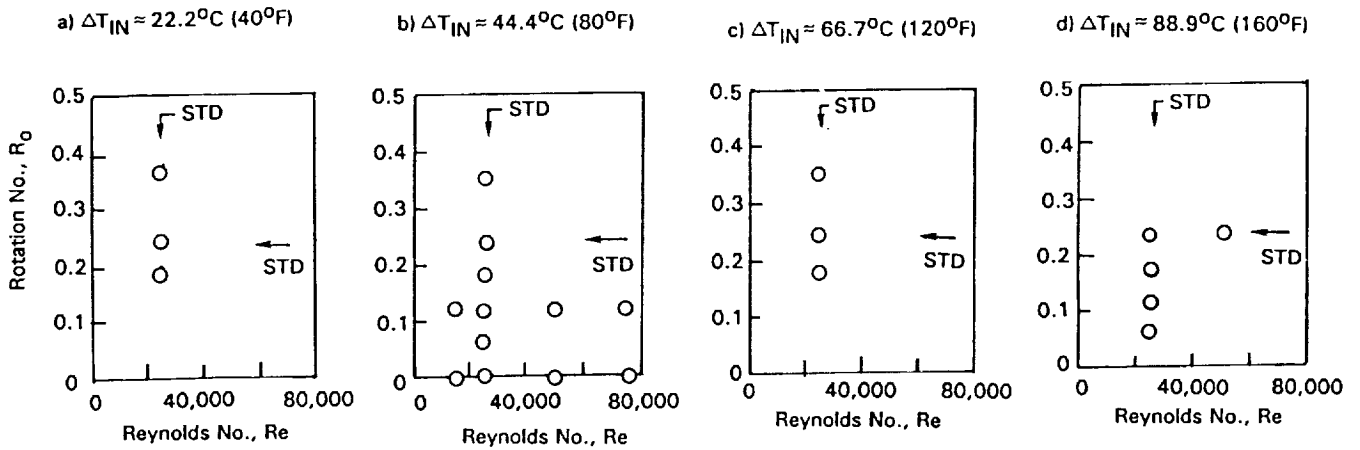


Figure 4.2- Test Conditions for Parametric Rotating Heat Transfer Study With Skewed Trips.

5.0 HEAT TRANSFER RESULTS FOR BASELINE FLOW CONDITIONS

Two baseline experiments, stationary and rotating, were conducted with both the normal and skewed trip models to obtain data for comparison with the smooth wall model data generated in this program. The stationary and rotating baseline experiments had dimensionless flow conditions which consisted of a Reynolds number of 25,000 and an inlet density ratio, $[(\rho_b - \rho_w)/\rho_b] = (T_w - T_b)/T_w$, of 0.13. The rotating baseline experiments had rotation numbers, $\Omega d/V$, of 0.24 and a radius ratio at the average model radius, R/d , equal 49. These values were selected because they are in the central region of the operating range of current large aircraft gas turbine engines.

5.1 Stationary Baseline Flow Condition

Streamwise variations of Nusselt number for the stationary baseline test are shown in Figure 5.1. The Nusselt number for fully developed, turbulent flow in a smooth tube with constant wall temperature and the results from the smooth wall experiments (Volume 1) are shown for comparison.

The heat transfer from the walls with normal and skewed trips (denoted leading and trailing surface, Figure 5.1) in the first outward straight ($3 < (X/d \text{ or } S/d) < 14$) passage have heat transfer coefficients more than two and three times the fully-developed, smooth-wall correlation. Note that the heat transfer coefficients for the models with the normal and skewed trips do not decrease significantly with X/d in each passage as they did for the model with the smooth wall. Some differences in heat transfer are observed between the leading and trailing surfaces in the two models for this stationary baseline condition. The exact cause of the difference is not known but may be due to the staggering of the trips on the two surfaces (Figures 3.4 & 3.5). The heat transfer coefficients on the side (or rib) walls (Figures 5.1) were less those that on the leading and trailing surfaces with trips. However the heat transfer with either set of trips was 20 to 100 percent greater than with the smooth walls. This increase in heat transfer on the side walls was attributed to increased velocity due to blockage of the trips for $X/d=4$ and to the increased turbulence level in the coolant passage for $X/d=8$ and 12. Note also that the heat transfer for sidewall segments 1-18 of the skewed trip model increases markedly at $X/d=8$ and 12. This increase was attributed to the secondary flow toward side test surfaces 1-5 (Figure 3.6) from the center of the coolant passage with a colder temperature. The secondary flow was caused by the trips skewed at 45 deg to the flow direction. The heat transfer coefficients on the trip model with skewed trips are 10 to 30 percent greater than those on the model with normal trips. The model with skewed trips has approximately five percent greater surface area on the leading surface than the model with normal trips. Therefore most of the increase in heat transfer with skewed trips compared to that with normal trips is attributed to the changes in the flow characteristics.

The heat transfer coefficients measured in the remaining two passages (i.e., $20 < S/d < 48$) show similar characteristics. The heat transfer characteristics in the second passage are generally similar to those in the first passage with heat transfer on all walls for the model with the skewed trips greater than that with the normal trips. The large increase in heat transfer on the leading side of the model at $S/d=21$ was attributed to the convection interaction of the secondary flow patterns (vorticity) in the first channel through the first 180 deg turn and the concentration of vorticity adjacent to the leading edge (for this stationary experiment).

The heat transfer in the turn regions was generally the same for the present experiment with normal and skewed trips compared to the previous smooth wall experiments. The modest changes on the leading and trailing surfaces of the turn sections are attributed in

Baseline temperature ratio, Reynolds number and geometry

$\Omega = 0$ rpm
 $Re = 25,000$
 $\Delta T \approx 44^\circ C (80^\circ F)$

$\bar{R}/d = 49$
 $\alpha = 0$
 $(\Delta T/T)_{in} = 0.13$

HP - High Pressure
 LP - Low Pressure

Symbol	○	●	◐
Model Config.	Smooth Wall	Normal Trips	Skewed Trips
Test No.	1 (Vol. I)	302	201

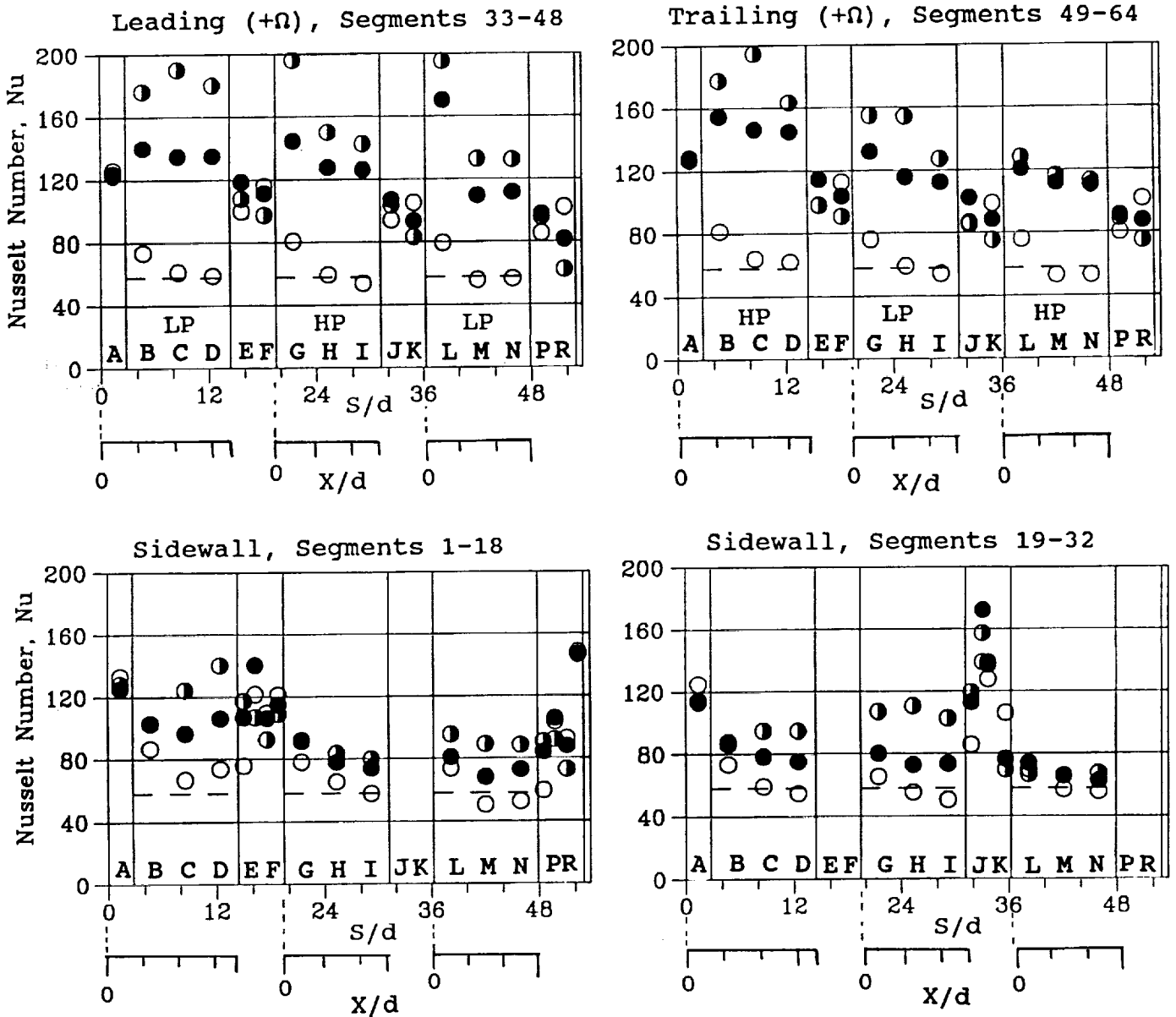


Figure 5.1- Effect of Trip Configuration on Heat Transfer for Stationary Baseline Flow Conditions.

part to the differences in the velocity profiles expected at the entrance to the turn regions. For the smooth wall flow condition, the velocities are expected to be high in the corners of the duct (e.g. Schlichting, 1968). For flow over normal trips, the velocity can be expected to be peaked in the center of the channel due to the large momentum losses at each trip. The changes in heat transfer on the sides (outside walls of turn sections) attest to the complexity of the flow structure in the turns and is not yet explained.

5.2 Rotating Baseline Flow Condition

The streamwise distribution of the dimensionless heat transfer coefficient (i.e. Nusselt Number) for the heat transfer models with normal and skewed trips for the Rotating Baseline Flow Condition [$Re=25,000$; $Ro=0.24$; $(\Delta\rho/\rho)_{inlet} = 0.13$] are presented in Fig. 5.2. Also shown are the results from the Rotating Baseline Flow Condition for the heat transfer model with smooth walls. The heat transfer characteristics for the models with trips and rotation are similar to those for the model with smoother walls. That is, in the first passage with flow outward, the heat transfer increases on the trailing side and decreases on the leading side. In addition, in the straight passages, the relative position of the heat transfer coefficients remain the same as for the Stationary Baseline Flow Condition.

The model with the skewed trips has the highest and the model with the smooth walls has the lowest heat transfer coefficients on the leading and trailing sides and on most of the side wall heat transfer surfaces. However, the ratio of the heat transfer coefficients at each streamwise location varies. At some locations, the heat transfer with the skewed trips is only 5 percent greater than that with normal trips; an increase approximately the same as the actual heat transfer surface area. (Recall that the heat transfer coefficients are based on projected surface area.)

The largest difference between the heat transfer from the models with skewed and normal heat transfer occurs on the trailing surfaces (Figure 5.2) in the second passage streamwise locations GHI or $19 < S/d < 31$. In this region, the heat transfer with the normal trips is closer to the smooth wall than that with the skewed trips. This anomaly is attributed to the formation of buoyancy-driven cells between the trips on this trailing surface with flow radially inward. The authors' hypothesis is that the secondary flow produced by the skewed trips precludes a recirculating flow, like that described for the normal trips, and the accompanying lower heat transfer coefficients with the normal trips. This model is compatible with the results for calculated flows in circular ducts with square trips (Taylor et al. 1991).

The heat transfer in the turn regions with rotation is more complex. For the first turn at the model tip (outside radius), the heat transfer coefficients with the smooth wall model are the highest on all three surfaces. For the second turn at the model root (inside radius), the heat transfer with the smooth model is the lowest. These effects are attributed to the complex flows produced during the convection of secondary flow patterns produced in the straight passage sections upstream of each turn by each of the three wall surfaces (smooth, normal trips, skewed trips). Additional analytical effort will be required to delineate the causes for these effects.

5.3 Comparison of Stationary and Rotating Results

The streamwise distributions of heat transfer ratio for the rotating baseline condition are also shown in Figures 5.3a and 5.3b for the models with the normal trips and the skewed trips. These data, previously presented in Figs. 5.1 and 5.2, show the effects of rotation. These results and those discussed in the following sections are shown as heat transfer ratio, Nu/Nu_{∞} . Nu_{∞} is that expected from the Kays and Perkins (1973) correlation for

Rotating baseline rotation number, temperature ratio and geometry

$\Omega = 550 \text{ rpm}$

$Re = 25,000$

$\Delta T \approx 44^\circ\text{C} (80^\circ\text{F})$

$\bar{R}/d = 49$

$\alpha = 0$

$(\Delta T/T)_{in} = 0.13$

HP - High Pressure

LP - Low Pressure

Symbol	\square	\blacksquare	\blacksquare
Model Config.	Smooth Wall	Normal Trips	Skewed Trips
Test No.	4 (Vol. I)	307	209

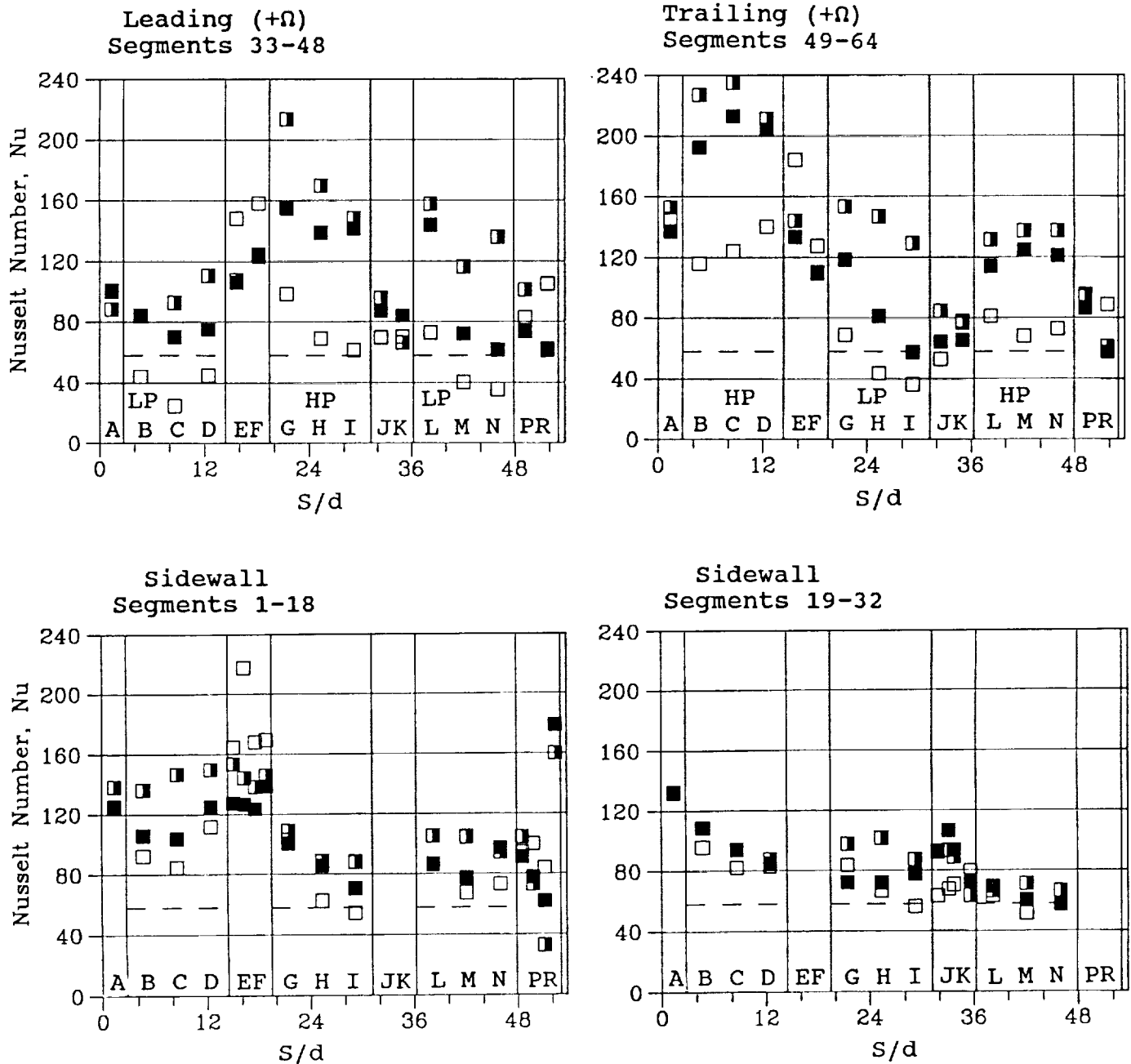


Figure 5.2- Effect of Trip Configuration on Heat Transfer for Rotating Baseline Flow Conditions.

fully developed, turbulent flow. The results are shown in this manner to minimize effects of Reynolds number variations from test to test.

The most important feature of the results from the model with the normal trips (Figure 5.3a) is the decrease in heat transfer on the "low pressure" sides of the model. The low pressure sides are the leading surfaces for flow outward ($X/d < 14$) and the trailing surfaces for flow inward ($X/d < 31$). The lowest values of Nu/Nu_{∞} are less than one-half the nonrotating values and approach 1.0, the value for flow for a smooth tube. The heat transfer on the high pressure side of the coolant passage with flow outward (i.e., the trailing surfaces) increases about 50 percent compared to the stationary case. However, the heat transfer on the leading surface for flow inward does not increase noticeably, but does decrease significantly on the trailing surface. These results are qualitatively similar to those obtained for the smooth wall model. Further comparison with the smooth wall model results will be made in a later section. The baseline results with rotation showed significant changes in the heat transfer in the first passage on the leading, trailing, and turn surfaces but relatively smaller changes on the sidewall surfaces, not shown in Figure 5-3a.

The streamwise distributions of heat transfer ratio for the rotating and stationary baseline flow conditions from the leading and trailing surfaces of the model with the skewed trips are shown in Figure 5.3b. The most important feature of these results is the decrease in heat transfer on the "low pressure" sides shown for the leading surfaces for flow outward ($S/d < 14$). The lowest values of Nu/Nu_{∞} are less than one-half the nonrotating values. The heat transfer on the high pressure side of the coolant passage with flow outward (i.e., the trailing surfaces) increases about 20 percent compared to the stationary case. However, the heat transfer on the leading and trailing surfaces for flow inward does not increase or decrease appreciably. These results are qualitatively similar to those obtained for the smooth wall model. The heat transfer coefficients on the leading surface of the third passage with flow upward did not decrease significantly due to rotation as occurred in the first passage. This difference is attributed to the secondary flows generated in the root turn. Further comparison with the smooth wall model results will be made in a later section.

The increase due to rotation in heat transfer from the models with the trips in the second and third passages was generally less than that obtained in the first outward straight section. This general reduction in heat transfer was attributed primarily to the development of well mixed flow in the coolant passages downstream of the turns and, possibly, the increased uncertainty in the bulk temperature at these downstream locations. (The increased heat transfer compared to the smooth wall model causes the difference between bulk temperature and the wall temperature to decrease and hence the uncertainty of the heat transfer coefficient determined to increase.)

5.4 Concluding Comments for Baseline Flow Conditions

The comparison of stationary and rotating results for the Baseline Flow Condition results from the models with normal and skew trips and previous results from the model with smooth walls showed several significant effects of rotation:

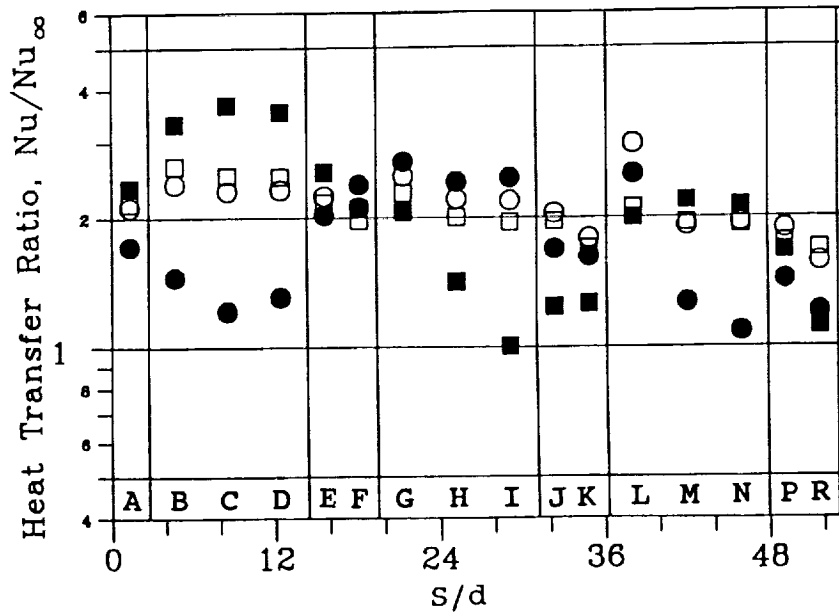
- On the low pressure surface (leading side on outward flow and trailing side on inward flow), rotation can decrease the heat transfer coefficient for normal trips to less than half the value for the stationary model. The effect of rotation is less significant for the skewed trips on the second and third passages.
- On the high pressure surface (trailing side on outward flow and leading side on inward flow), heat transfer coefficients increase significantly with rotation in the first passage, but are approximately the same for the second and third passages.

$\overline{R/d} = 49$
 $\alpha = 0$
 $Re = 25,000$

$\Delta T \approx 44^\circ C (80^\circ F)$
 $(\Delta T/T)_{in} = 0.13$

Symbol	○	●	□	■
Surface	Leading	Leading	Trailing	Trailing
R_o	0.0	0.23	0.0	0.23

a) Normal Trip Configuration (Tests No. 302 & 307)



b) Skewed Trip Configuration (Tests No. 201 & 209)

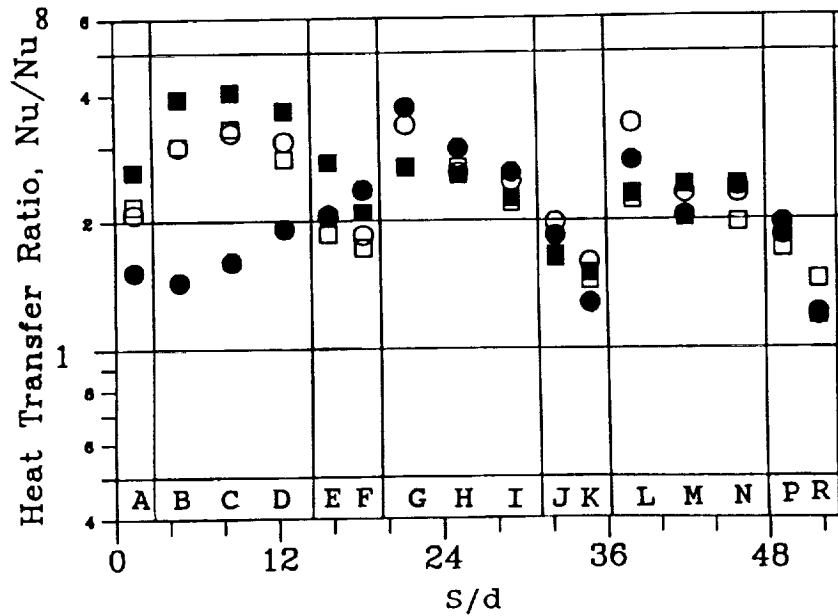


Figure 5.3- Comparison of Heat Transfer for Stationary and Rotating Baseline Flow Conditions.

6.0 HEAT TRANSFER RESULTS FOR VARIATION OF PARAMETERS ABOUT BASELINE FLOW CONDITIONS

The test matrices for all three wall configurations, i.e., smooth, normal trips, skewed trips, were originally planned to have only variations of the flow parameters about the Rotating Baseline Flow Condition. During the experiments with the smooth wall model it became apparent that the character of the heat transfer and flow was complex and changed markedly with changes in the rotation number ($\Omega d/V$) and the inlet density ratio $(\Delta\rho/\rho)_{\text{inlet}}$. Subsequently, the test matrices were enlarged for all three model wall configurations to include more test conditions with varying inlet density ratios and for the rotation numbers where the character of the flow changes. Results from the variations about the rotating baseline flow conditions provide a great deal of insight into the cause/effect relationships.

The results from the experiments will be presented in two manners. First, the effects of varying each flow parameter about the Rotating Baseline Flow Condition on the local heat transfer coefficients in each model will be shown (Section 6) as a variation with the streamwise location for each surface. In addition, the effects of varying the Reynolds number about the Stationary Baseline Flow Conditions for each configuration will be shown. These stationary results will be used to establish the use of the Reynolds number exponent (i.e., 0.8) relationship for the comparison of results. Second, the effects of varying all the flow conditions on the heat transfer coefficients at specific locations within the model will be shown in Sections 7 to 9 for the models with the normal and skew trips. The results from previous tests in this program for the model with smooth walls will also be compared at these specific locations.

6.1 Effects of Reynolds Number

The variation of the heat transfer ratio, Nu/Nu_{∞} , at stationary conditions on the leading and trailing surfaces with streamwise location (S/d), are presented in Figures 6.1 and 6.2 for Reynolds numbers of approximately 12,500, 25,000, 50,000 and 75,000. The heat transfer coefficients are normalized with those expected for fully developed flow in a smooth tube at the same streamwise Reynolds number (note the local bulk and film properties were used in the calculation of the heat transfer ratio).

The heat transfer ratios for the three highest Reynolds numbers are identical within the accuracy of the experiment for the model with normal trips (Figure 6.1). The heat transfer ratio for $Re = 12,500$ is 10 to 15 percent higher than those for the higher Reynolds numbers. This increase in heat transfer ratio is attributed to Reynolds number effects. However, some of the differences could be attributed to uncertainties in the results at the lower Reynolds number where the effects of the uncertainty in the heat losses through the model increase as the convective heat flux decreases.

The variation of the heat transfer ratio at stationary conditions with Reynolds number for skewed trips (Figure 6.2) is larger than for the model with normal trips. The results for $Re = 50,000$ and 75,000 are essentially identical. However, the results for $Re = 12,500$ and 25,000 are 10 to 20 percent greater than those for $Re = 50,000$ and 75,000. The heat transfer ratio on the side (or rib walls - not shown) were approximately the same (i.e. within 5 percent) for the flow in the first two channels for both models.

The streamwise variation of heat transfer ratio, Nu/Nu_{∞} , is presented in Figures 6.3 and 6.4 for Reynolds numbers from 12,500 to 75,000, for a fixed rotation number, $Ro = 0.12$, and a fixed inlet density ratio, $(\Delta\rho/\rho)_{\text{inlet}} = 0.13$ from models with normal (Figure 6.3) and skew trips (Figure 6.4). The heat transfer coefficient from each streamwise

location is made dimensionless with respect to the heat transfer coefficient for a fully developed flow in a smooth duct.

The heat transfer ratio for $Re = 50,000$ and $75,000$ at all locations in both models are well correlated by use of the Kays and Perkins correlation. Results for the leading surfaces in the first passage of both models and the trailing surfaces in the second passage with the skewed trip model are especially well correlated. The variations between the heat transfer ratios for Reynolds number equal $25,000$ and those for $50,000$ and $75,000$ are generally less than 10 percent for both models with trips. The variation for Reynolds numbers of $12,500$ is somewhat greater, especially in regions with the highest heat transfer coefficients.

The conclusion from these rotating and stationary experiments was that the relationship for fully developed flow in a square duct with smooth walls, $Nu_{\infty} = 0.0176 Re^{0.8}$, would be adequate for scaling the effects of Reynolds number on the heat transfer ratio.

6.2 Effect of Rotation

The rotation number, $\Omega d/V$, was varied from 0 to 0.35 for this series of flow conditions. The Reynolds number, inlet density ratio and radius ratio were held constant at the nominal values of $25,000$, 0.13 and 49 , respectively. The heat transfer ratios for the models with the normal and skewed trips are presented in Figures 6.5 and 6.6, respectively.

The heat transfer ratios for both models vary significantly, i.e. a factor of 2, on the leading and trailing surfaces. The decrease in heat transfer coefficient due to rotation on the leading surface of the first passage is approximately the same for both models, that is, the heat transfer decreases to approximately one-half the stationary value for $Ro = 0.24$. However, the effects of rotation are somewhat different in the two models on the other surfaces and in the second and third passages. The variations are attributed to the different secondary flow patterns induced in each model by the normal or skewed trip configurations and the different effects of the conservation of vorticity through turn regions on the heat transfer in the second and third passage. These effects will be noted in this and following sections. Although the various effects are recognized, their relative importance regarding the heat transfer is difficult to estimate. The current (i.e. 1989-1991) analyses of flows in complex rotating coolant passages are providing insight into the flow and heat transfer characteristics of turbine blade internal cooling.

Normal Trips

High Pressure Surfaces. Increasing the rotation rate causes significant increases in heat transfer on the trailing surfaces (Figure 6.5) of the first passage but relatively small increases occurred on the leading surfaces in the second passage. Heat transfer in the first passage increased by more than 60 percent for the largest value of rotation parameter (0.35) compared to stationary heat transfer values. The substantial increases in heat transfer in the first passage are consistent with the results of Rothe and Johnston (1979). They found that as rotation rate was increased, the reattachment length after a step decreased. For the trip spacing of the present program ($P/e = 10$), this would translate into an increase in the effective heat transfer area between the trips with attached, turbulent flow, thereby, causing an increase in the heat transfer. Compared to the stationary results, the heat transfer on the leading, high pressure side of the second passage increased approximately 10 percent. The effects on heat transfer due to Coriolis generated secondary flows and flow reattachment might be expected to be approximately the same for the first and second passages. The differences in heat transfer between the outward and inward

$\Omega = 0$ rpm
 $\overline{R}/d = 49$
 $\alpha = 0$

$\Delta T \approx 44^\circ\text{C}$ (80°F)
 $(\Delta T/T)_{in} = 0.13$

HP - High Pressure
 LP - Low Pressure

Symbol	□	○	△	◇
Reynolds No.	12,500	25,000	50,000	75,000
Test No.	302	301	303	304

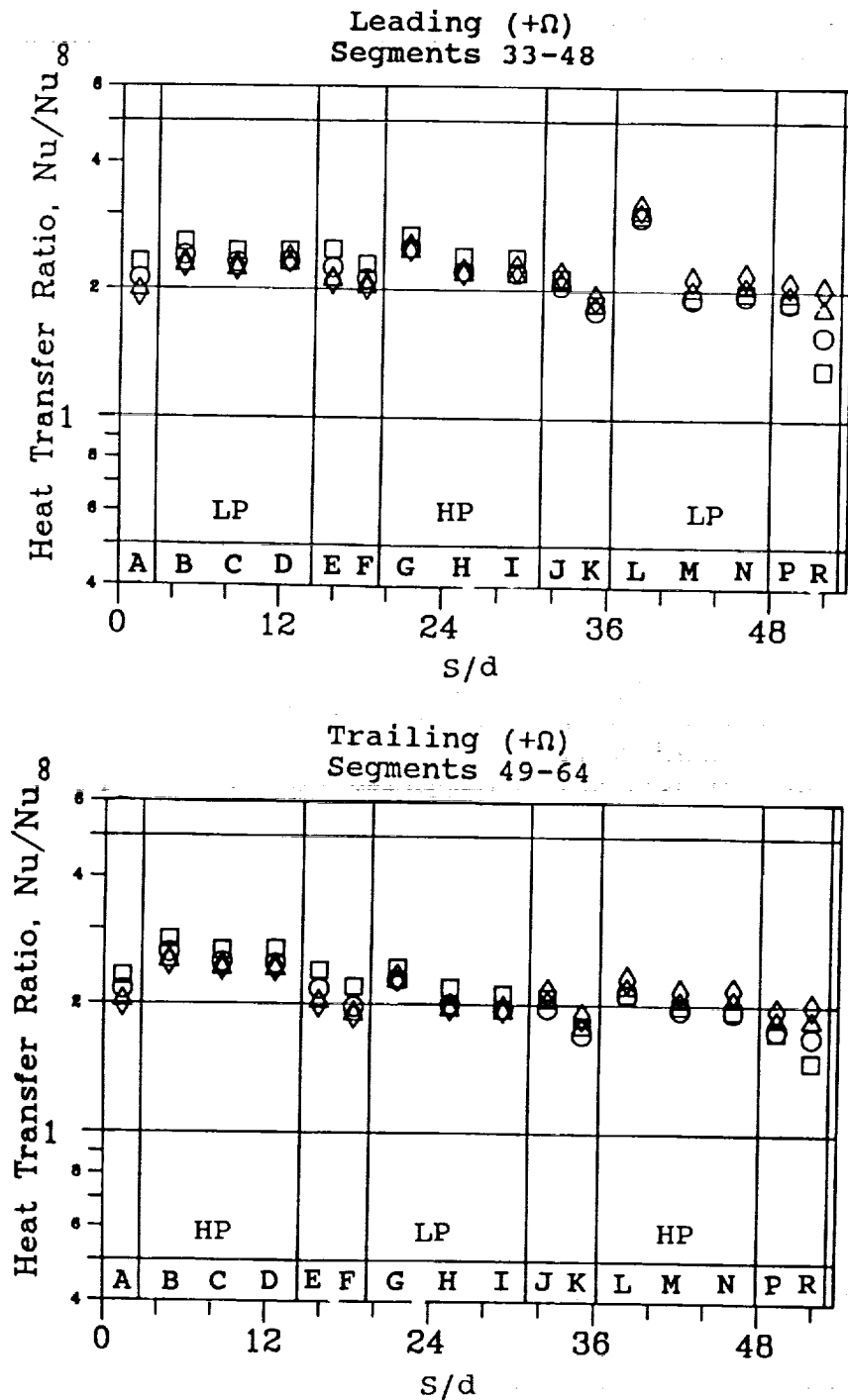


Figure 6.1- Effect of Reynolds Number on Heat Transfer Ratio for Normal Trips and No Rotation.

$\Omega = 0$ rpm

$\overline{R}/d = 49$

$\alpha = 0$

$\Delta T \approx 44^\circ\text{C}$ (80°F)

$(\Delta T/T)_{in} = 0.13$

HP - High Pressure

LP - Low Pressure

Symbol	□	○	△	◇
Reynolds No.	12,500	25,000	50,000	75,000
Test No.	202	201	203	204

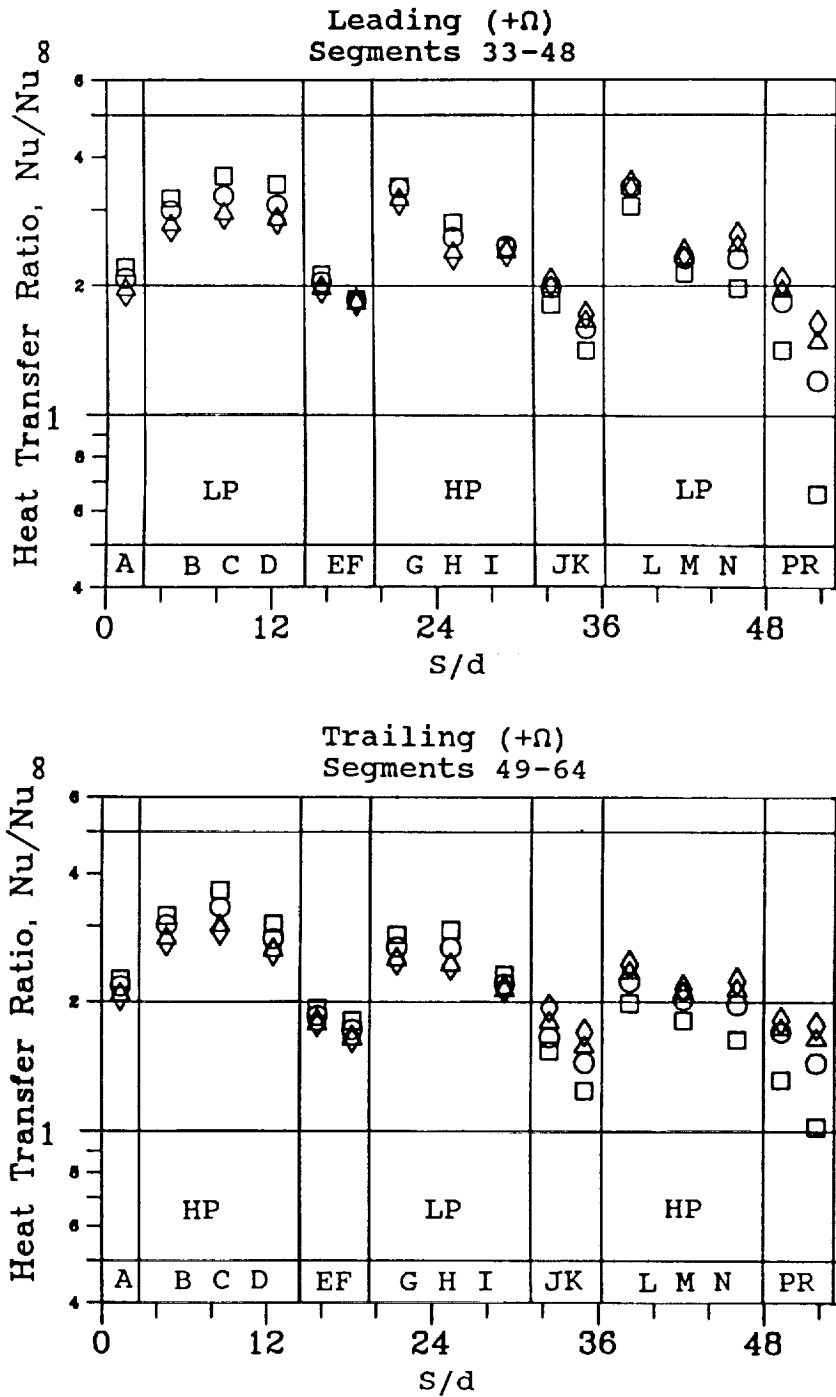


Figure 6.2- Effect of Reynolds Number on Heat Transfer Ratio for Skewed Trips and No Rotation.

$\bar{R}/d = 49$
 $\alpha = 0$
 $R_o = 0.12$

$\Delta T \approx 44^\circ\text{C} (80^\circ\text{F})$
 $(\Delta T/T)_{in} = 0.13$

HP - High Pressure
 LP - Low Pressure

Symbol	□	○	△	◇
Reynolds No.	12,500	25,000	50,000	75,000
Test No.	309	306	310	311

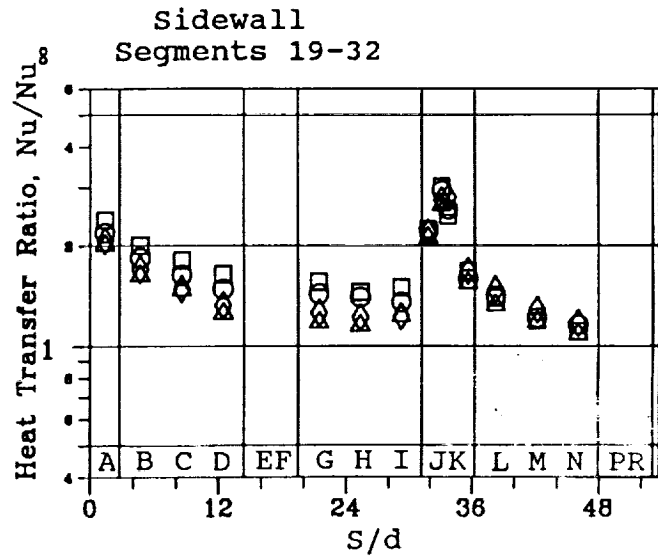
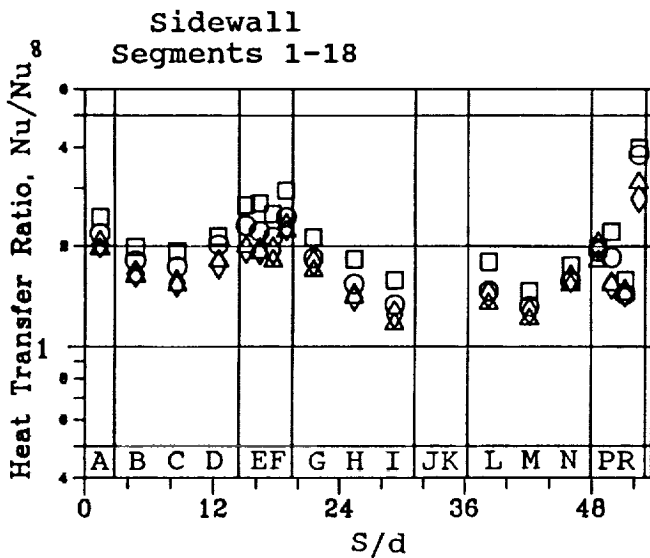
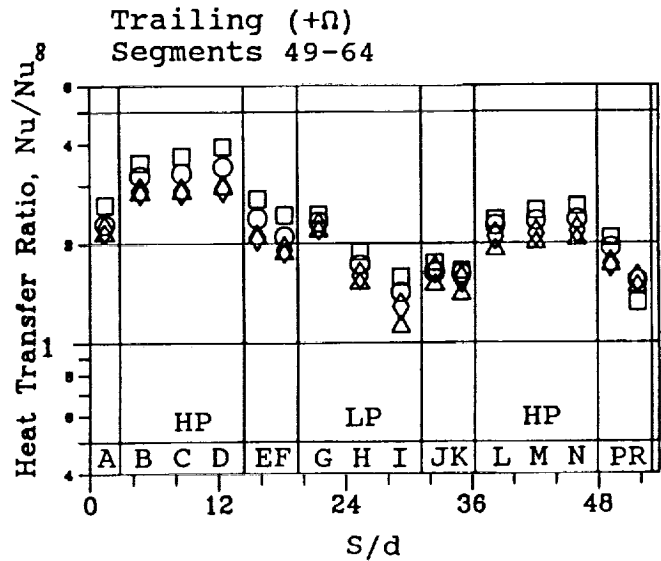
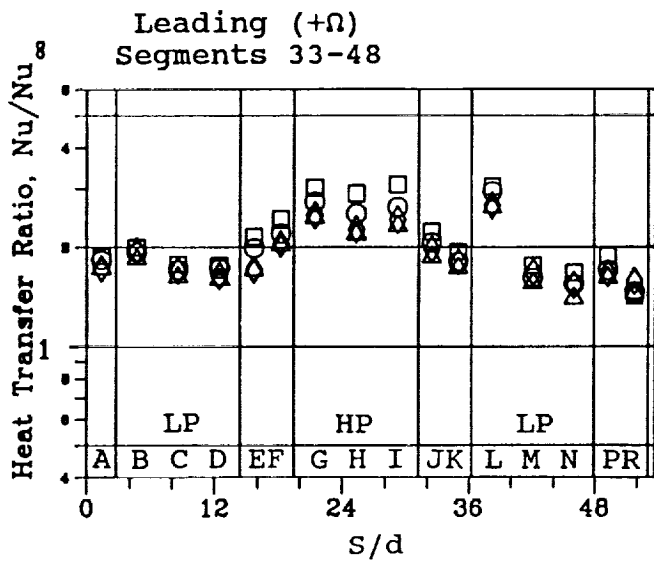


Figure 6.3- Effect of Reynolds Number on Heat Transfer Ratio for Normal Trips and a Rotation Number of 0.12.

$R/d = 49$
 $\alpha = 0$
 $R_o = 0.12$

$\Delta T \approx 44^\circ\text{C} (80^\circ\text{F})$
 $(\Delta T/T)_{in} = 0.13$

HP - High Pressure
 LP - Low Pressure

Symbol	□	○	△	◇
Reynolds No.	12,500	25,000	50,000	75,000
Test No.	211	207	212	213

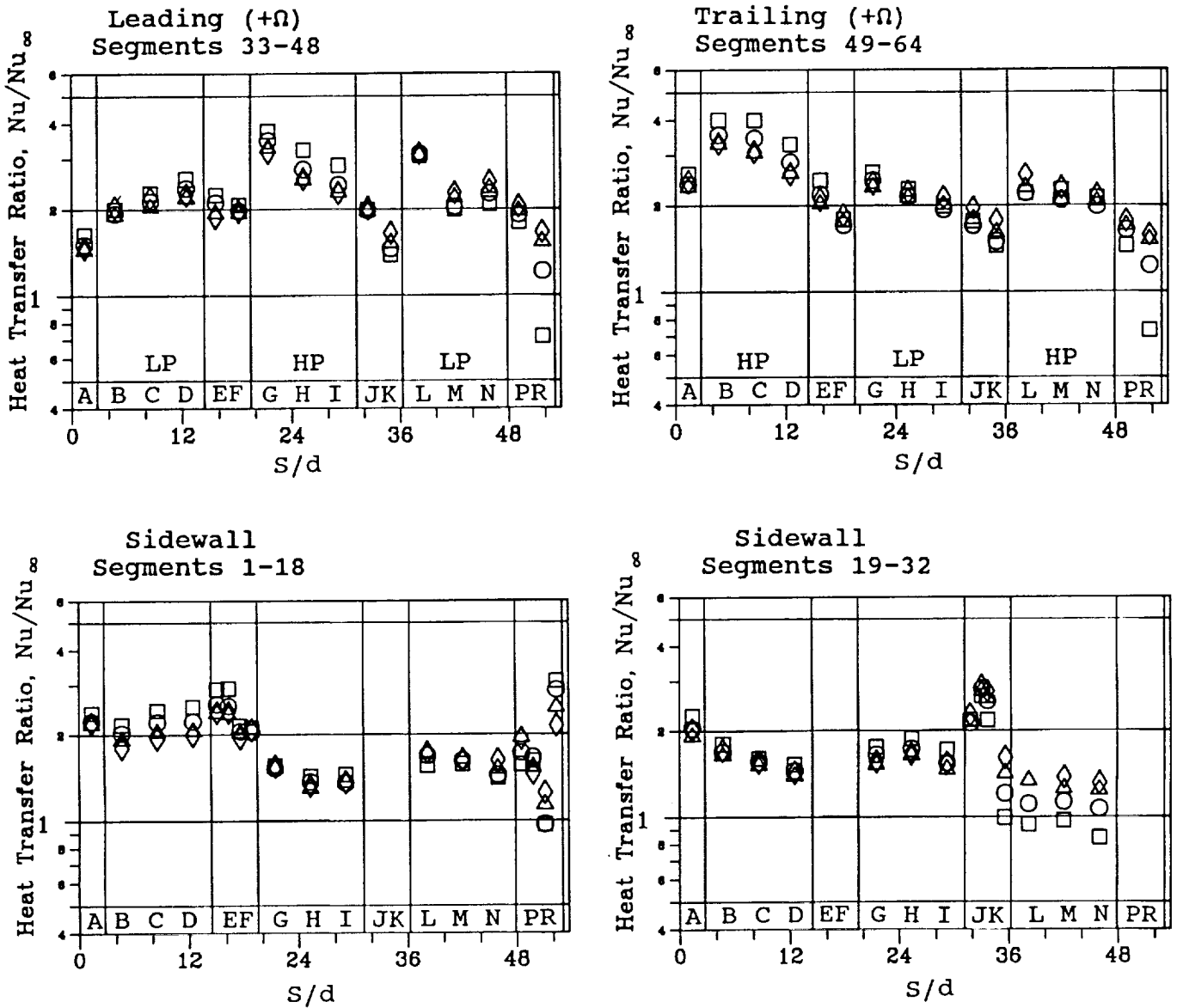


Figure 6.4- Effect of Reynolds Number on Heat Transfer Ratio for Skewed Trips and a Rotation Number of 0.12.

$\bar{R}/d = 49$
 $\alpha = 0$
 $Re = 25,000$

$\Delta T \approx 44^\circ C (80^\circ F)$
 $(\Delta T/T)_{in} = 0.13$

HP - High Pressure
 LP - Low Pressure

Symbol	○	□	△	◇	▽
Rotation No.	0.00	0.06	0.12	0.23	0.35
Test No.	301	305	306	307	308

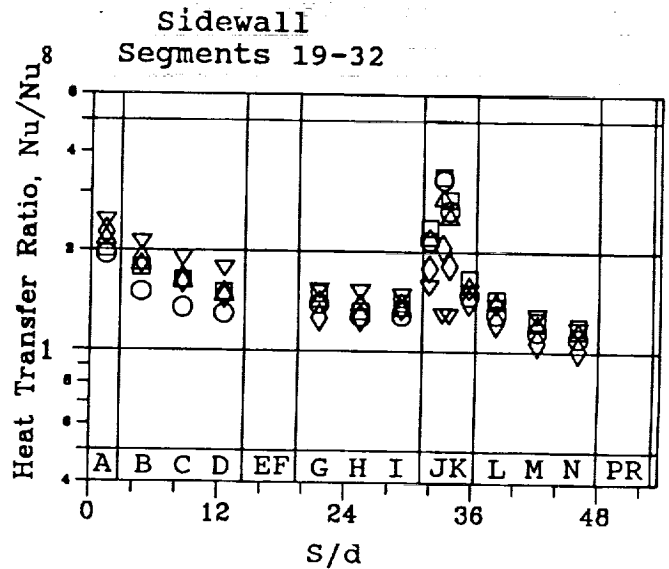
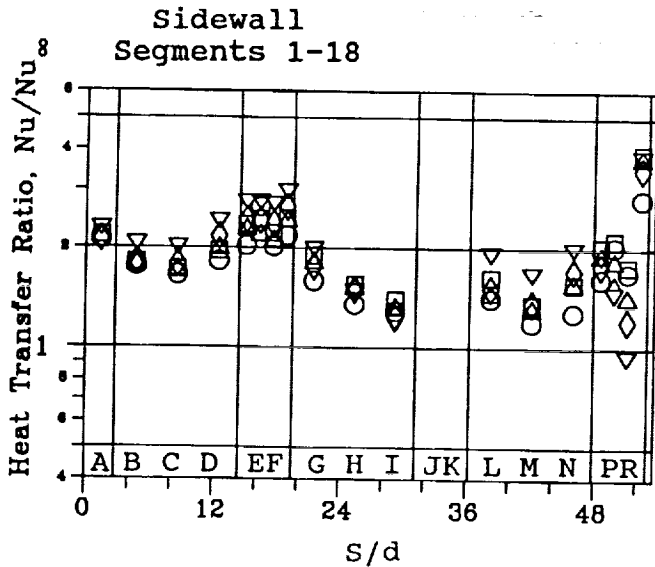
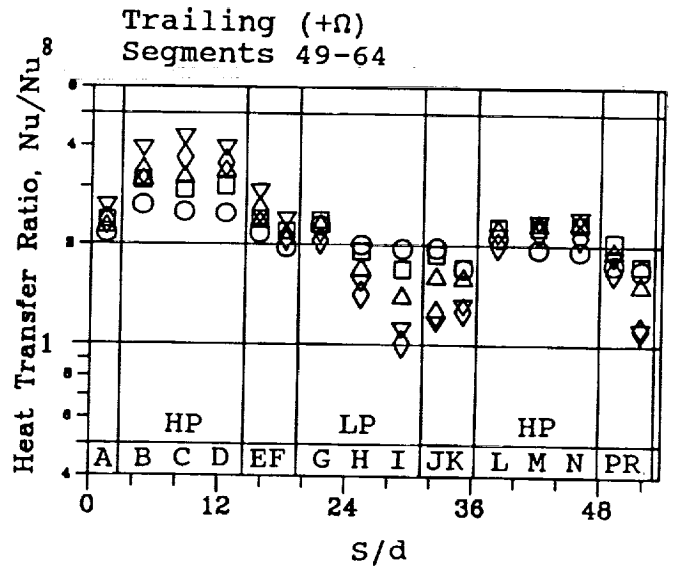
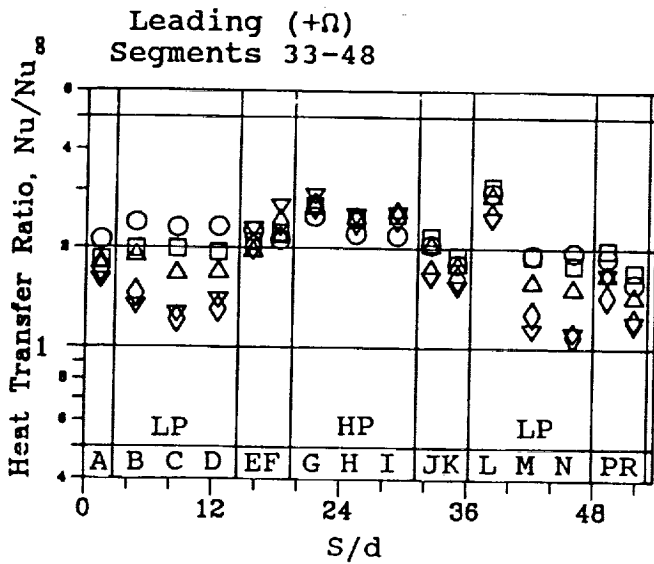


Figure 6.5- Effect of Rotation Number on Heat Transfer Ratio for Normal Trips.

$\bar{R}/d = 49$
 $\alpha = 0$
 $Re = 25,000$

$\Delta T \approx 44^\circ C (80^\circ F)$
 $(\Delta T/T)_{in} = 0.13$

HP - High Pressure
 LP - Low Pressure

Symbol	○	□	△	◇	▽	△	D
Rotation No.	0.00	0.006	0.06	0.12	0.18	0.23	0.34
Test No.	201	205	206	207	208	209	210

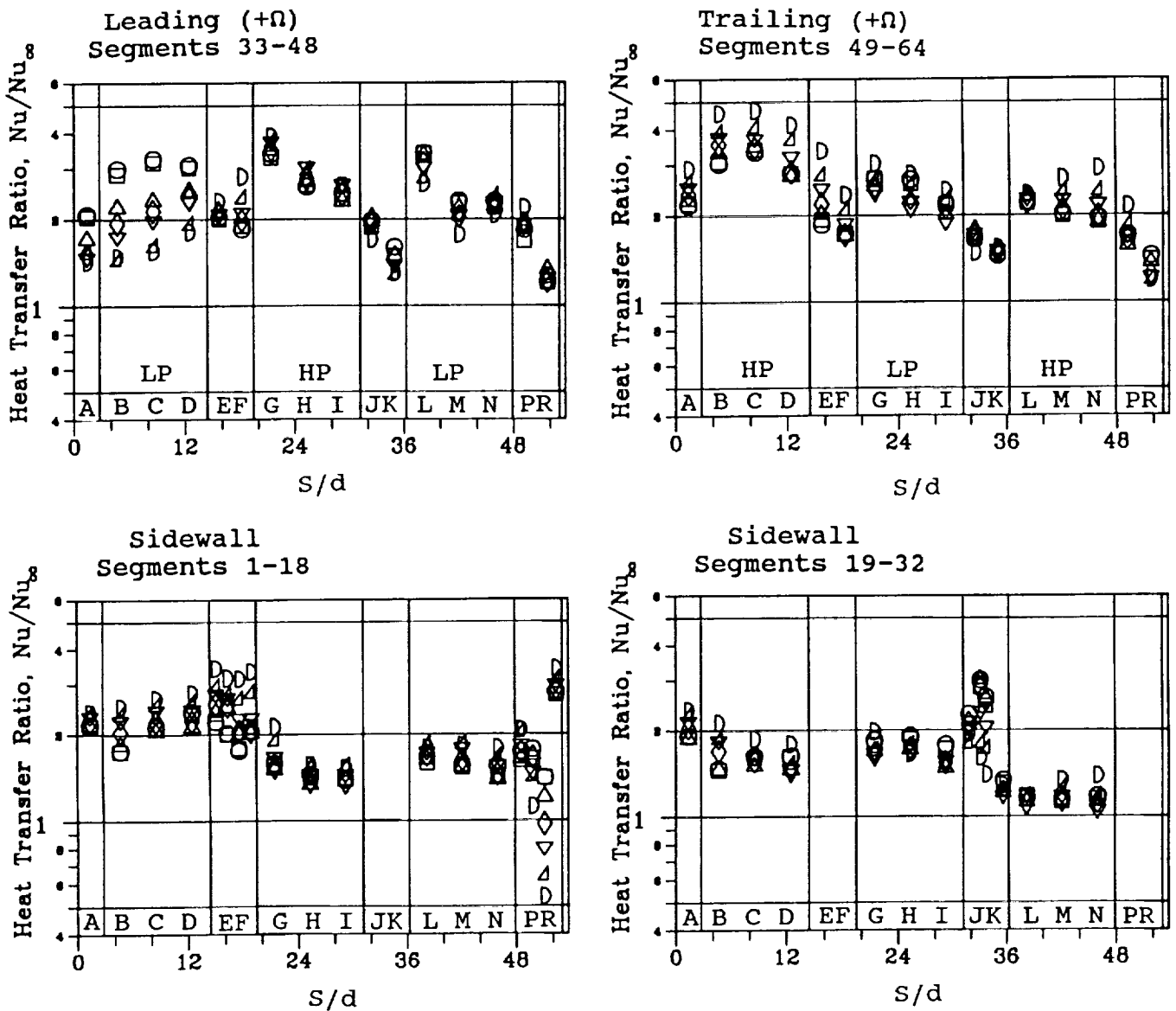


Figure 6.6- Effect of Rotation Number on Heat Transfer Ratio for Skewed Trips.

flowing passages are therefore attributed to the different effects of buoyancy in the counter-flowing first passage (radially outward flow) and the co-flowing second passage (radially inward flow). In general, the trends noted above are compatible with those obtained for the smooth wall test surfaces in the same model (Wagner et al., 1990).

The small increase in the heat transfer ratio on the high pressure (leading surface) side of the second passage (trailing surface) relative to the first passage is attributed to a reduction in the generation of near-wall turbulence. In the first passage, the near-wall buoyancy driven flow was inward toward the axis of rotation and the coolant flow was outward. This counter flow is expected to generate additional near-wall turbulence due to the strong shear gradient. The large increases in heat transfer in the first passage are attributed to the destabilizing effects of the shear flow combined with the cross stream secondary flows generated by Coriolis forces. However, when the average flow direction and the buoyancy-driven near-wall flow direction are coincident, as in the second passage, the generation of near-wall turbulence may be diminished because of the relatively weaker near-wall shear layer. The expected lower near-wall turbulence and weaker shear flows may also contribute to increases in reattachment lengths following the trips. Therefore, the reduced effects of the buoyant and the cross stream secondary flows coupled with possible increases in reattachment lengths in the second passage may have resulted in lesser changes in heat transfer. The magnitude of the buoyancy effect on the heat transfer is unclear in that the buoyancy effect on the heat transfer in the second passage may be zero (which implies a modest Coriolis dominated heat transfer increase) or negative (which implies a larger Coriolis dominated heat transfer increase which is offset by a reduction due to buoyancy). Future results from concurrent numerical simulations of these flow conditions are expected to assist in the understanding of this complex flow field.

Low Pressure Surfaces. In contrast to the continual increase in heat transfer with increasing rotation number on the trailing side, the heat transfer ratio decreases with increasing rotation number on the leading side of the passage near the inlet, i.e. $x/D < 4$ (Figure 6.5). For the remaining locations on the leading side of the passage, the heat transfer ratio decreases and then increases again with increasing rotation number. Heat transfer from the trailing, low pressure surfaces of the second passage also had large decreases in heat transfer. Heat transfer in the first passage leading surface and second passage trailing surface decreased to almost 50 percent of the stationary heat transfer levels. In both passages, the heat transfer decreased and then subsequently increased again as the rotation rate was increased.

The decreases in the heat transfer ratio are attributed to the cross-stream flow patterns as well as the stabilization of the near-wall flow on the leading side of the passage, e.g. Johnston et al. (1972). The cross-stream flows cause heated, near-wall fluid from the trailing and sidewall surfaces to accumulate near the leading side of the coolant passage resulting in reduced heat transfer. In addition, as described by Rothe and Johnston (1979), it can be expected that flow reattachment after trips on low pressure surfaces occurs at larger distances from the trips with increasing rotation number. Longer reattachment lengths, due to the stabilizing effects, will decrease the effective heat transfer area between trips, thereby, further reducing the turbulent transport of heat. The increase in the heat transfer ratio in the latter half of the coolant passage for the larger rotation numbers is attributed to buoyancy effects, possibly caused by buoyancy enhanced flow in the recirculation cells downstream of the trips. These effects of rotation are noted for the low pressure surfaces in both the first and second passages, with flow radially outward and radially inward, respectively. These results suggest that the decrease in heat transfer on low pressure surfaces with trips is dominated by Coriolis generated cross-stream flows which cause a stabilization of the near-wall flows and that the heat transfer on the high pressure surfaces is affected by a combination of Coriolis and buoyant effects. Therefore,

it can be expected that the correlations of local heat transfer data may be substantially different, depending on local flow conditions (i.e. due to differing near-wall shear gradients).

The effects of rotation on the heat transfer in the model with normal trips were significant in several locations. The decreases in heat transfer on the low pressure surfaces of the first (leading surface) and second (trailing surface) passages are approximately 50 percent of the stationary values. The decreases in the heat transfer on the side walls and on the trailing surfaces of the second turns (root location) are similar (40 to 60 percent). The increase in heat transfer coefficient on the trailing surface of the first passage is significant: from 2.5 times Nu_{∞} (stationary) to 4.0 times Nu_{∞} ($Ro = 0.35$). Note that smaller increases occurred due to rotation on the leading surface of the second passage and the trailing surface of the third passage. The small effects of rotation on the leading surface of the second passage were attributed to changes in the turbulent transport for the smooth wall model. The smaller increases in the trailing surface of third passage are attributed to unknown interactions through the second turn.

Skewed Trips

The effects of rotation on the heat transfer in the model with skewed trip strips shown in Figure 6.6 were similar in most respects to the effects from the model with normal trips. The differences are discussed in the following paragraphs.

The heat transfer on the first test surface (streamwise location G) of the leading surface downstream of the first turn was consistently higher than at other locations. This increase was attributed to the vorticity distribution downstream of the turn which was a result of the secondary flow caused by the skewed trips in the first passage. This particular effect was not measured for the models with smooth walls or normal trips (see Figure 5.3).

The heat transfer on the trailing surface of the second passage and on the leading surface of the third passage was less sensitive to rotation than the same surfaces with normal trips. The decreased sensitivity is attributed to the secondary flow patterns caused by the skewed trips. These differences will be discussed again when the full set of data is presented.

Streamwise Location

With trips, the heat transfer does not usually vary appreciably with streamwise location. The large decrease in heat transfer with increasing distance from the inlet measured in the model with smooth walls does occur with the trips. The exception occurs for flow downstream of turns with the skewed trips where the upstream vorticity has been convected to one side of the model and the flow readjusts in the new passage. The effects of flow direction were generally the same for the models with trips as for the models with smooth walls. The largest effects of flow direction occurred on the high pressure side of the coolant passage. For flow outward, a modest increase in heat transfer ratio occurred for the trailing surface. For flow inward, the heat transfer on the leading surface was essentially independent of rotation number and density ratio.

6.3 Effect of Density Ratio

The inlet density ratio, $(\Delta\rho/\rho)_{in}$, was varied from 0.07 to 0.23 for this series of flow conditions shown in Figures 6.7 and 6.8. The Reynolds number, rotation number and radius ratio were held constant at the baseline values of 25,000, 0.24 and 49, respectively. Heat transfer was obtained at a fixed rotation number and, therefore, conclusions can be

$\bar{R}/d = 49$
 $\alpha = 0$

$Re = 25,000$
 $R_o = 0.24$

HP - High Pressure
 LP - Low Pressure

Symbol	□	○	△
$(\Delta\rho/\rho)_i$	0.07	0.13	0.23
Test No.	312	307	313

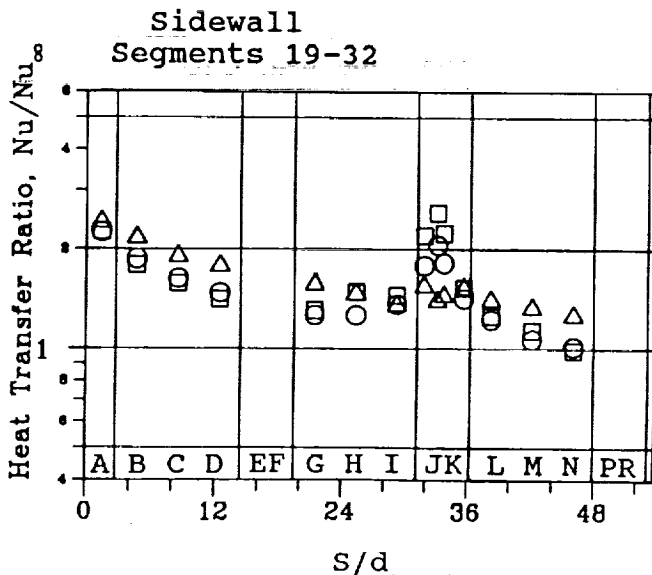
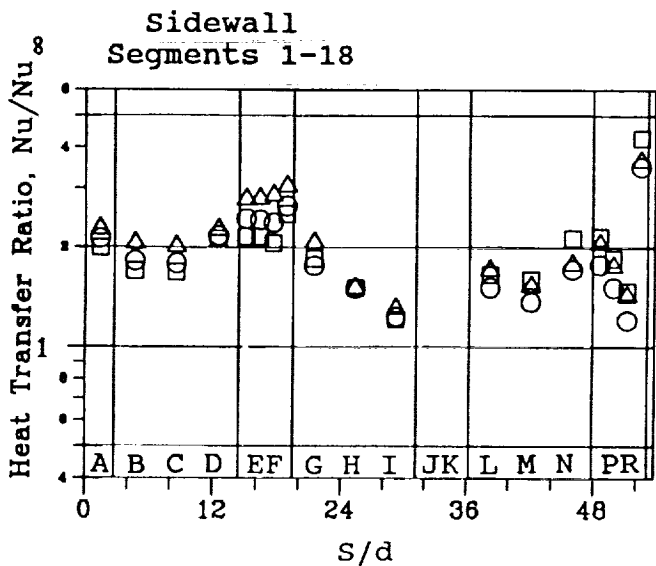
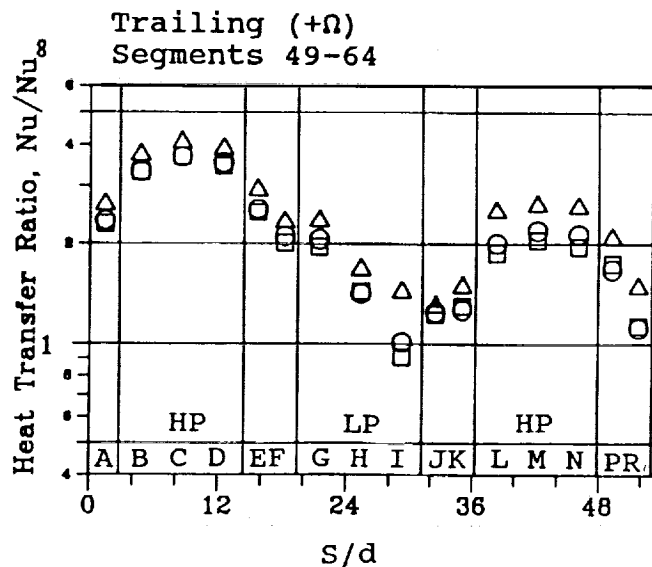
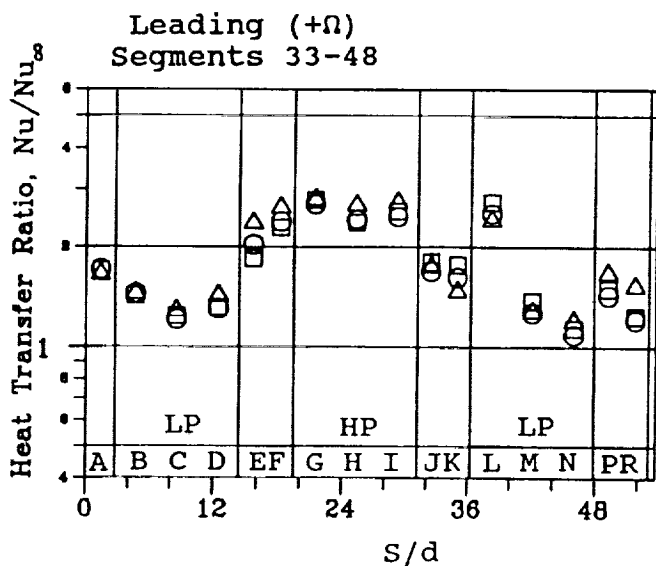


Figure 6.7- Effect of Density Ratio on Heat Transfer Ratio for Normal Trips.

$\overline{R}/d = 49$
 $\alpha = 0$

$Re = 25,000$
 $R_o = 0.24$

HP - High Pressure
 LP - Low Pressure

Symbol	○	□	△	◇
$(\Delta\rho/\rho)_{in}$	0.07	0.12	0.13	0.23
Test No.	220	209	221	222

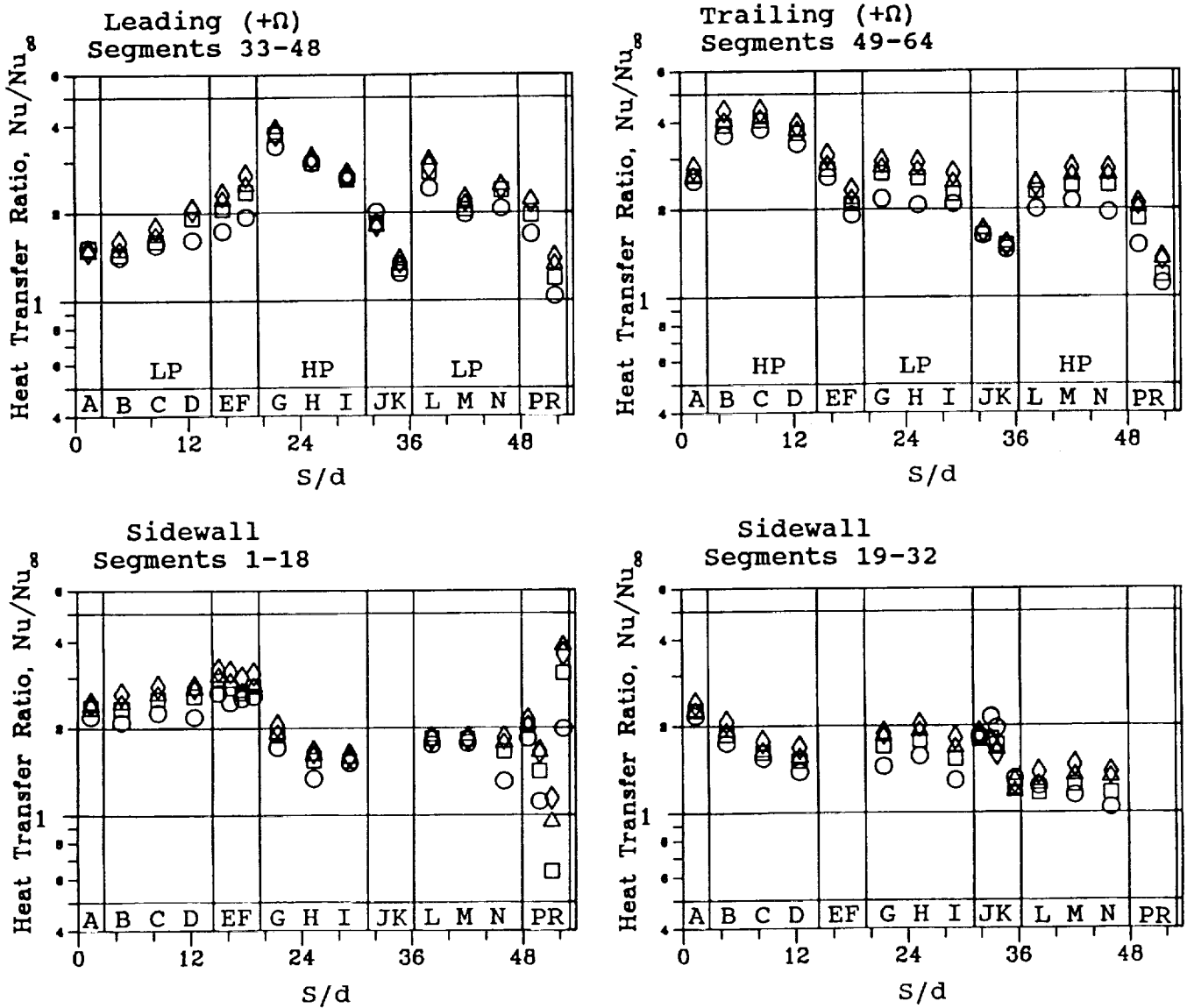


Figure 6.8- Effect of Density Ratio on Heat Transfer Ratio for Skewed Trips.

obtained regarding the effects of buoyancy for flow conditions near the rotating baseline flow conditions.

Increasing the inlet density ratio (i.e., the wall-to-coolant temperature difference) from 0.07 to 0.23 causes the heat transfer ratio in the first passage of the model with normal trips to increase on all trailing surfaces by as much as 25 percent and on the leading surfaces by as much as 15 percent. The exception to the general increase in heat transfer with increasing density ratio occurred near the inlet of the first passage on the leading side, where the heat transfer ratio is observed to be relatively unaffected by varying density ratio. Heat transfer in the second, inward flowing passage on the low pressure side increased as much as 70 percent with increases in the temperature difference (Figure 6.7). (Larger effects of density ratio were obtained for a rotation number of 0.35.)

The effect of inlet density ratio on the streamwise distribution of heat transfer ratio for the model with skewed trips and at the other baseline flow conditions is shown in Figure 6.8. The effects of density ratio on the leading and trailing surfaces are somewhat larger for the model with skewed trips than were measured for the model with normal trips for $R_o = 0.24$.

6.4 Effects of Model Orientation

Heat transfer experiments were conducted with the plane of the coolant passages rotated 45 degrees to the axis of rotation ($\alpha = 45$ deg) for the model with skewed trips. See Figure 3.7 for the model orientation. The scope of the program did not permit experiments with the coolant passages rotated in the same orientation for the model with normal trips.

The effect of model orientation on the streamwise distribution of heat transfer ratio for the four surfaces is presented in Figure 6.9. The heat transfer ratios for the Rotating Baseline Flow Conditions are presented for $\alpha = 0$ and 45 degrees. In the first coolant passage, orientation of the model from $\alpha = 0$ to $\alpha = 45$ degrees caused the heat transfer ratio to decrease on both side walls and the trailing side and to increase or remain the same on the leading side. In the second passage, small decreases in the heat transfer ratio occurred on all four sides of the coolant passage. The conclusion from this presentation is that the heat transfer ratios can increase or decrease 20 to 30 percent with the coolant passage orientation up to 45 degrees from the $\alpha = 0$ orientation.

$\bar{R}/d = 49$
 $Re = 25,000$
 $R_o = 0.23$

$\Delta T \approx 44^\circ C (80^\circ F)$
 $(\Delta T/T)_{in} = 0.13$

HP - High Pressure
 LP - Low Pressure

Symbol	○	□
α	0 deg	45 deg
Test No.	209	226

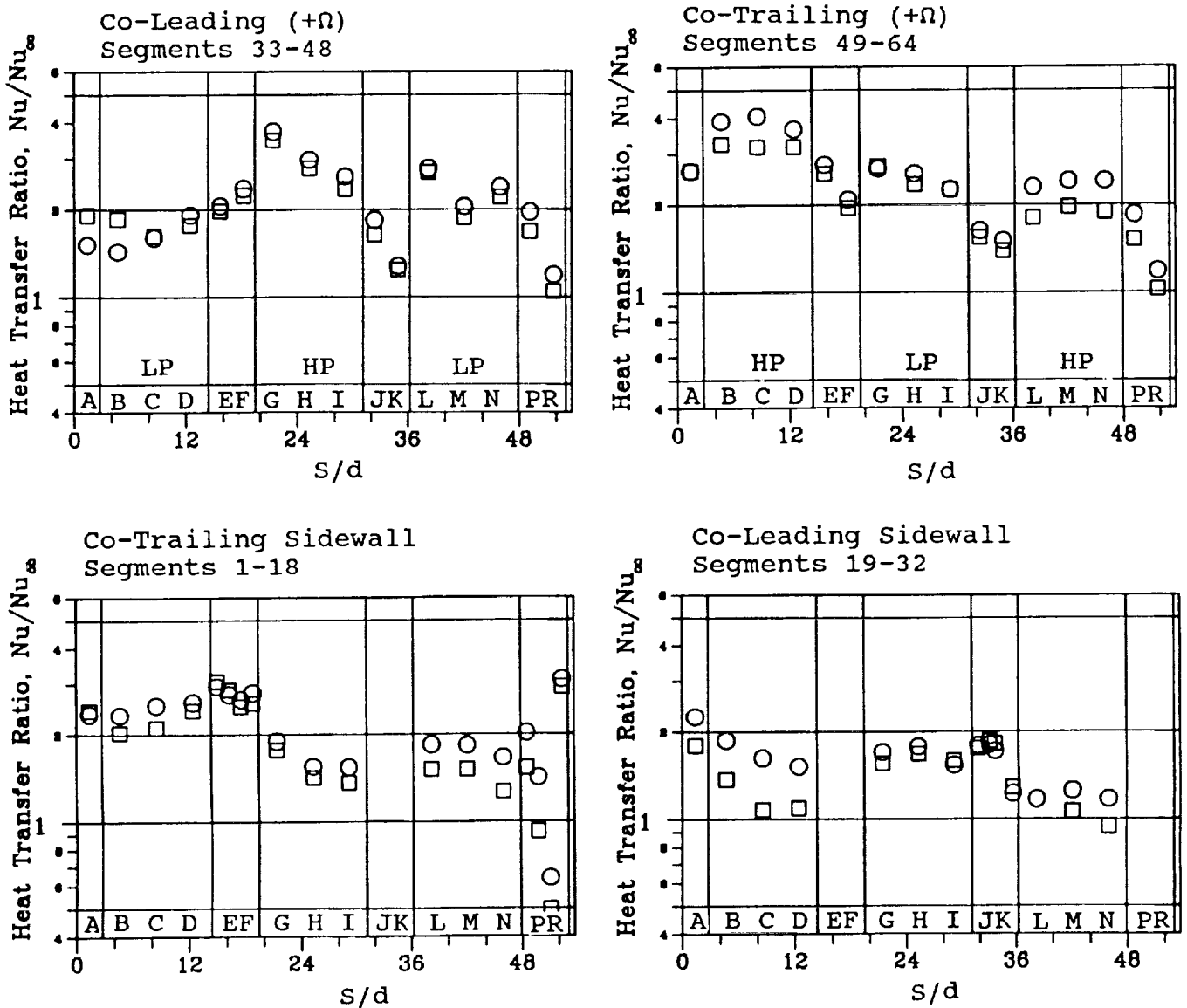


Figure 6.9- Effect of Model Orientation (Alpha) on Heat Transfer Ratio for Skewed Trips.

7.0 HEAT TRANSFER RESULTS FOR LEADING AND TRAILING SURFACES

The heat transfer relationships in the models with normal and skewed trips are complex. The spatial variations in the heat transfer ratio caused by the variation of the individual flow parameters about the Rotating Baseline Flow Condition were discerned in Section 6. In this section, the heat transfer ratios will be presented for specific locations on the leading and trailing surfaces in the three passages. The heat transfer ratios will be presented as

- 1) the variation of local rotation number for each inlet density ratio,
- 2) the variation with local density ratio for each rotation rate, and
- 3) the variation with the buoyancy parameter (identifying results from each rotation rate).

The results from the model with smooth walls are also presented for comparison. With these three presentations, the similarities and differences of the heat transfer characteristics from the three models with normal and skewed trips and with smooth walls can be identified and discussed. This presentation also serves as a data base for thermal design of radial rotating coolant passages.

7.1 Variation with Rotation Number

The heat transfer ratios for the leading and trailing surfaces in the three straight passages are presented in Figures 7.1, 7.2 and 7.3. The test surface identification number (Fig. 3.6), the streamwise location (Fig. 3.1) and the X/d ratio from the start of each straight section are also shown on each panel of the figure.

High Pressure Surfaces. The trailing surfaces of the first and third passages and the leading surface of the second passage are denoted as the high pressure surfaces (Figures 7.1, 7.2, and 7.3). In the first and third passages of both models with trips, the heat transfer coefficients increase with increasing rotation number at approximately half the slope as the model with smooth walls. In the first two passages, the heat transfer from the models with trips is essentially independent of inlet density for $Ro \leq 0.24$. The uncertainty in the heat transfer measurements in the third channel increases due to small bulk to wall temperature differences for the low inlet density ratios. However, the results for the third passages with trips show characteristics similar to those for the third passage with smooth walls. Increasing the rotation number caused the trip strip model's heat transfer ratios to increase up to 75 percent over the non-rotating condition.

Low Pressure Surfaces. The heat transfer behavior for the low pressure surfaces is more complex than for the high pressure surfaces. The heat transfer ratio in the first passage with both the normal and skewed trips decreases with increasing rotation number for low values of the rotation number, i.e. $\Omega d/V < 0.25$ and then increases with increases in rotation for larger values of rotation number depending on density ratio. The heat transfer ratio increases with increases in the density ratio, similar to the results obtained for the trailing surface of the first passage.

The effects of varying inlet density ratio (from 0.07 to 0.23) on the heat transfer ratio are larger in the second passage with normal trips radially inward flow than in first passage (a factor of three for the second passage compared to a factor less than two for the first passage). Note that the local density ratios in the second passage are about half of the inlet values as will be shown in Figure 7.5a. For the model with skewed trips, the decrease

in the heat transfer ratio with increasing rotation number is less than for the models with normal trips or smooth walls.

The heat transfer characteristics of the third passage are more similar to those of the second passage than those of the first passage for each model. The model with skewed trips showed less decrease in heat transfer with increasing rotation than the model with normal trips.

The more complicated heat transfer distributions on the low pressure surfaces of the coolant passages are attributed to 1) the combination of buoyancy forces and the stabilization of the near-wall flow for low values of the rotation number, 2) the developing, Coriolis driven secondary flow cells and 3), the increases in flow reattachment lengths after trips for the larger values of the rotation number. It is postulated that the relatively small effects from variations in density ratio near the inlet of the second passage and the large effects near the end of the second passage are due to the development of the near-wall thermal layers (i.e. thickening for the normal trip model compared to thinning for the smooth wall model). Near the inlet of the second passage, the thermal layers are postulated to be thin because of the strong secondary flows in the first turn region. With increasing X/d , the turn dominated secondary flows diminish and the counteracting effect of buoyancy and the Coriolis generated secondary flow increases.

The heat transfer in the model with skewed trips was less sensitive to rotation in the second and third passages than in the model with normal trips. This decrease in sensitivity was attributed to the additional secondary flow induced by the skewed trips and the interactions with the secondary flows induced by the Coriolis forces.

The rotation number correlates the heat transfer ratios for models with trips better and for more surface locations and flow conditions than it did for the model with smooth walls. The percent decrease in heat transfer ratio from the stationary value on the low pressure side of the first coolant passage is well correlated by the rotation number for $Ro \leq 0.24$ and was independent of the three wall surface geometries.

7.2 Variation with Density Ratio

This presentation uses the local density ratio rather than the inlet density ratio used for test identification purposes. Note that for the models with the normal and skewed trips, the largest value of density ratio in the third passage is only one half the value with the smooth walls. This presentation also permits an extrapolation of the results to a density ratio of zero and therefore allows comparison (a) with the results from analytical predictions with constant density models, and (b) with the results from naphthalene experiments using a mass transfer/heat transfer analogy.

In the first passage (Figure 7.4), the variation of heat transfer ratio with density ratio is greater for the models with normal than with skewed trips. The slope of the variation for the model with normal trips is approximately the same as obtained for results from the model with smooth walls. Note that the heat transfer ratio does not vary with density ratio for $Ro = 0.05$ or 0.12 and does not become appreciable until $Ro = 0.35$. The variation of heat transfer ratio with density ratio is always expected to be zero for $Ro = 0$ when the film properties are used to evaluate the Reynolds and the Nusselt numbers. Note also that the largest variation of heat transfer ratio with density ratio occurs for test section 36 (leading surface, $X/d = 12.4$) for both the normal and skewed trips. Note that these larger variations with density ratio occurred at $Ro = 0.24$ for the model with smooth walls. The conclusion is that, for the first passage, the trips cause turbulence and/or secondary flows which diminish the buoyancy effects in this region. Note also that there is less effect of

Symbol	○	◇	☆	△	∅	□	▵
Rotation No.	0.00	0.006	0.05	0.12	0.18	0.25	0.35

Symbol Flag	$\Delta T_{in}/\Delta T_{out}$ (σ_F)
○	22.4 (40)
○	44.4 (80)
○	66.7 (120)
○	88.9 (160)

Re = 25,000 $\alpha = 0$ $\bar{R}/d = 49$

Normal Trips - open symbols LP - Low Pressure
 Smooth Wall - solid symbols HP - High Pressure

----- Estimate for $\Delta T \rightarrow 0$

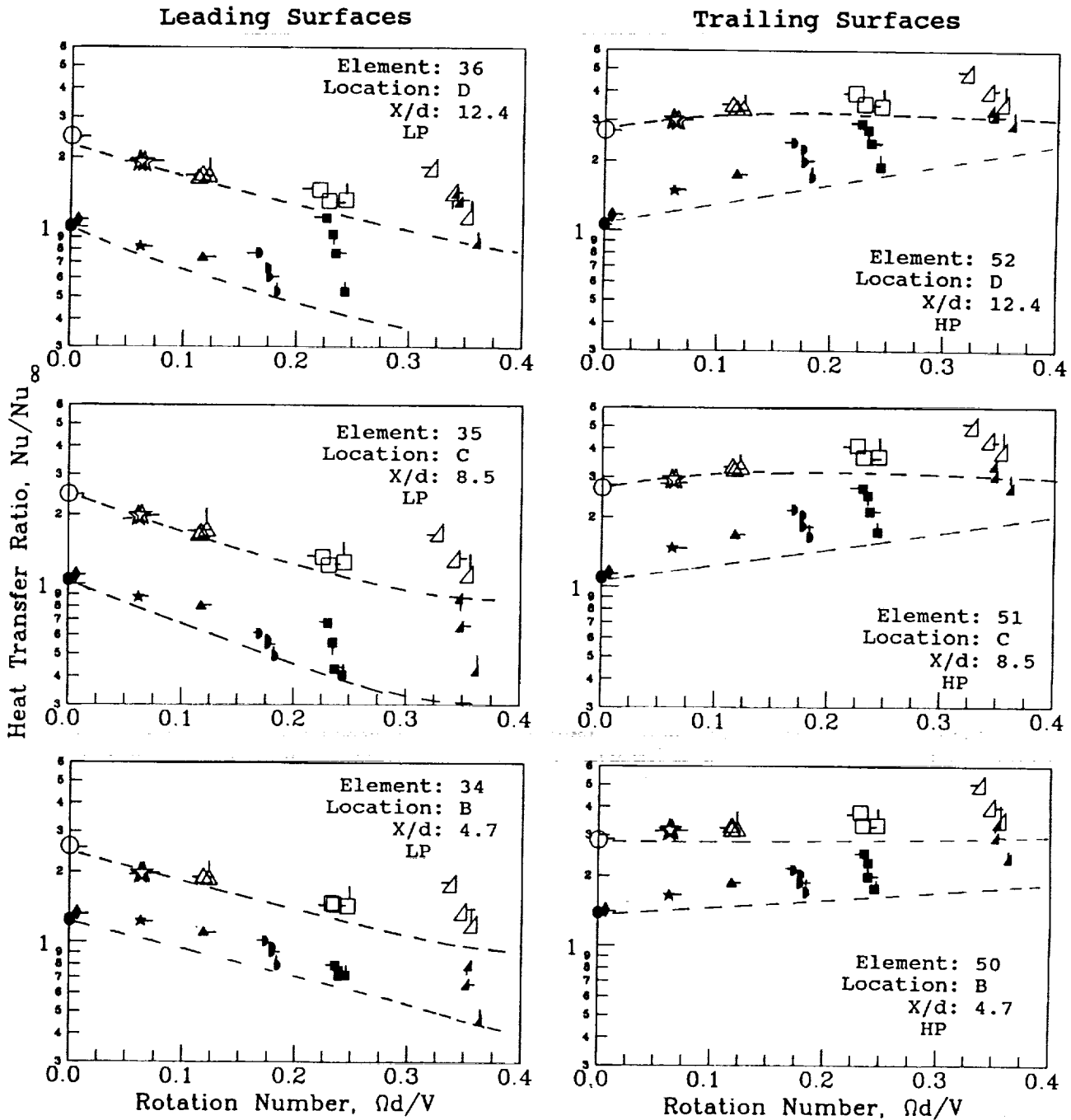


Figure 7.1a- Effect of Rotation Number on Heat Transfer Ratios in the First Passage.

Symbol	○	◇	☆	△	D	□	△
Rotation No.	0.00	0.006	0.05	0.12	0.18	0.25	0.35

Symbol Flag	$\Delta T_{in, C} (^\circ F)$
○	22.4 (40)
◇	44.4 (80)
☆	66.7 (120)
△	88.9 (160)

Re = 25,000

$\alpha = 0$

$\bar{R}/d = 49$

Skewed Trips - open symbols
Smooth Wall - solid symbols

LP - Low Pressure
HP - High Pressure

----- Estimate for $\Delta T \rightarrow 0$

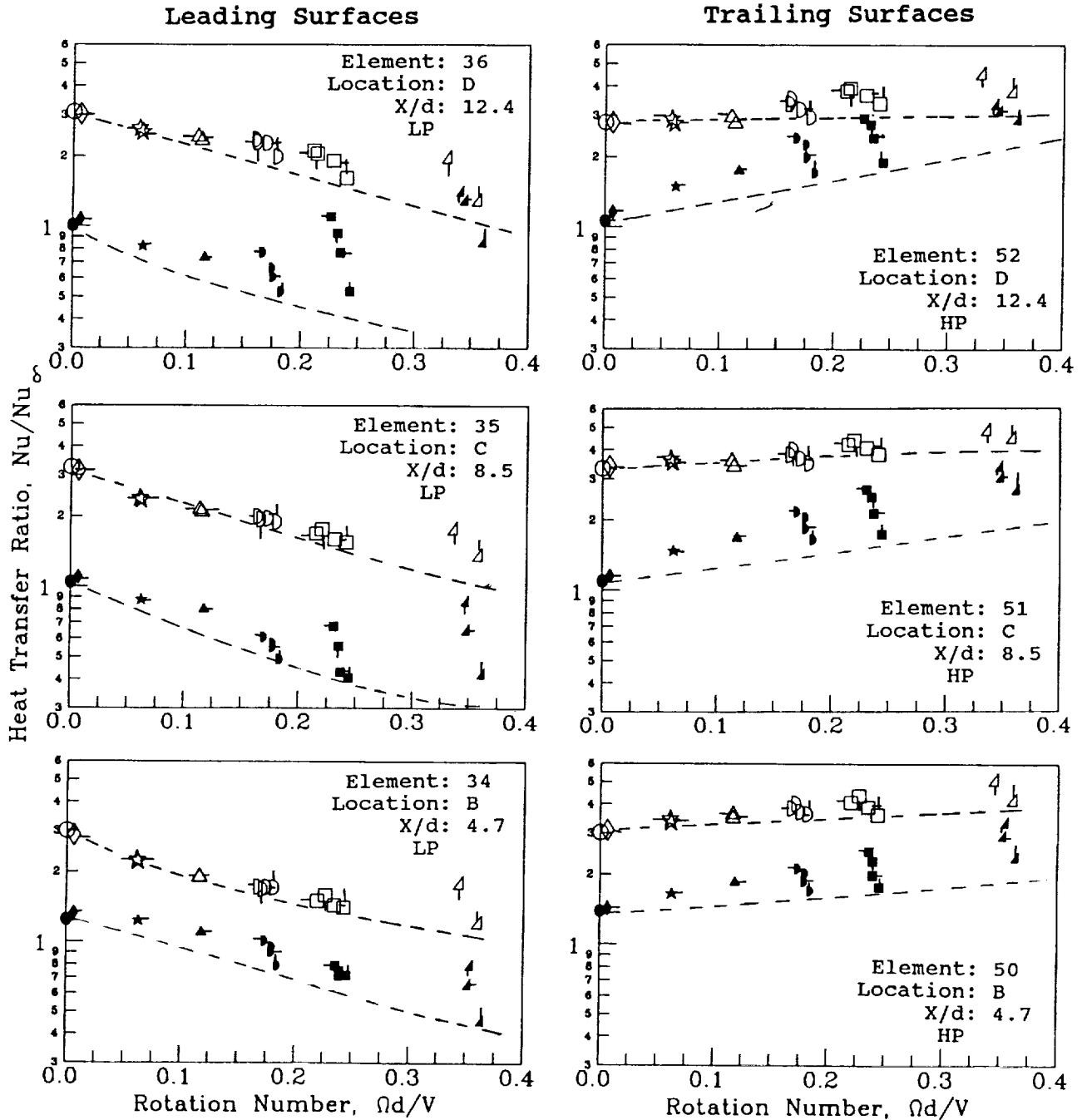


Figure 7.1b- Effect of Rotation Number on Heat Transfer Ratios in the First Passage.

Symbol	○	◇	☆	△	D	□	△
Rotation No.	0.00	0.006	0.05	0.12	0.18	0.25	0.35

Symbol Flag	ΔT_{in} °C (°F)
○	22.4 (40)
○	44.4 (80)
○	66.7 (120)
○	88.9 (160)

Re = 25,000

$\alpha = 0$

$\bar{R}/d = 49$

Normal Trips - open symbols
Smooth Wall - solid symbols

LP - Low Pressure
HP - High Pressure

----- Estimate for $\Delta T \rightarrow 0$

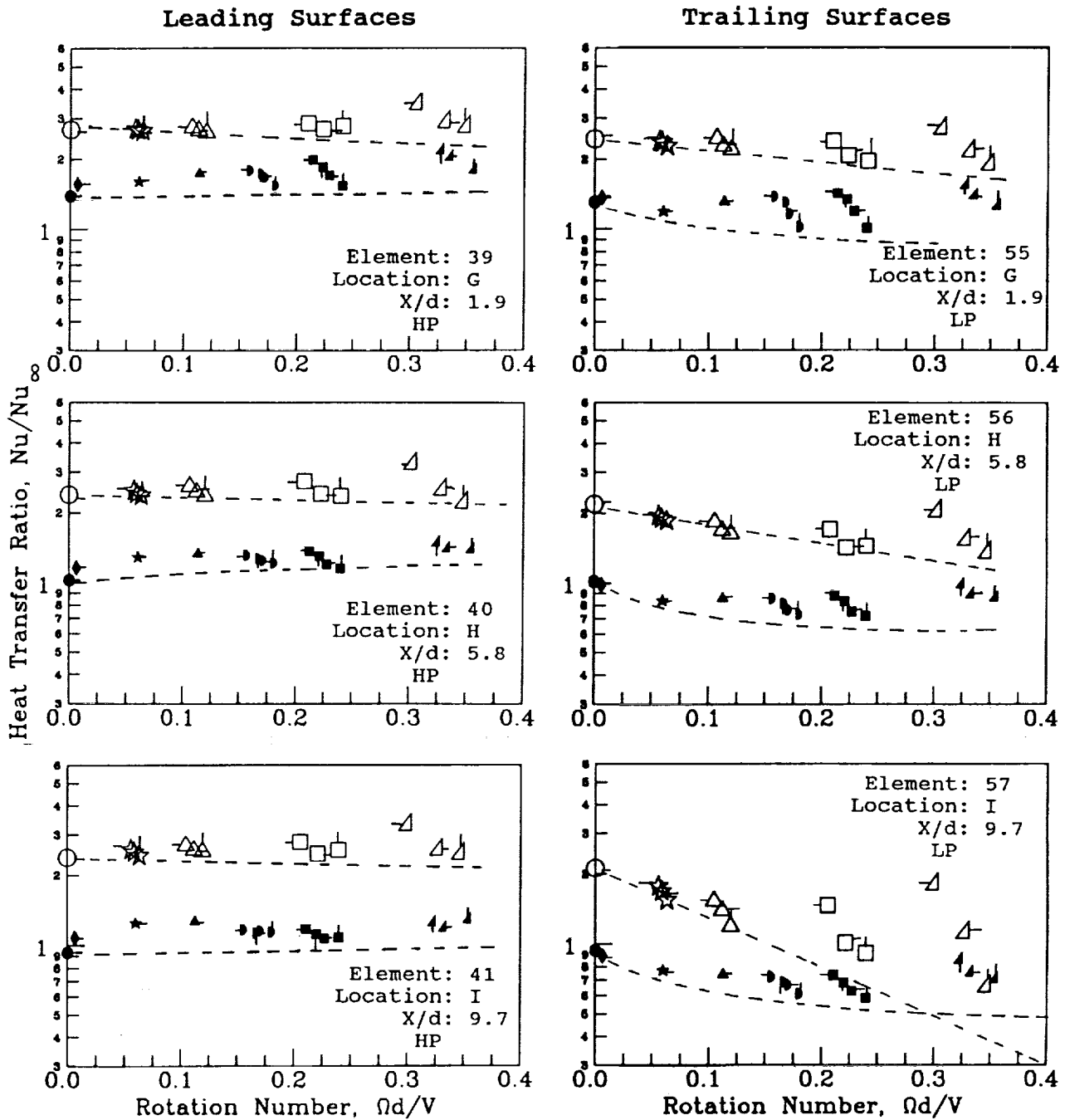


Figure 7.2a- Effect of Rotation Number on Heat Transfer Ratios in the Second Passage.

Symbol	○	◇	☆	△	D	□	△
Rotation No.	0.00	0.006	0.05	0.12	0.18	0.25	0.35

Symbol Flag	ΔT_{in} °C (°F)
○	22.4 (40)
○	44.4 (80)
○	66.7 (120)
○	88.9 (160)

Re = 25,000

$\alpha = 0$

$\bar{R}/d = 49$

Skewed Trips - open symbols
Smooth Wall - solid symbols

LP - Low Pressure
HP - High Pressure

----- Estimate for $\Delta T \rightarrow 0$

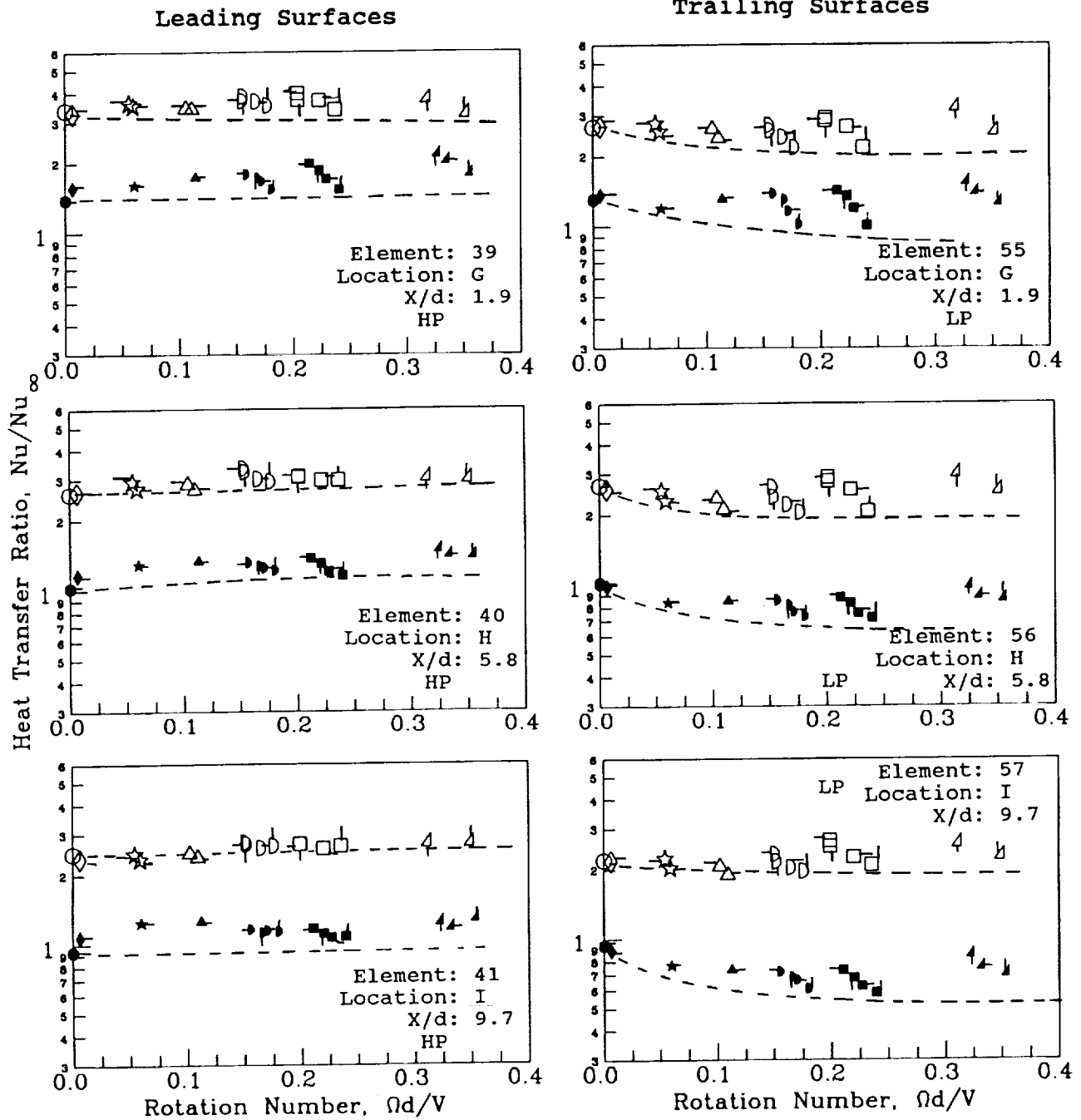


Figure 7.2b- Effect of Rotation Number on Heat Transfer Ratios in the Second Passage.

Symbol	○	◇	☆	△	∩	□	△
Rotation No.	0.00	0.006	0.05	0.12	0.18	0.25	0.35

Symbol Flag	$\Delta T_{in,OC}$ (°F)
○	22.4 (40)
○	44.4 (80)
○	66.7 (120)
○	88.9 (160)

Re = 25,000

$\alpha = 0$

$\bar{R}/d = 49$

Normal Trips - open symbols
Smooth Wall - solid symbols

LP - Low Pressure
HP - High Pressure

----- Estimate for $\Delta T \rightarrow 0$

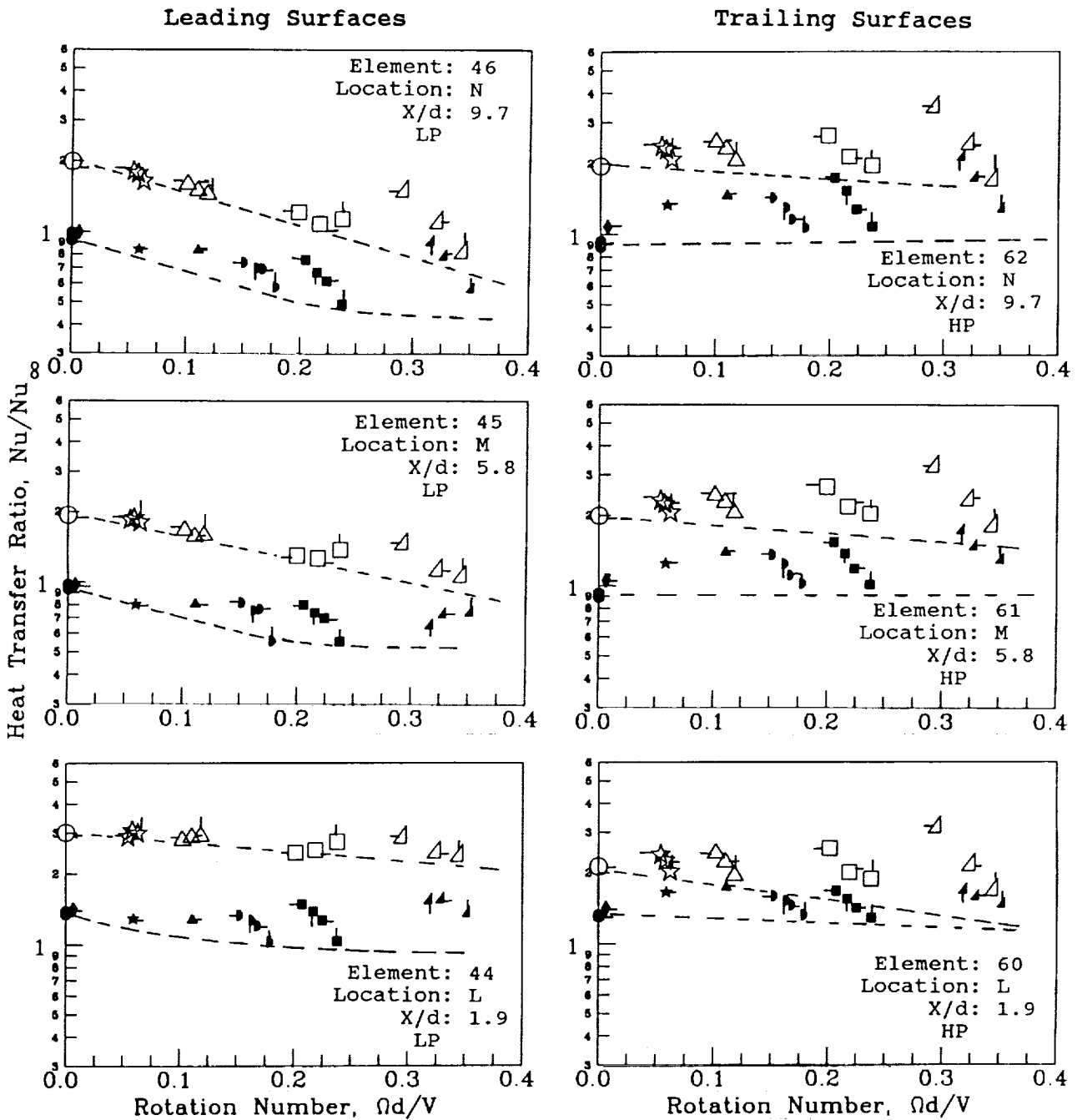


Figure 7.3a- Effect of Rotation Number on Heat Transfer Ratios in the Third Passage.

Symbol	○	◇	☆	△	D	□	△
Rotation No.	0.00	0.006	0.05	0.12	0.18	0.25	0.35

Symbol Flag	$\Delta T_{in} / \Delta T_{out} (^\circ F)$
○	22.4 (40)
○	44.4 (80)
○	66.7 (120)
○	88.9 (160)

Re = 25,000

$\alpha = 0$

$\bar{R}/d = 49$

Skewed Trips - open symbols
Smooth Wall - solid symbols

LP - Low Pressure
HP - High Pressure

----- Estimate for $\Delta T \rightarrow 0$

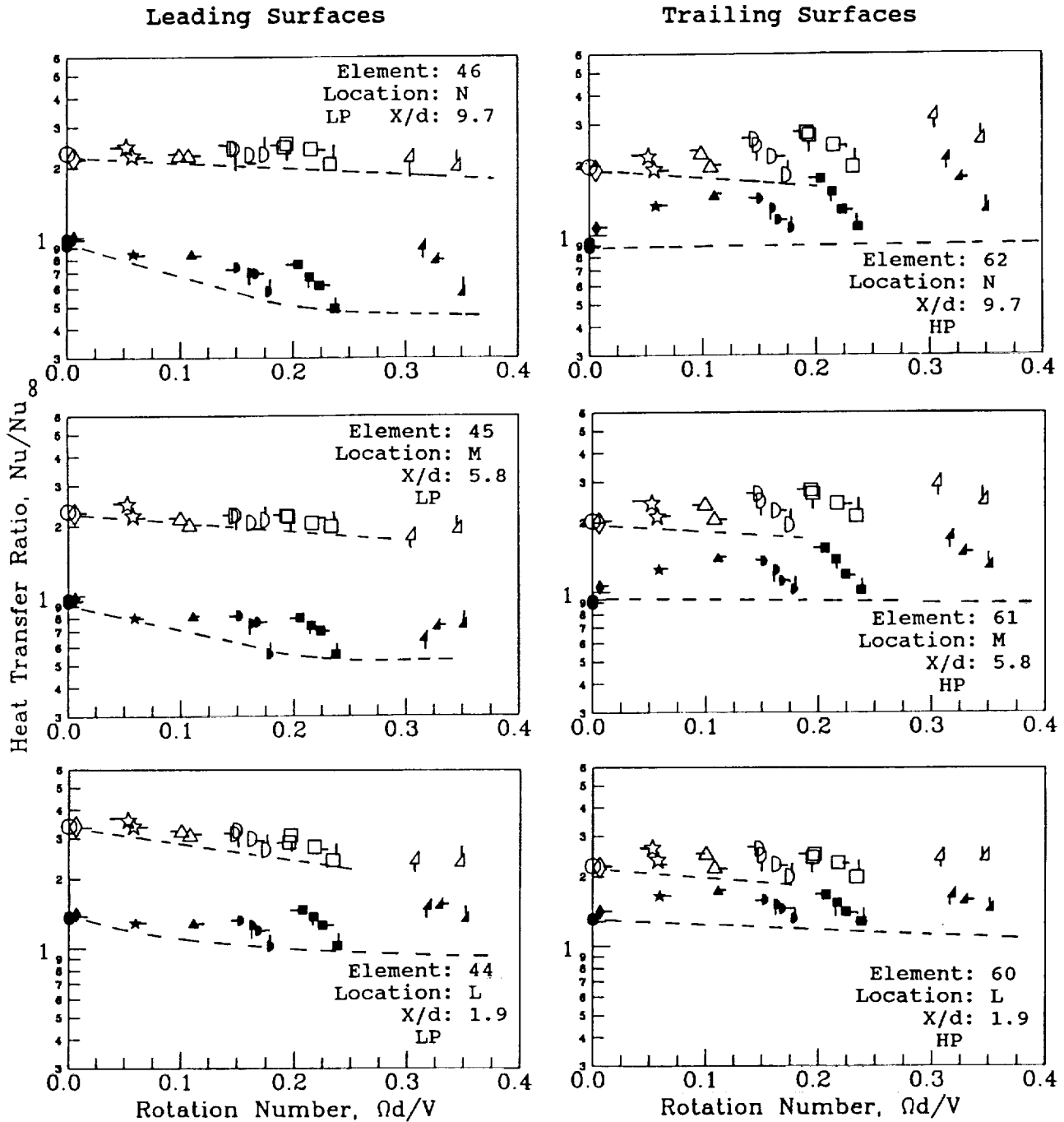


Figure 7.3b- Effect of Rotation Number on Heat Transfer Ratios in the Third Passage.

Symbol	○	◇	☆	△	D	□	△
Rotation No.	0.00	0.006	0.05	0.12	0.18	0.25	0.35

Symbol Flag	$\Delta T_{in}/\Delta T_{oc}$ ($^{\circ}F$)
○	22.4 (40)
○	44.4 (80)
○	66.7 (120)
○	88.9 (160)

Re = 25,000 $\alpha = 0$ $\bar{R}/d = 49$

Normal Trips - open symbols LP - Low Pressure
Smooth Wall - solid symbols HP - High Pressure

----- Estimate for $\Delta T \rightarrow 0$

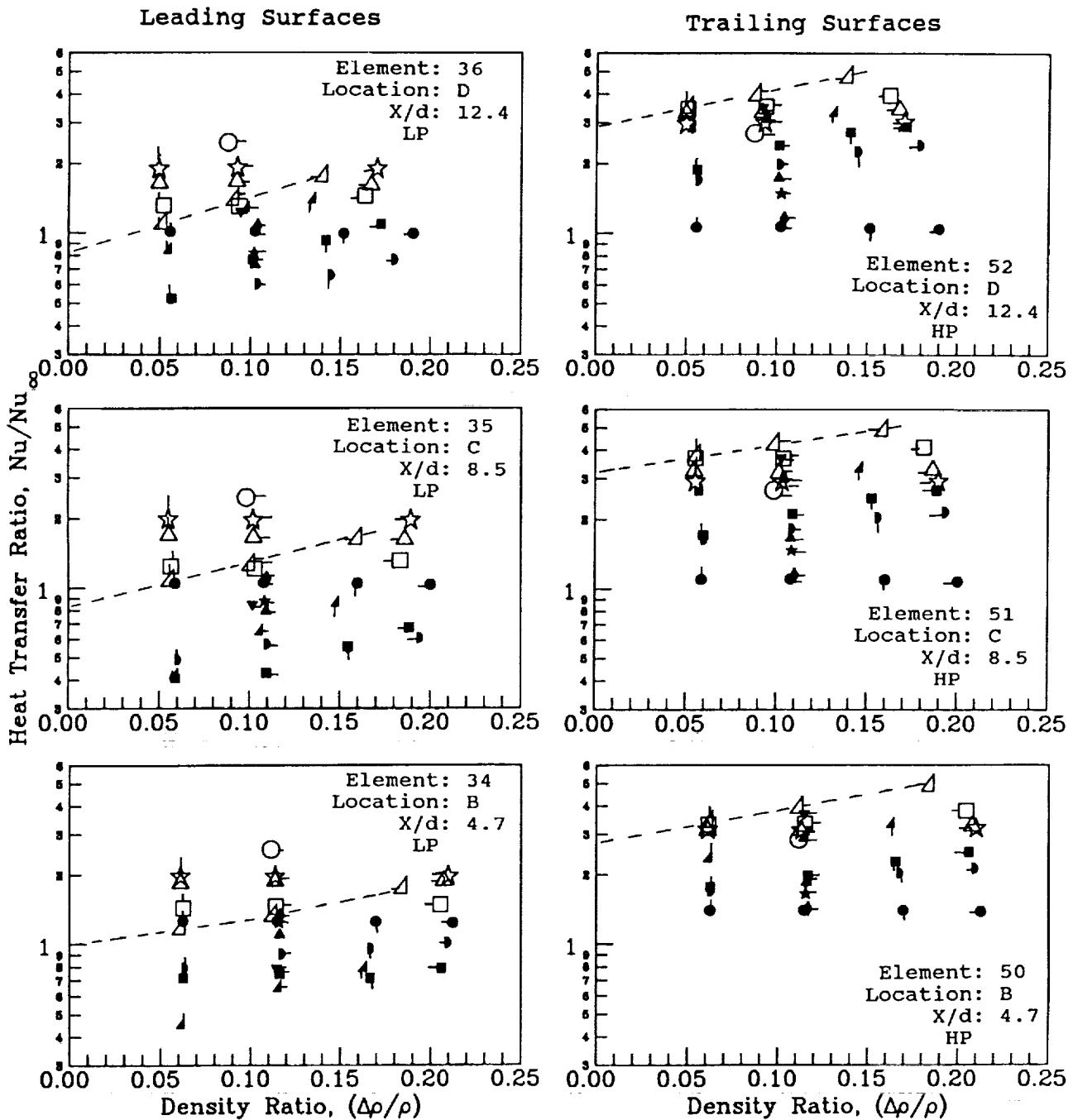


Figure 7.4a- Effect of Density Ratio on Heat Transfer Ratios in the First Passage.

Symbol	○	◇	☆	△	D	□	△
Rotation No.	0.00	0.006	0.05	0.12	0.18	0.25	0.35

Symbol Flag	$\Delta T_{in, C} / (T_{in, OF})$
○	22.4 (40)
○	44.4 (80)
○	66.7 (120)
○	88.9 (160)

Re = 25,000 $\alpha = 0$ $\bar{R}/d = 49$

Skewed Trips - open symbols LP - Low Pressure
Smooth Wall - solid symbols HP - High Pressure

----- Estimate for $\Delta T \rightarrow 0$

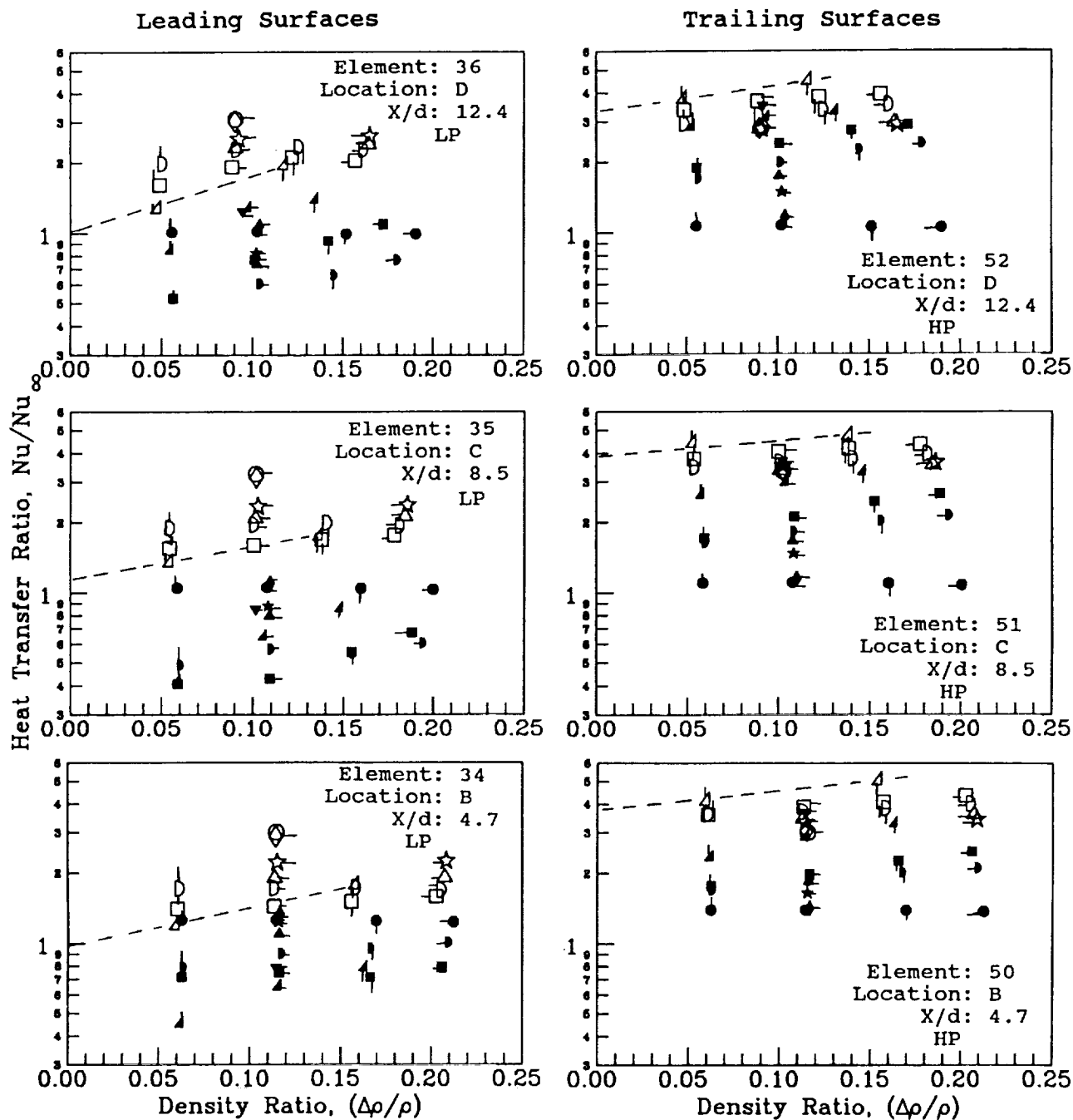


Figure 7.4b- Effect of Density Ratio on Heat Transfer Ratios in the First Passage.

Symbol	○	◇	☆	△	D	□	▴
Rotation No.	0.00	0.006	0.05	0.12	0.18	0.25	0.35

Symbol Flag	$\Delta T_{in} / \Delta T_{out} (^\circ F)$
○	22.4 (40)
○	44.4 (80)
○	66.7 (120)
○	88.9 (160)

Re = 25,000 $\alpha = 0$ $\bar{R}/d = 49$

Normal Trips - open symbols LP - Low Pressure
Smooth Wall - solid symbols HP - High Pressure

----- Estimate for $\Delta T \rightarrow 0$

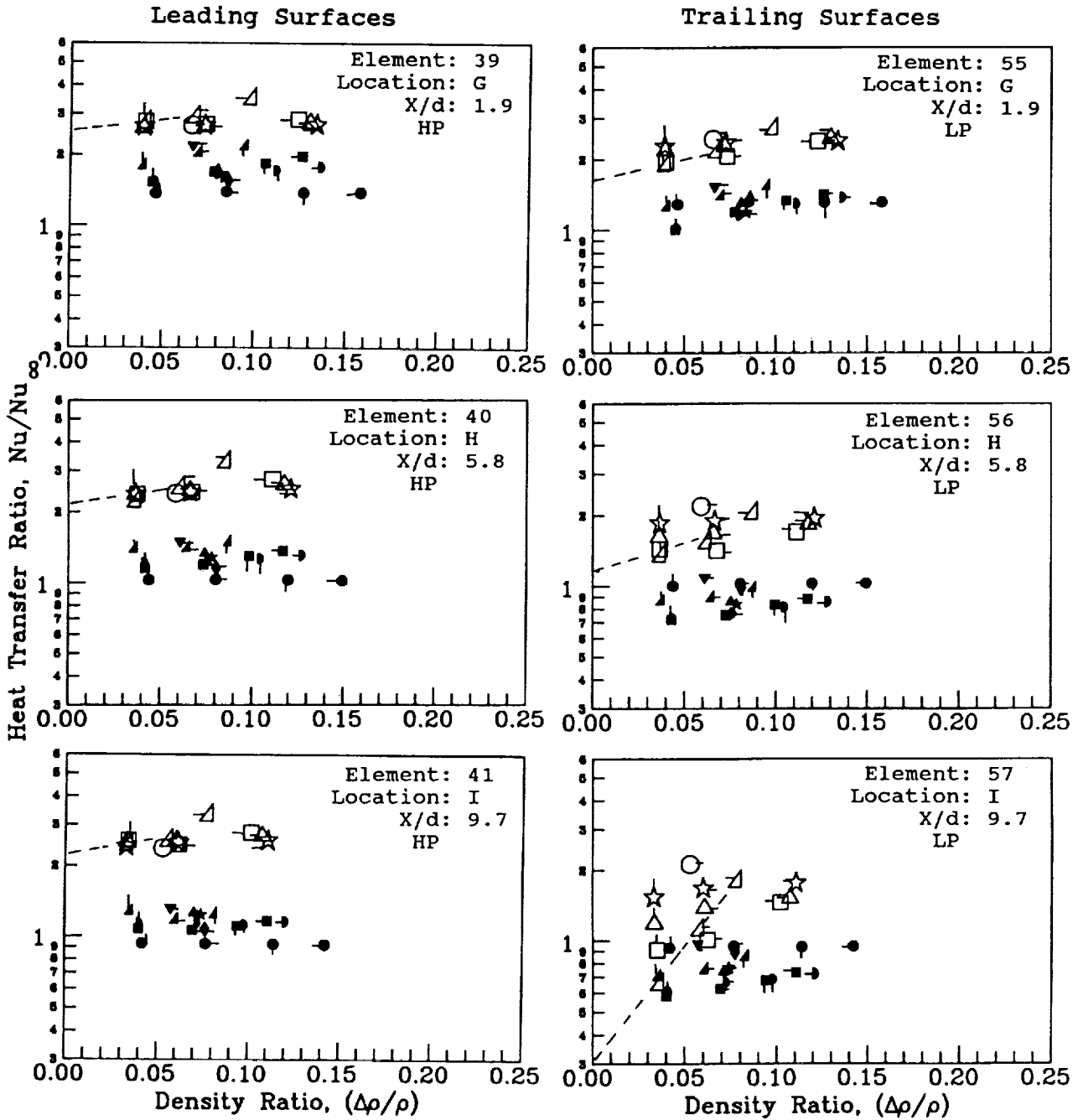


Figure 7.5a- Effect of Density Ratio on Heat Transfer Ratios in the Second Passage.

Symbol	○	◇	☆	△	D	□	△
Rotation No.	0.00	0.006	0.05	0.12	0.18	0.25	0.35

Symbol Flag	$\Delta T_{in}/\Delta T_{OC} (^{\circ}F)$
○	22.4 (40)
○	44.4 (80)
○	66.7 (120)
○	88.9 (160)

Re = 25,000

$\alpha = 0$

$R\bar{d} = 49$

Skewed Trips - open symbols
Smooth Wall - solid symbols

LP - Low Pressure
HP - High Pressure

----- Estimate for $\Delta T \rightarrow 0$

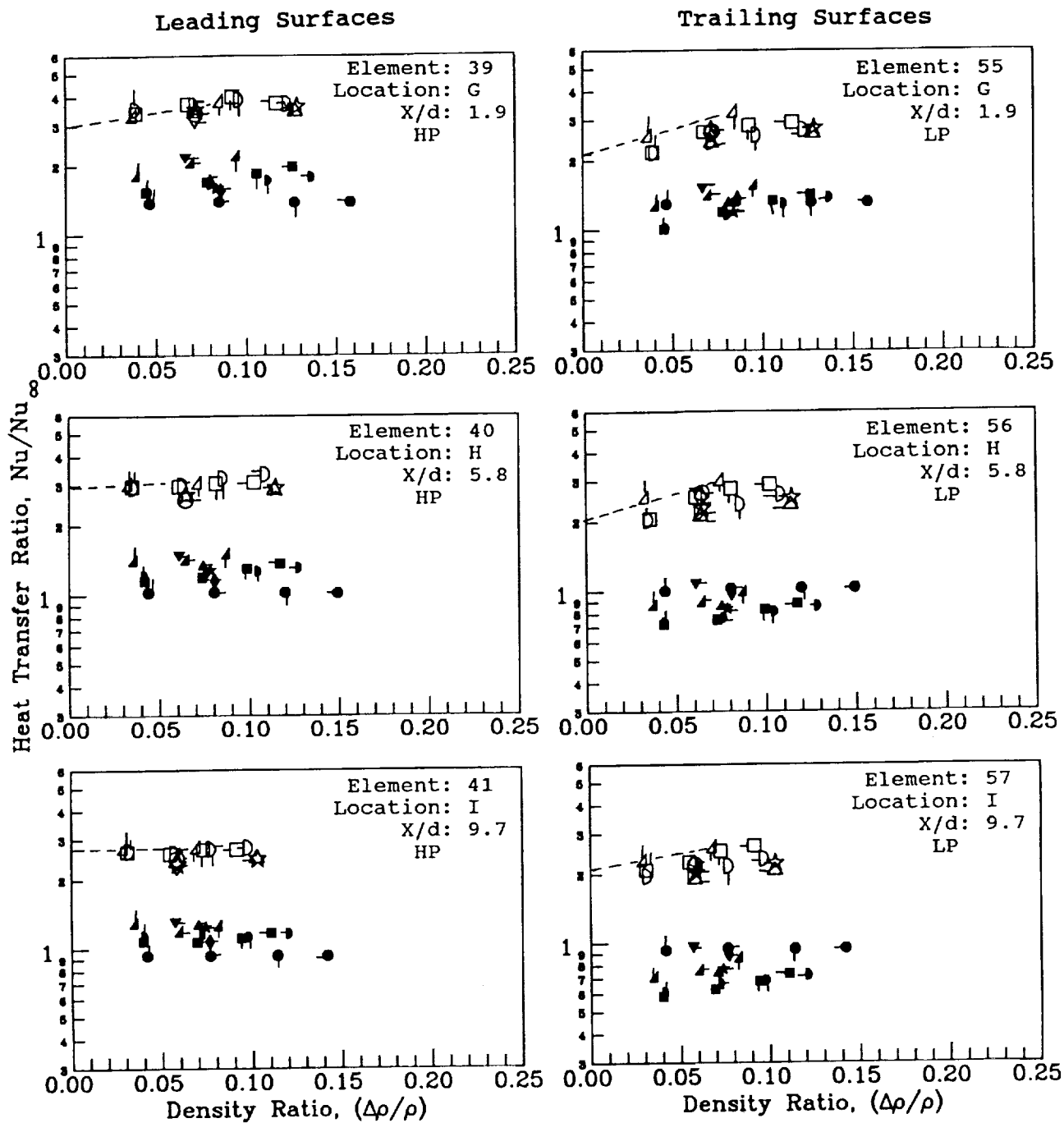


Figure 7.5b- Effect of Density Ratio on Heat Transfer Ratios in the Second Passage.

Symbol	○	◇	☆	△	∩	□	▵
Rotation No.	0.00	0.006	0.05	0.12	0.18	0.25	0.35

Symbol Flag	$\Delta T_{in} / \Delta T_{OC} (^{\circ}F)$
○	22.4 (40)
○	44.4 (80)
○	66.7 (120)
○	88.9 (160)

Re = 25,000 $\alpha = 0$ $\bar{R}/d = 49$

Normal Trips - open symbols LP - Low Pressure
Smooth Wall - solid symbols HP - High Pressure

----- Estimate for $\Delta T \rightarrow 0$

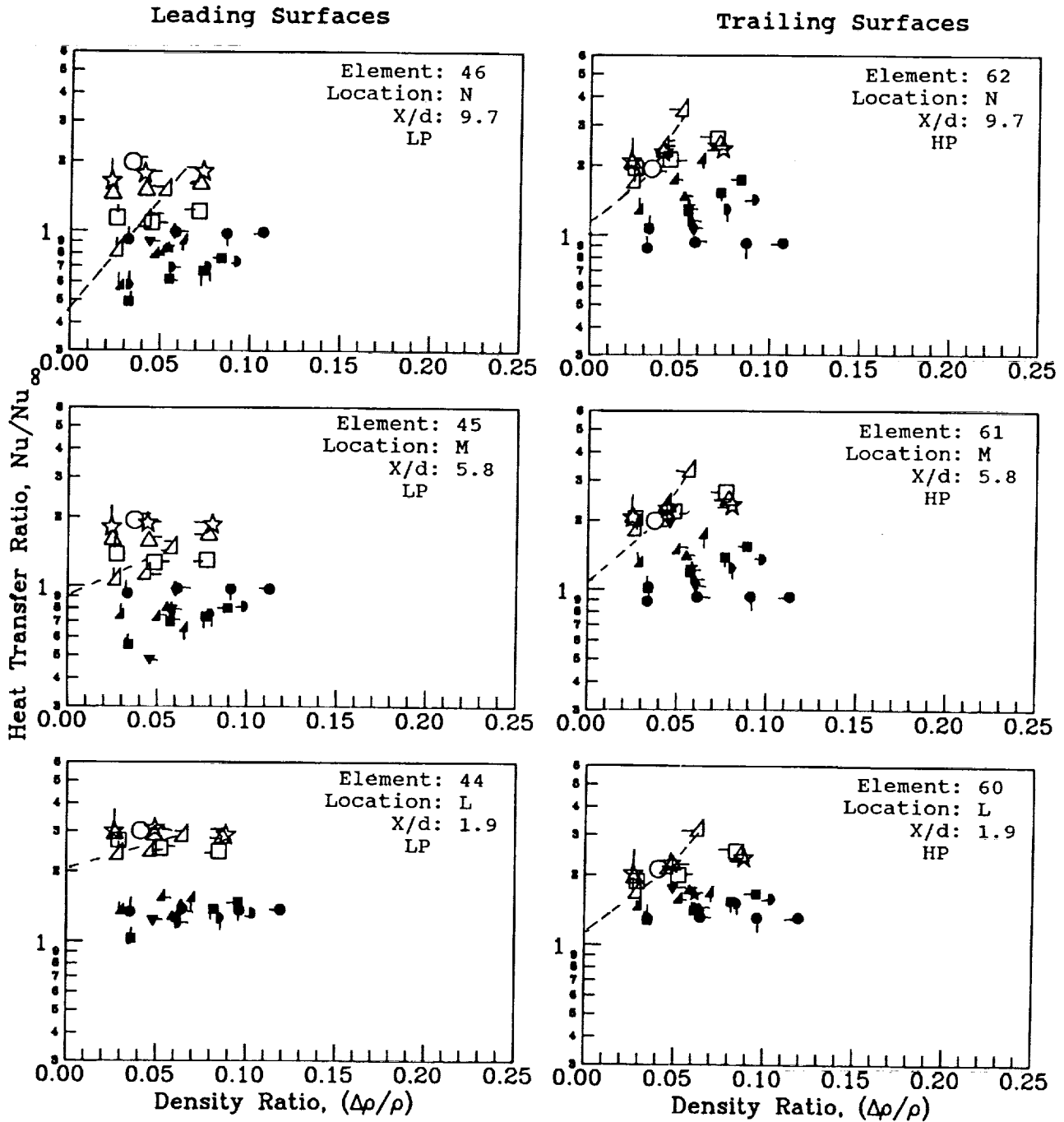


Figure 7.6a- Effect of Density Ratio on Heat Transfer Ratios in the Third Passage.

Symbol	○	◇	☆	△	D	□	▴
Rotation No.	0.00	0.006	0.05	0.12	0.18	0.25	0.35

Symbol Flag	$\frac{\Delta T_{in}}{O_C} (O_F)$
○	22.4 (40)
○	44.4 (80)
○	66.7 (120)
○	88.9 (160)

Re = 25,000 $\alpha = 0$ $\bar{R}/d = 49$

Skewed Trips - open symbols LP - Low Pressure
 Smooth Wall - solid symbols HP - High Pressure

----- Estimate for $\Delta T \rightarrow 0$

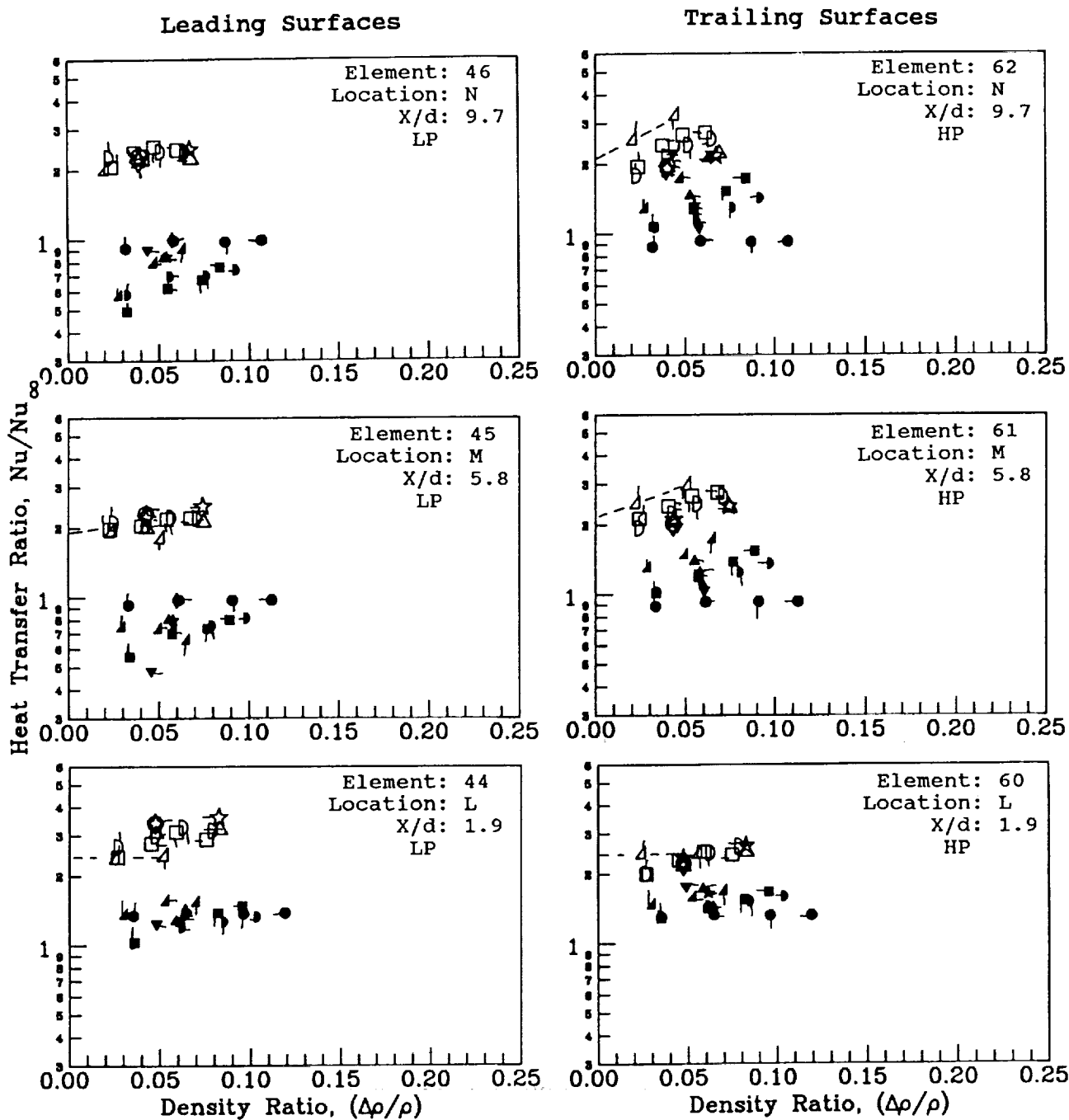


Figure 7.6b- Effect of Density Ratio on Heat Transfer Ratios in the Third Passage.

density ratio on the trailing surface (high pressure side) for the skewed trips than for the normal trips.

On the trailing surfaces of the second passage of the model with the normal trips (Figure 7.5a), the slopes of the variations of heat flux ratio with density ratio increase significantly as the X/d increases for all values of the rotation number 0.24 and 0.35. The effects of density ratio measured at $X/d = 9.7$ were the greatest for all three models; however, it should be noted that the results for the model with the normal trips generally lie between those from the model with the skewed trips and the model with smooth walls. This phenomena of very large density effects is attributed to the flow structures with separated and attached flow on the wall adjacent to the trips.

The heat transfer results on both the leading and trailing surfaces in the second passage with skewed trips (Figure 7.5b) show much less effect of density ratio than those with normal trips. The conclusion is that the secondary flows produced by the trips can have a large effect on heat transfer. The skewed trips apparently caused secondary flow patterns which did not produce strong effects of density ratio. The normal trips apparently caused flow patterns which produced strong effects on density ratio. The variation of heat transfer ratios with increasing density ratio on the trailing surfaces in the second passage of the model with skewed trips also occurs at lower values of the rotation number than occurred in the first passage. However, the slopes were close to those measured in the model with smooth walls.

The heat transfer characteristics in the third passage (Figure 7.6) were similar to those in the second passage. The heat transfer ratios for the model with normal trips were more sensitive to density ratio for $Ro = 0.35$ than those for the model with skewed trips.

The density ratio is a lesser factor in heat transfer when the flow in the coolant passage is well mixed. For most flow situations with the skewed trips, the flow is apparently well mixed and the effects of density ratio are minimal for $Ro \leq 0.25$. However, for the model with the normal trips, secondary flow patterns are postulated to occur where the recirculating flow is driven by the buoyancy terms. For these cases, the density ratio and therefore the buoyancy parameter are important. The principal results from this presentation are that the variations of heat transfer ratio with density ratio do not become appreciable until the rotation number is 0.24 or 0.35, depending on the passage, and that the heat transfer from the model with skewed trips was much less sensitive to the local density ratio than was the heat transfer from the model with normal trips. The first result was attributed to the influence of the trips on the secondary flows and turbulence characteristics. The second result was attributed to the formulation of buoyancy driven flow patterns for the normal trips and the preclusion of these patterns by the secondary flows due to the skewed trips.

7.3 Variation with Buoyancy Parameter

The buoyancy parameter, $(\Delta\rho/\rho)(\Omega R/V)(\Omega d/V)$, has been effective for the correlation of heat transfer results from the model with smooth walls (Volume I). The best correlation occurred for streamwise locations of $X/d = 12$ and for values of the buoyancy parameter greater than 0.20. In this sub section, the heat transfer ratios from the leading and trailing surfaces in the three passages are presented and compared with results from the model with smooth walls.

The variation of the local heat transfer ratio with the buoyancy parameter in the first passage with flow outward for both models is shown in Figure 7.7. The trailing surfaces for both models are correlated better with the buoyancy parameter than with the rotation number (Figure 7.1) or the inlet density ratio (Figure 7.4). Note that the heat transfer

ratios of test surface 52 for the normal and skewed trips are 20 and 25 percent greater than the heat transfer ratios for the smooth walls and for buoyancy parameters > 0.6 . (Recall that the total surface areas for the normal and skewed trips are 10 and 15 percent greater than for the smooth walls and that the heat transfer coefficients and hence heat transfer ratios are based on the projected area.) On an absolute basis (i.e. ΔNu), the increases are 30 and 45 percent of Nu_∞ . The conclusion is that half or more of the increase in heat transfer occurs due to the increased surface area. The increase in local heat transfer coefficient due to trips (10 percent) for high rotation numbers and high values of the buoyancy parameters is a small fraction of the 150 to 200 percent increase obtained from trips for zero rotation.

The variations of heat transfer ratio with buoyancy parameter for the leading (low pressure) surfaces in the first passages show several of the same characteristics previously shown for the results from the smooth model. However, for $Ro \leq 0.25$, the heat transfer ratios are correlated better by the rotation number (Figure 7.1) than by the buoyancy parameter. The distribution of results at all streamwise locations, i.e. $X/d = 4.7, 8.5$ and 12.4 for the models with trips resemble the distribution of results for $X/d = 4.7$ for the model with smooth walls. One possible cause for this relationship is that the trips cause the flow to mix near the wall and perhaps prevent the radial recirculation expected from strong buoyancy forces and low convection velocities near the leading surface. For test surface 36 and at values of the buoyancy parameters greater than 0.6 , the increase in the heat transfer ratio with normal trips is approximately 20 percent greater than with the smooth wall. For the same surface and flow condition and with the skewed trips, the increase is 35 percent above the values obtained with the smooth wall. However, the heat transfer on both surfaces with trips is approximately 30 percent less than the values obtained without rotation!

The variation of the heat transfer ratio with the buoyancy parameter in the second passage with flow radially inward (Figure 7.8) shows markedly different results from the two models with trips. For the model with skewed trips, the leading surfaces are well correlated by the buoyancy parameter but have values of the heat transfer ratio not more than 10 to 30 percent greater than the value for the stationary model. For the highest values of the buoyancy parameter at $X/d = 12.4$ the increase in heat transfer ratio is greater at the other values of X/d and lower values of the buoyancy parameter. The trailing surfaces are reasonably well correlated by the buoyancy parameter. However, the maximum decrease in heat transfer ratio from the stationary ratio due to buoyancy is less than 30 percent whereas the smooth wall model had decreases of approximately 40 percent. It should be noted that the decrease in absolute values are greater for the model with skewed trips ($0.75 Nu_\infty$) than for the model with smooth walls ($0.45 Nu_\infty$).

The heat transfer characteristics from the trailing surfaces in the second passage with flow inward for the model with normal trips (Figure 7.8a) are markedly different than those from the model with skewed trips (Figure 7.8b). At an $X/d = 9.7$ (element 57), the heat transfer for the lowest $(\Delta\rho/\rho)_{in}$ decreases from $2.1 Nu_\infty$ ($Ro = 0$) to $0.63 Nu_\infty$ ($Ro = 0.35$). In addition, the local heat transfer ratio increases markedly with increasing $(\Delta\rho/\rho)$ as the rotation number increases from 0.05 to 0.35 . These effects were previously attributed to the buoyancy driven flow structure caused by the normal trips and the separation, reattachment and radial recirculation zones associated with the trips. Note that at $X/d = 9.7$ (element 57) for $Ro = 0.35$ and the lowest $(\Delta\rho/\rho)_{in}$ the heat transfer ratio with the normal trips is approximately equal to that with smooth walls at the same location, i.e. $0.63 Nu_\infty$.

The results for the leading surfaces of the second passage in the model with normal trips are similar to those from the model with the skewed trips. Differences occur for Ro

Symbol	○	◇	☆	△	∩	□	▴	▽
Rotation No.	0.00	0.006	0.05	0.12	0.18	0.25	0.35	0.50

Symbol Flag	ΔT_{in} °C (°F)
○	22.4 (40)
○	44.4 (80)
○	66.7 (120)
○	88.9 (160)

Re = 25,000

$\alpha = 0$

$\bar{R}/d = 49$

Normal Trips - open symbols
Smooth Wall - solid symbols

HP - High Pressure
LP - Low Pressure

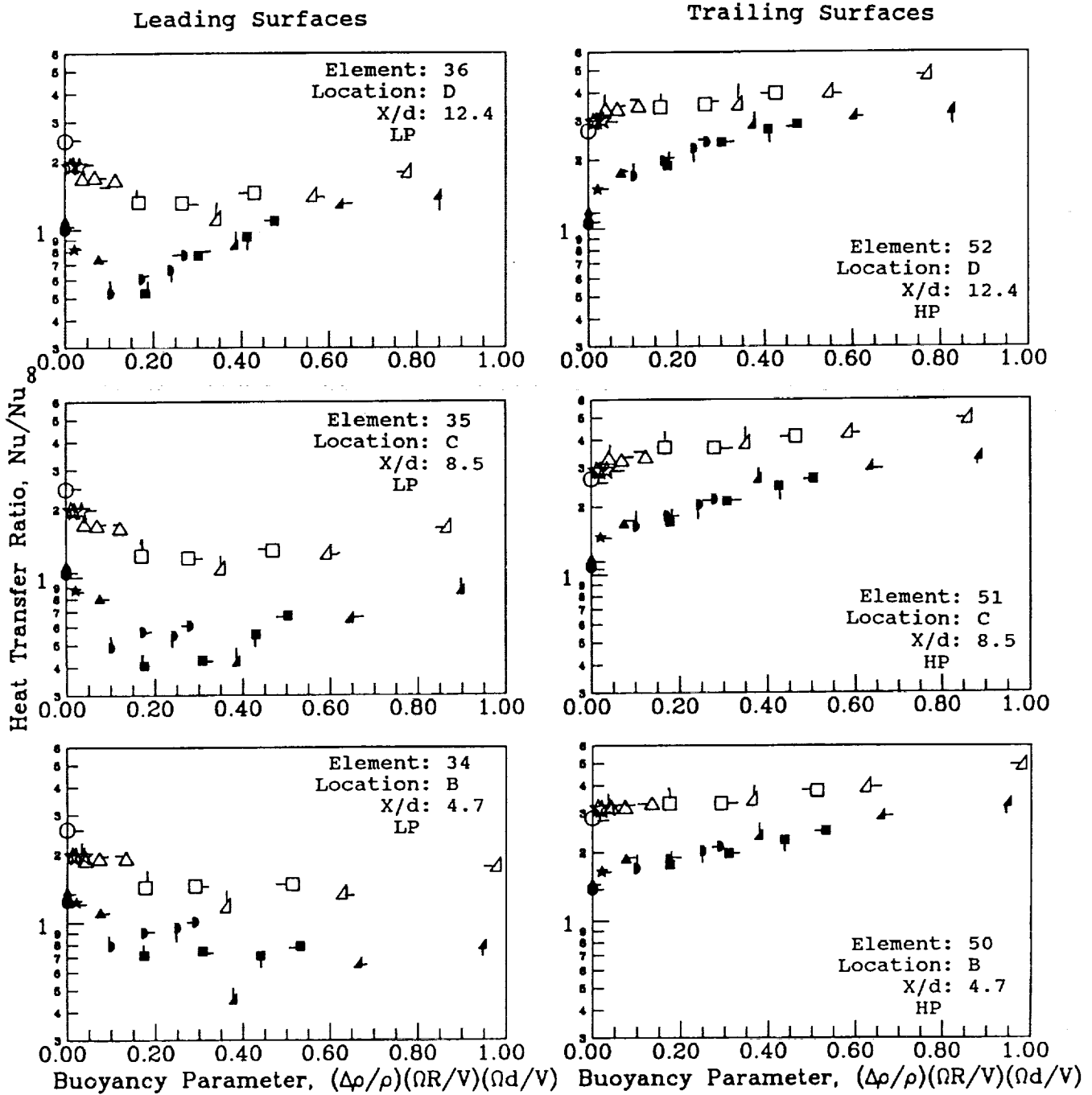


Figure 7.7a- Effect of Buoyancy Parameter on Heat Transfer Ratios in the First Passage.

Symbol	○	◇	☆	△	D	□	△	▽
Rotation No.	0.00	0.006	0.05	0.12	0.18	0.25	0.35	0.50

Symbol Flag	$\Delta T_{in}/\Delta T_{OC}$ (°F)
○	22.4 (40)
○	44.4 (80)
○	66.7 (120)
○	88.9 (160)

Re = 25,000

$\alpha = 0$

$\bar{R}/d = 49$

Skewed Trips - open symbols
Smooth Wall - solid symbols

HP - High Pressure
LP - Low Pressure

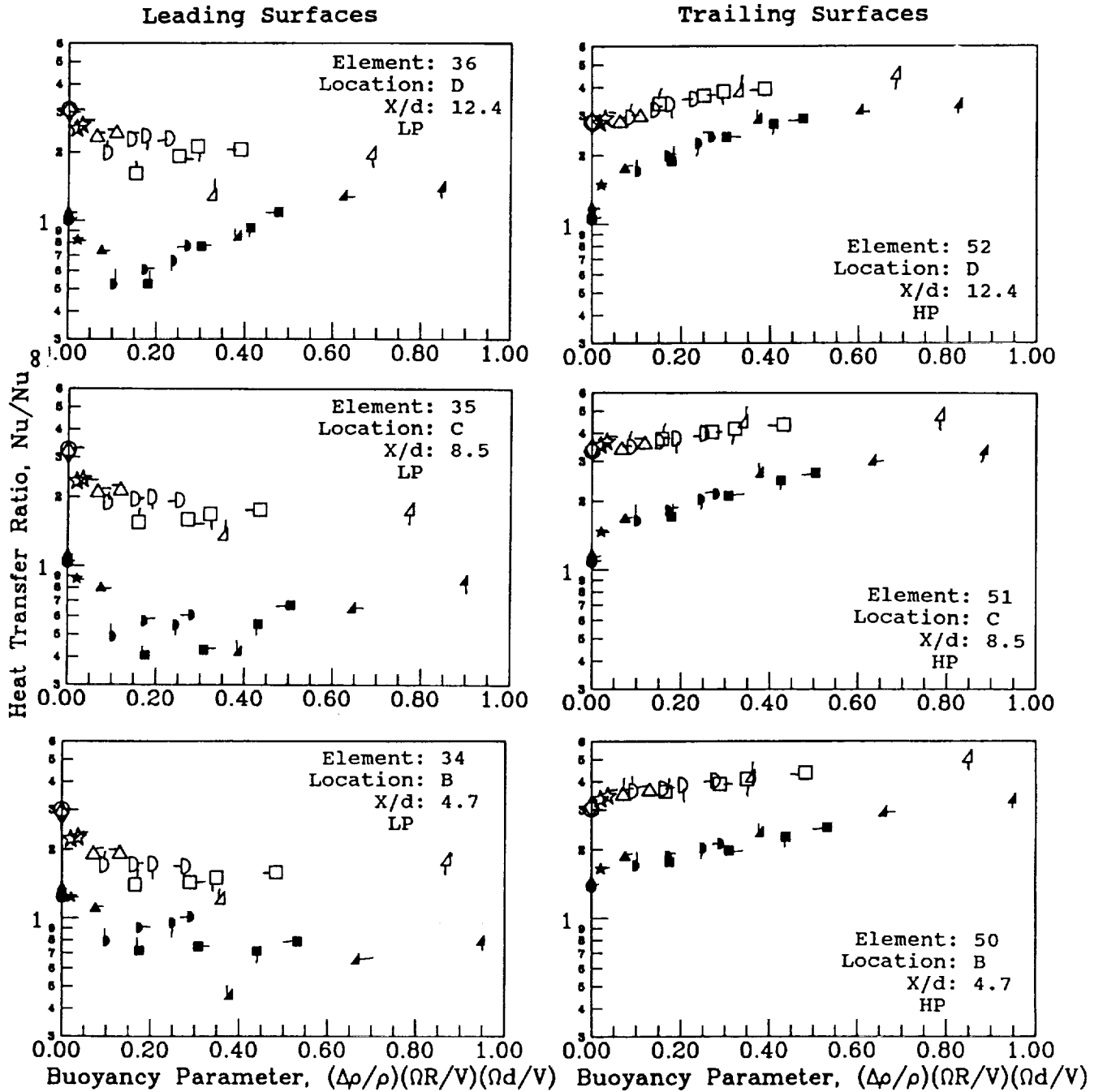


Figure 7.7b- Effect of Buoyancy Parameter on Heat Transfer Ratios in the First Passage.

Symbol	○	◇	☆	△	∩	□	▴	▽
Rotation No.	0.00	0.006	0.05	0.12	0.18	0.25	0.35	0.50

Symbol Flag	ΔT_{in} ΔT_{in} ΔT_{in} ΔT_{in}	ΔT_{in} ΔT_{in} ΔT_{in} ΔT_{in}	ΔT_{in} ΔT_{in} ΔT_{in} ΔT_{in}
○	22.4	(40)	
○	44.4	(80)	
○	66.7	(120)	
○	88.9	(160)	

Re = 25,000

$\alpha = 0$

$\bar{R}/d = 49$

Normal Trips - open symbols
Smooth Wall - solid symbols

HP - High Pressure
LP - Low Pressure

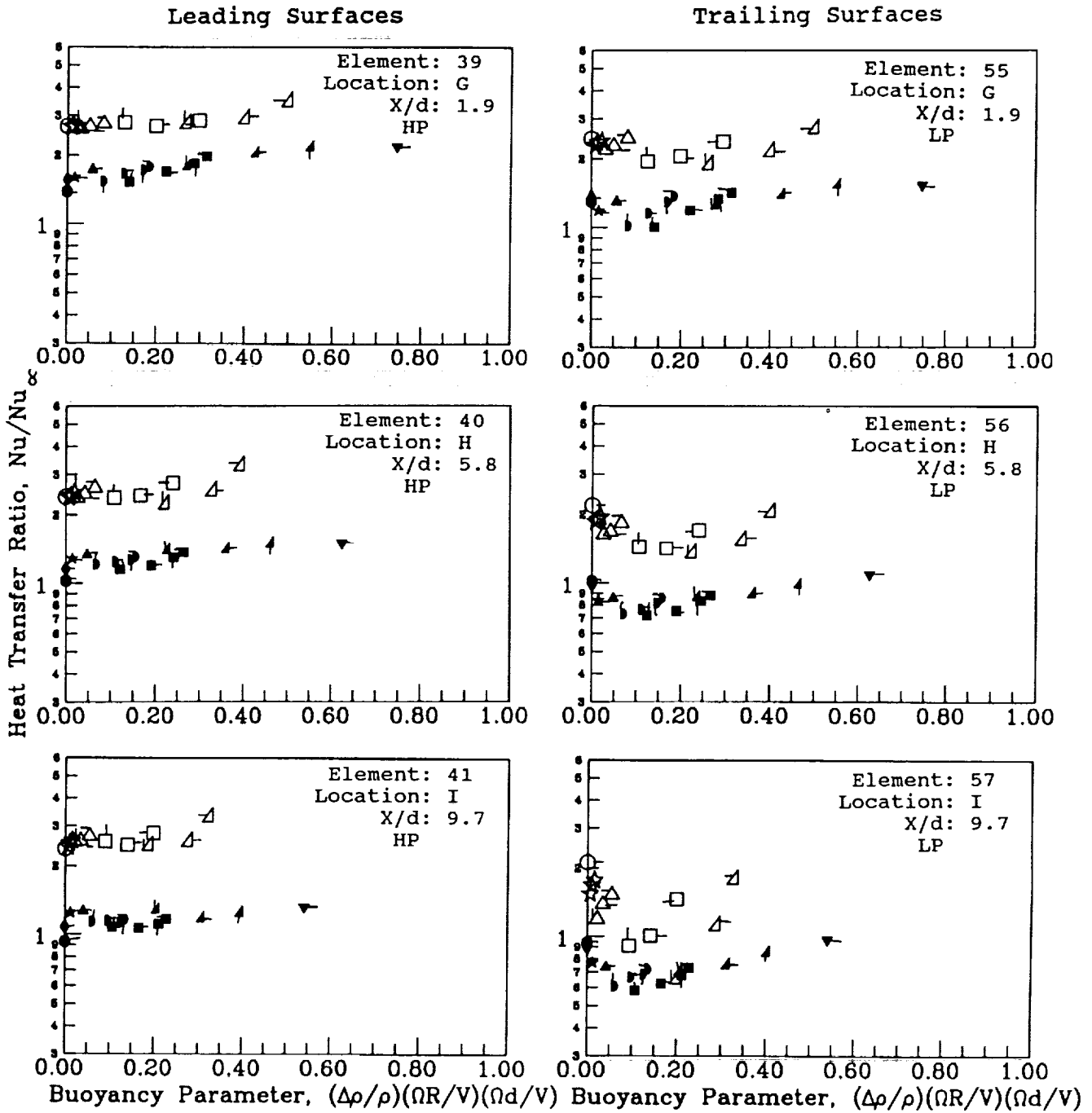


Figure 7.8a- Effect of Buoyancy Parameter on Heat Transfer Ratios in the Second Passage.

Symbol	○	◇	☆	△	D	□	△	▽
Rotation No.	0.00	0.006	0.05	0.12	0.18	0.25	0.35	0.50

Symbol Flag	ΔT_{in} °C (°F)
○	22.4 (40)
○	44.4 (80)
○	66.7 (120)
○	88.9 (160)

Re = 25,000

$\alpha = 0$

$\bar{R}/d = 49$

Skewed Trips - open symbols
Smooth Wall - solid symbols

HP - High Pressure
LP - Low Pressure

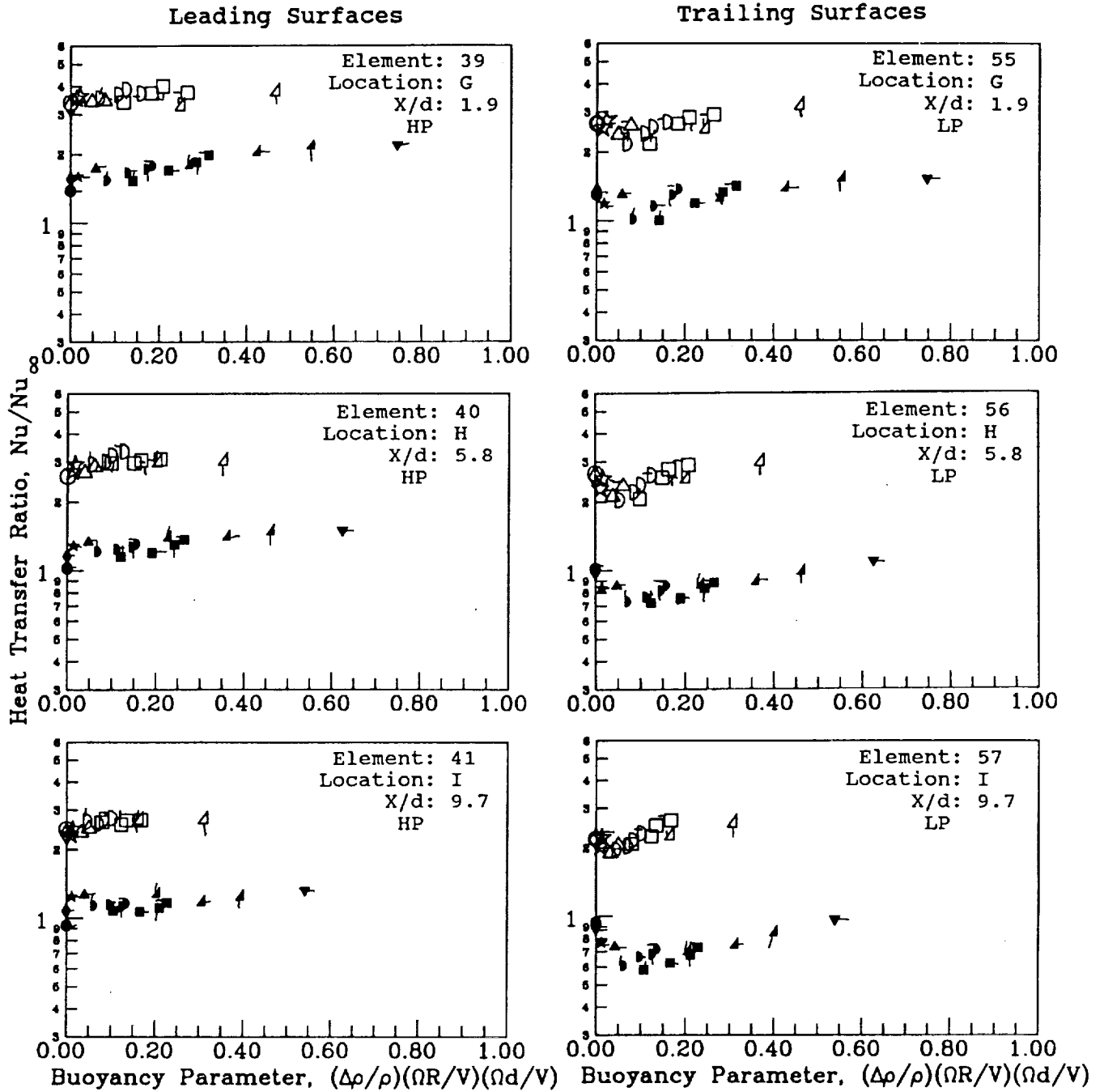


Figure 7.8b- Effect of Buoyancy Parameter on Heat Transfer Ratios in the Second Passage.

Symbol	○	◇	☆	△	◐	□	▵	▽
Rotation No.	0.00	0.006	0.05	0.12	0.18	0.25	0.35	0.50

Re = 25,000

$\alpha = 0$

$\bar{R}/d = 49$

Normal Trips - open symbols
Smooth Wall - solid symbols

HP - High Pressure
LP - Low Pressure

Symbol Flag	ΔT_{in} $^{\circ}C$ ($^{\circ}F$)
○	22.4 (40)
◐	44.4 (80)
◑	66.7 (120)
◒	88.9 (160)

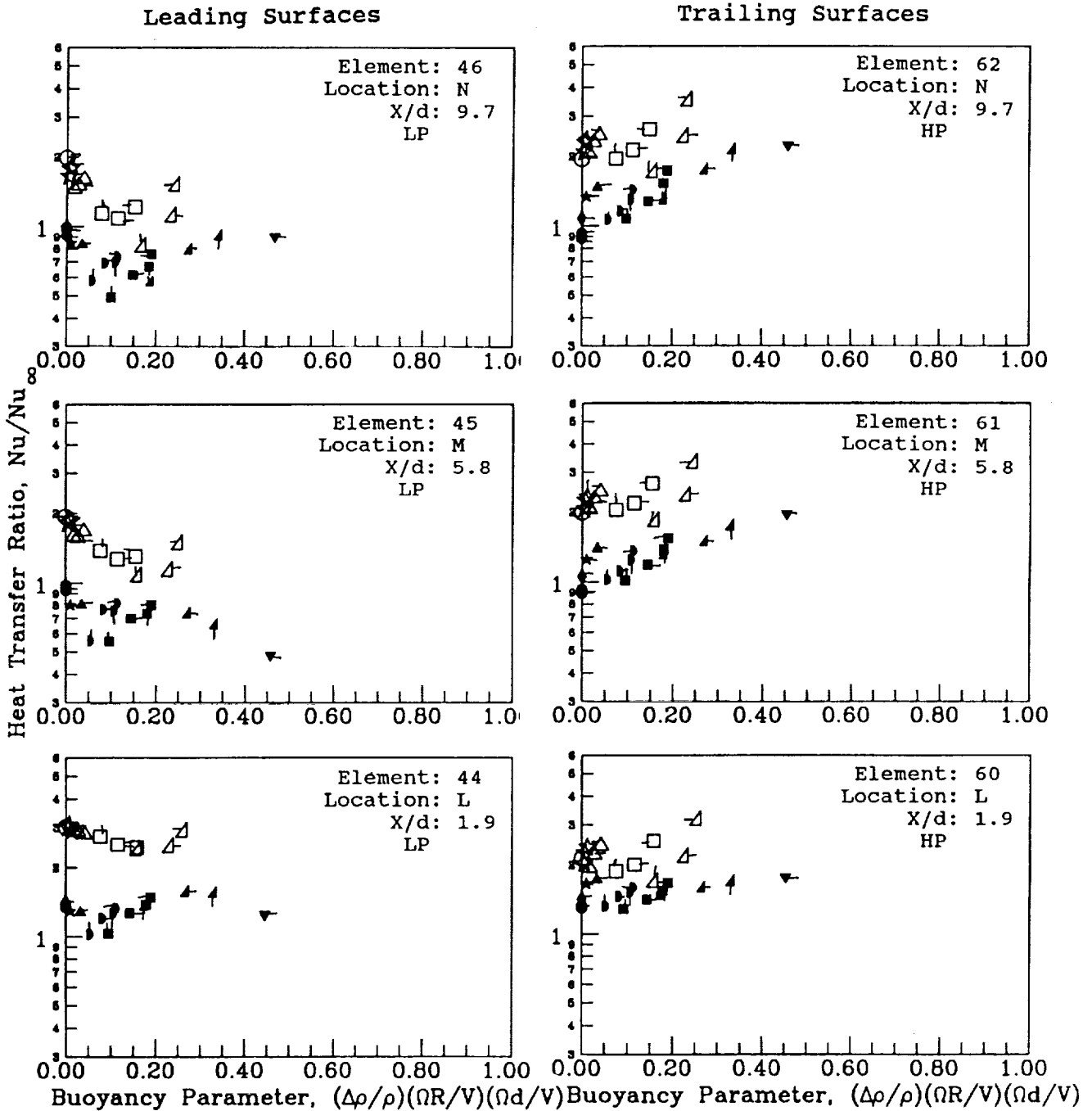


Figure 7.9a- Effect of Buoyancy Parameter on Heat Transfer Ratios in the Third Passage.

Symbol	○	◇	☆	△	D	□	△	▽
Rotation No.	0.00	0.006	0.05	0.12	0.18	0.25	0.35	0.50

Symbol Flag	$\Delta T_{in} / \Delta T_{out} (^\circ F)$
○	22.4 (40)
○-	44.4 (80)
○	66.7 (120)
○-	88.9 (160)

Re = 25,000

$\alpha = 0$

$\bar{R}/d = 49$

Skewed Trips - open symbols
Smooth Wall - solid symbols

HP - High Pressure
LP - Low Pressure

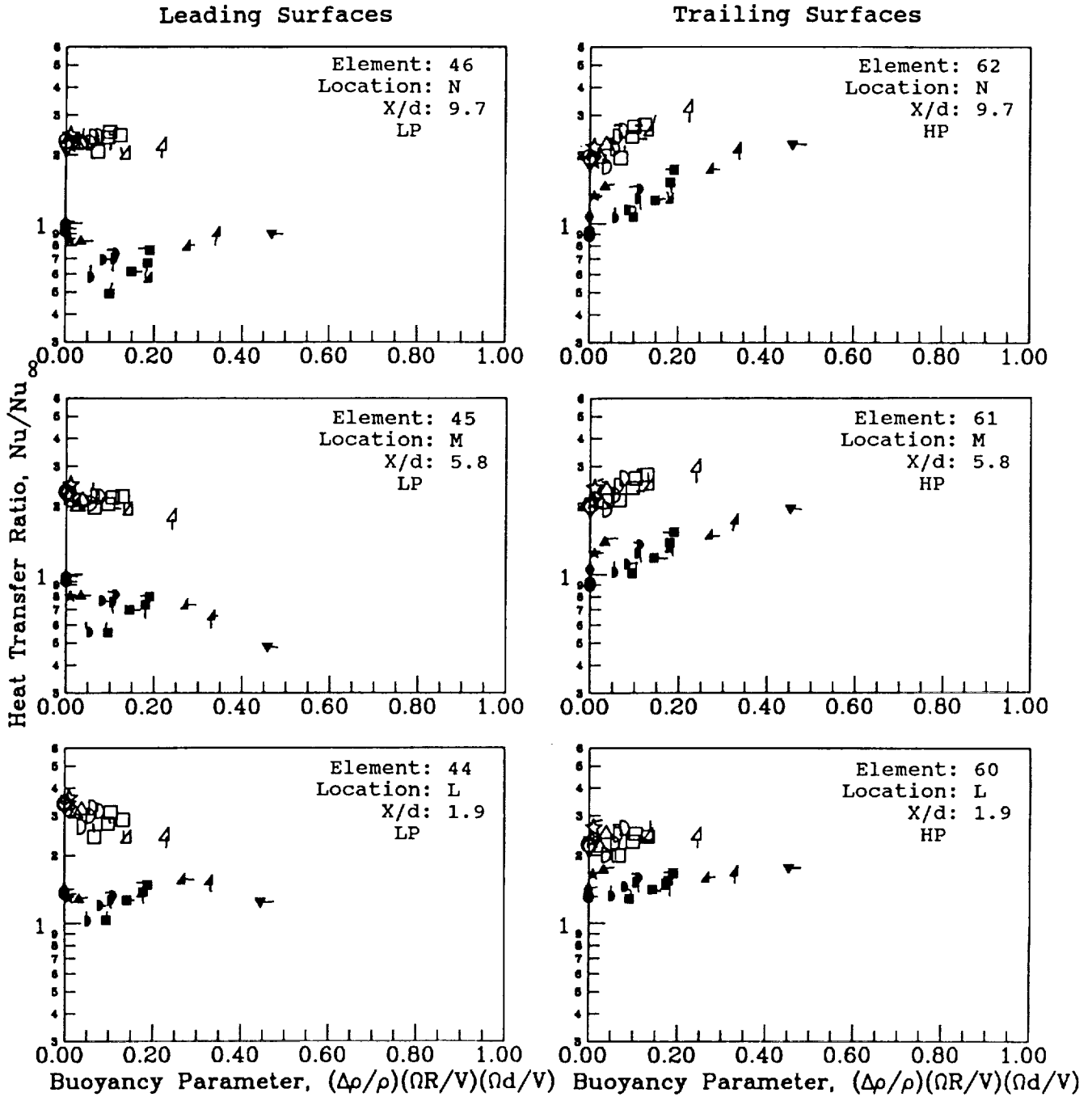


Figure 7.9b- Effect of Buoyancy Parameter on Heat Transfer Ratios in the Third Passage.

Symbol	○	◇	☆	△	D	□	△	▽
Rotation No.	0.00	0.006	0.05	0.12	0.18	0.25	0.35	0.50

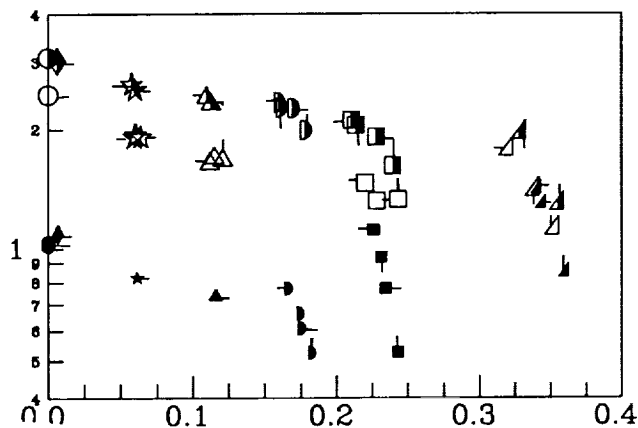
Symbol Flag	$\Delta T_{in,OC}$ (°F)
○	22.4 (40)
○	44.4 (80)
○	66.7 (120)
○	88.9 (160)

Re = 25,000 $\alpha = 0$ $\bar{R}/d = 49$

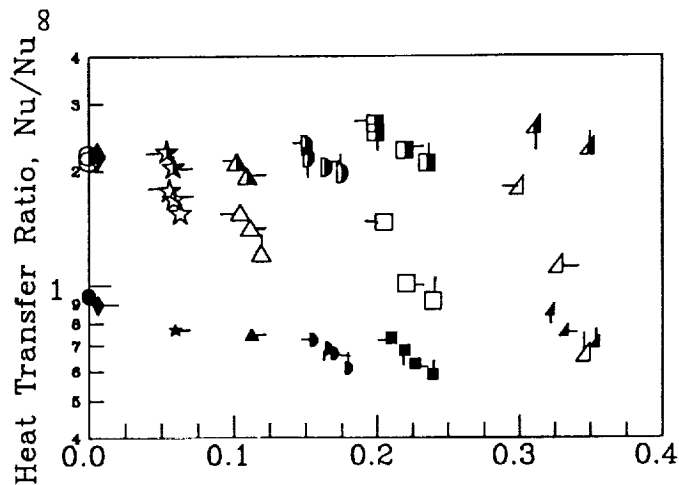
■ - Smooth Wall □ - Normal Trips ▣ - Skewed Trips

Low Pressure Sides of Passages

First Leg
Outward Flow
X/d = 12.4
Leading Surface
Element: 36
Location: D



Second Leg
Inward Flow
X/d = 9.7
Trailing Surface
Element: 57
Location: I



Third Leg
Outward Flow
X/d = 9.7
Leading Surface
Element: 46
Location: N

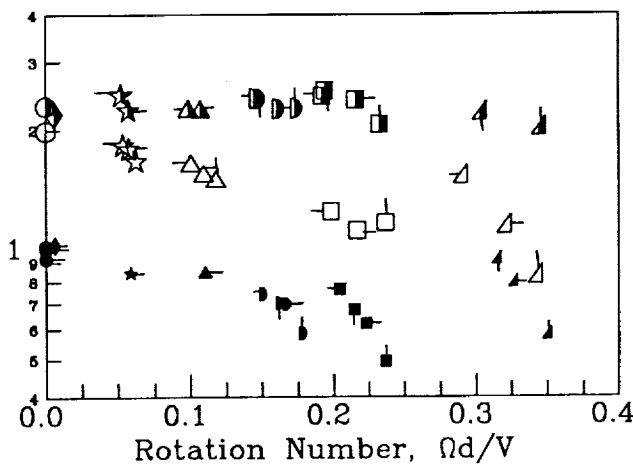


Figure 7.10a- Comparison of Effects of Rotation and Flow Direction on Heat Transfer Ratios.

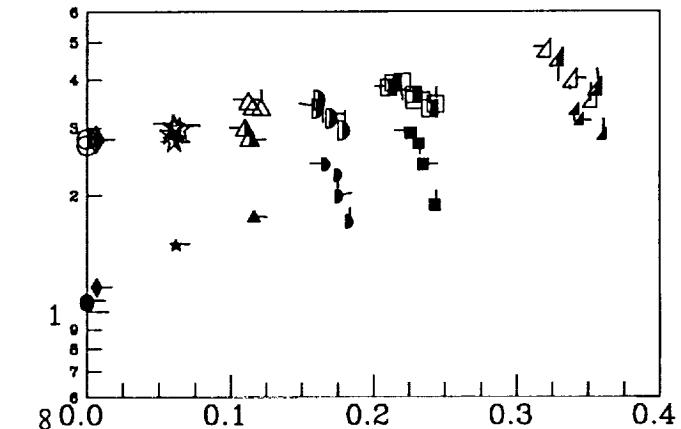
Symbol	○	◇	☆	△	D	□	▴	▽
Rotation No.	0.00	0.006	0.05	0.12	0.18	0.25	0.35	0.50

Symbol Flag	ΔT_{in} ΔT_{oc} ($^{\circ}F$)
○	22.4 (40)
○-	44.4 (80)
○	66.7 (120)
○	88.9 (160)

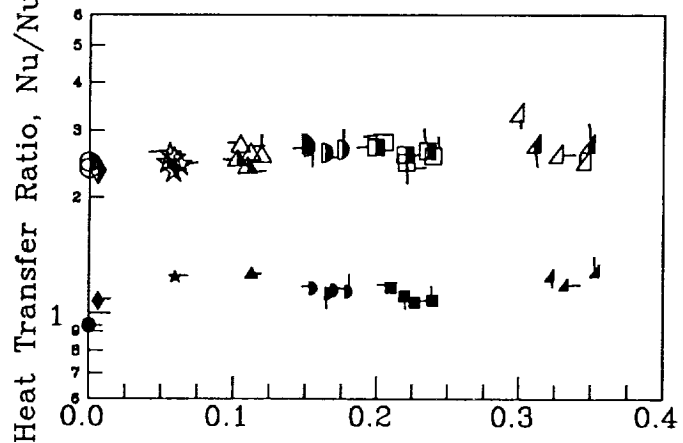
$Re = 25,000$ $\alpha = 0$ $\bar{R}/d = 49$
 ■ - Smooth Wall □ - Normal Trips ▣ - Skewed Trips

High Pressure Sides of Passages

First Leg
 Outward Flow
 $X/d = 12.4$
 Trailing Surface
 Element: 52
 Location: D



Second Leg
 Inward Flow
 $X/d = 9.7$
 Leading Surface
 Element: 41
 Location: I



Third Leg
 Outward Flow
 $X/d = 9.7$
 Trailing Surface
 Element: 62
 Location: N

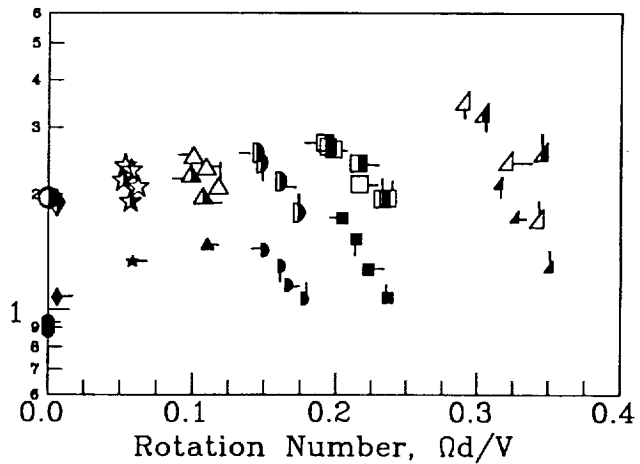


Figure 7.10b- Comparison of Effects of Rotation and Flow Direction on Heat Transfer Ratios.

Symbol	○	◇	☆	△	D	□	▴	▽
Rotation No.	0.00	0.006	0.05	0.12	0.18	0.25	0.35	0.50

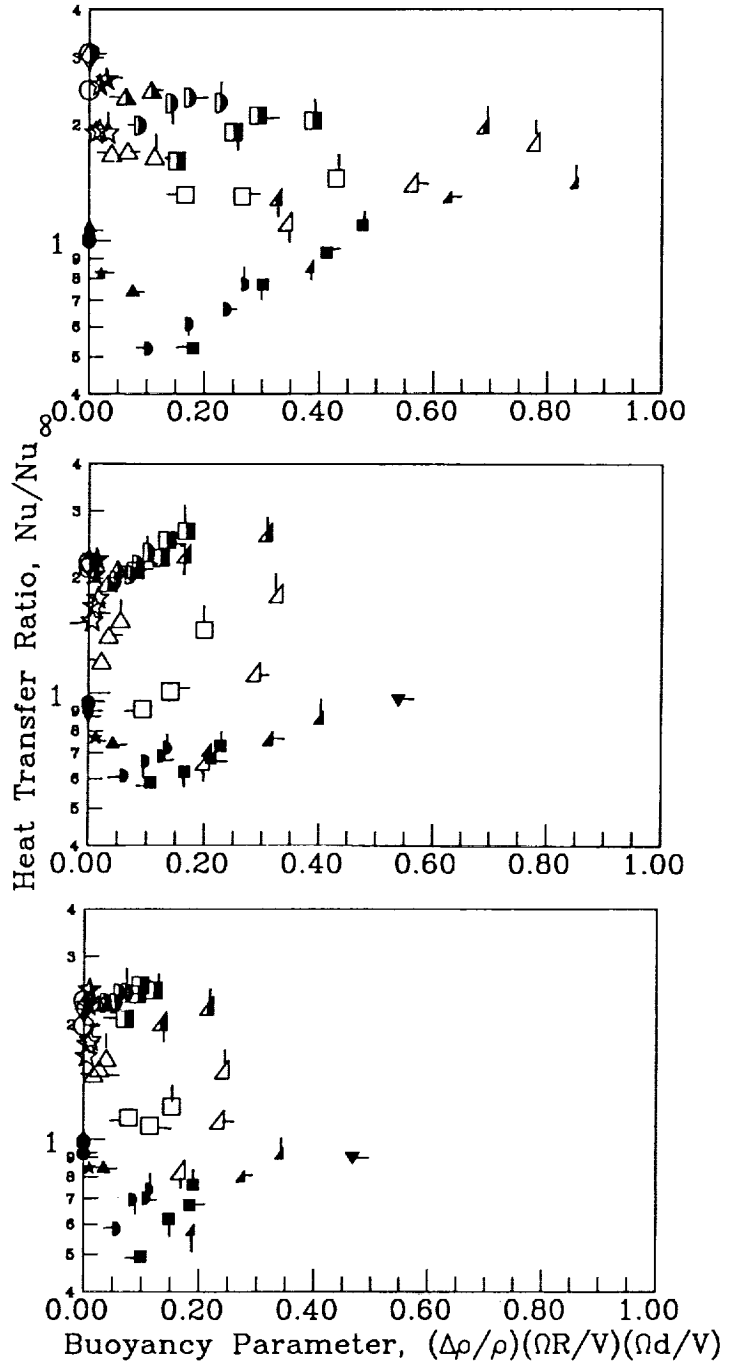
Symbol Flag	ΔT_{in} $^{\circ}C$ ($^{\circ}F$)
○	22.4 (40)
○	44.4 (80)
○	66.7 (120)
○	88.9 (160)

Re = 25,000 $\alpha = 0$ $\bar{R}/d = 49$

■ - Smooth Wall □ - Normal Trips ▴ - Skewed Trips

First Leg
Outward Flow
X/d = 12.4
Leading Surface
Element: 36
Location: D

Low Pressure Sides of Passages



Second Leg
Inward Flow
X/d = 9.7
Trailing Surface
Element: 57
Location: I

Third Leg
Outward Flow
X/d = 9.7
Leading Surface
Element: 46
Location: N

Figure 7.11a- Comparison of Effects of Buoyancy Parameter and Flow Direction on Heat Transfer Ratios.

Symbol	○	◇	☆	△	∅	□	▵	▽
Rotation No.	0.00	0.006	0.05	0.12	0.18	0.25	0.35	0.50

Symbol Flag	ΔT_{in} °C (°F)
○	22.4 (40)
○	44.4 (80)
○	66.7 (120)
○	88.9 (160)

$Re = 25,000$ $\alpha = 0$ $\bar{R}/d = 49$
 ■ - Smooth Wall □ - Normal Trips ▣ - Skewed Trips

First Leg
 Outward Flow
 $X/d = 12.4$
 Trailing Surface
 Element: 52
 Location: D

Second Leg
 Inward Flow
 $X/d = 9.7$
 Leading Surface
 Element: 41
 Location: I

Third Leg
 Outward Flow
 $X/d = 9.7$
 Trailing Surface
 Element: 62
 Location: N

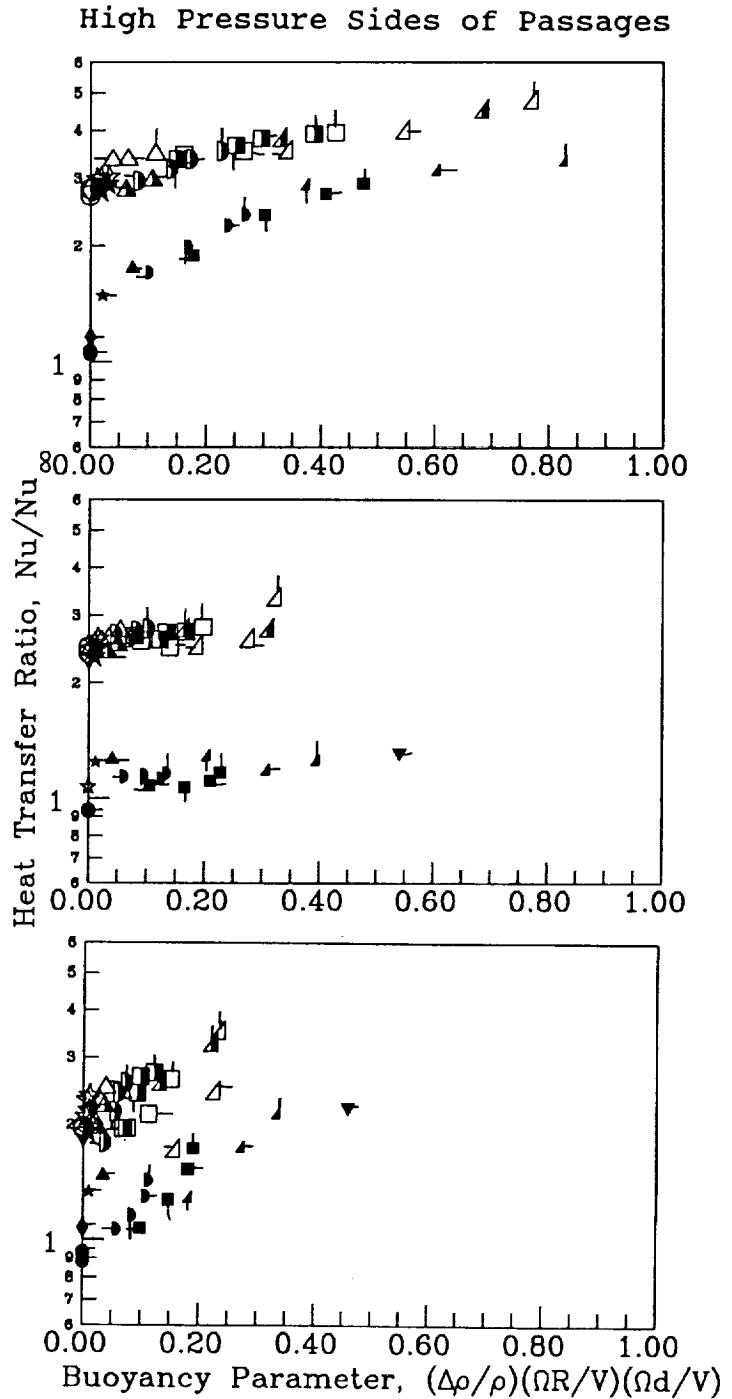


Figure 7.11b- Comparison of Effects of Buoyancy Parameter and Flow Direction on Heat Transfer Ratios.

= 0.35 and 0.24 where there is a greater dependency upon the density ratio than observed for either the smooth wall or skewed trip configurations at these locations.

7.4 Variation with Flow Direction

Rotation Number. The variation with rotation number heat transfer ratios for the downstream leading and trailing surfaces in the three straight passages are presented in Figure 7.10. These results were previously shown as part of Figures 7.1 through 7.3. Portions of the previous discussion will be repeated as applied to the figures. The test surface identification number, the streamwise location and the X/d ratio from the start of each straight section are also shown on each panel of the figure.

The trailing surfaces of the first and third passages and the leading surface of the second passage are the high pressure surfaces. In the first and third passages of both models with trips, the heat transfer coefficients increase with increasing rotation number at approximately half the slope as the heat transfer coefficients for the model with smooth walls (Figure 7.10b). The increases in heat transfer ratios, due to rotation, are as much as 75 percent compared to the heat transfer ratios for the same models with trips and no rotation. Also, the heat transfer ratios in the second passage with flow radially inward are essentially independent of rotation. Note that the heat transfer from the models with trips is essentially independent of inlet density for $Ro \leq 0.24$ in the first two passages. The uncertainty in the heat transfer measurements in the third channel increases due to small bulk to wall temperature differences for the low inlet density ratios. However, the results for the third passages with trips show characteristics similar to those for the third passage with smooth walls.

The heat transfer from the low pressure surfaces is more complex than that from the high pressure surfaces (Figure 7.10a). The heat transfer ratio in the first passage with both the normal and skewed trips decreases with increasing rotation number at the downstream location for the range of values tested, i.e. $\Omega d/V \leq 0.36$. At the larger values of $\Omega d/V$, 0.24–0.36, the heat transfer ratio increases with increases in the density ratio, similar to the results obtained for the trailing surface of the first passage.

The effects of inlet density ratio on the heat transfer ratio in the second passage are of order 10 percent for the model with skewed trips and with flow radially inward. Note that large variations of order 300 percent were obtained for the model with normal trips in this passage for $\Omega d/V \geq 0.3$. Note also that the local density ratios in the second passage are about half of the inlet values.

The heat transfer characteristics of the third passage are more similar to those of the second passage than to those of the first passage for each model. The model with skewed trips showed less decrease in heat transfer with increasing rotation than the models with the normal trips or the smooth walls.

The more complicated heat transfer distributions on the low pressure surfaces of the coolant passages are attributed to 1) the combination of buoyancy forces and the stabilization of the near-wall flow for low values of the rotation number, 2) the developing, Coriolis driven secondary flow cells, and 3) the increases in flow reattachment lengths after trips for the larger values of the rotation number. It is postulated that the relatively small effects from variations in density ratio near the inlet of the second passage and the large effects near the end of the second passage are due to the development of the near-wall thermal layers (i.e. thickening for the normal trip model compared to thinning for the smooth wall model). Near the inlet of the second passage, the thermal layers are postulated to be thin because of the strong secondary flows in the first turn region. With increasing

X/d, the turn dominated secondary flows diminish and the counteracting effects of buoyancy and the Coriolis generated secondary flow increase.

Buoyancy Parameter. The buoyancy parameter, $(\Delta\rho/\rho)(\Omega R/V)(\Omega d/V)$, has been effective for the correlation of heat transfer results from the model with smooth walls (Wagner et al., 1991a & 1991b). The best correlation was made for streamwise locations of $X/d = 12$ and for values of the buoyancy parameter greater than 0.20. In this section, the heat transfer ratios from the leading and trailing surfaces in the three passages are presented and compared with results from the models with smooth walls and with normal trips. These results were previously presented as parts of Figures 7.7 through 7.9. Portions of the previous discussion will be repeated as applied to the figures.

The variations of the local heat transfer ratio with buoyancy parameter for the normal and skewed trip walls are somewhat different than for the smooth walls. The comparison of the heat transfer on the low pressure side of the passage from the downstream test surfaces of each test leg is shown in Figure 7.11a. Note that the heat transfer ratios for the smooth wall model at values of the buoyancy parameter greater than 0.2 all lie in the same data band (see also Figure 33 of Volume I). The results for the normal trip model do not appear to be correlated by the buoyancy parameter for values less than 0.4 (reached only in the first leg). The heat transfer results for the skewed trip model vary somewhat between legs.

The comparison between legs of the heat transfer characteristics on the high pressure side of the passages with trips is better (Figure 7.11b). For both the first and third legs with flow outward, the heat transfer ratios increase modestly with increasing buoyancy parameter. For the second leg with flow inward, the heat transfer is less sensitive to the buoyancy parameter than for the first and third leg. This result for the models with trips is similar to that for the second leg of the smooth wall model. The tentative conclusion is that the changes in the turbulent transport due to buoyancy, which affects the heat transfer in the smooth wall model, also occur in rotating coolant passages with trips.

7.5 Concluding Discussion for Leading and Trailing Surfaces

As expected, the heat transfer results from the models with the normal and skewed trips show complex relationships occur because of the wall geometry. Following is a summary of comments regarding the importance of each of the parameters identified in Section 4.

- **Reynolds Number** – The heat transfer ratios for stationary and rotating conditions are reasonably well correlated by $Nu \sim Re^{0.8}$ relationship. For low Reynolds numbers, i.e. $Re \sim 12,500$, the exponent may be less.
- **Rotation Number** – The rotation number correlates the heat transfer ratios for models with trips better and for more surface locations and flow conditions than it did for the model with smooth walls. The percent decrease in heat transfer ratio from the stationary value on the low pressure side of the first coolant passage is well correlated by the rotation number for $R_o \leq 0.24$ and was independent of the three wall surface geometries.
- **Density Ratio and Buoyancy Parameter** – For these tests with a constant value of R/d, the density ratio, the rotation number and the Reynolds numbers are independent flow parameters and the buoyancy is determined by the variations of the density ratio and the rotation number, i.e. $(\Delta\rho/\rho)(\Omega d/V)^2 (R/d)$. The density ratio is a lesser factor in heat transfer when the flow in the coolant passage is well mixed. For most flow situations with the skewed trips, the flow

is apparently well mixed and the effects of density ratio are minimal for $Ro \leq 0.25$. However, for the model with the normal trips, secondary flow patterns are postulated to occur where the recirculating flow is driven by the buoyancy terms. For these cases, the density ratio and therefore the buoyancy parameter are important.

- **Streamwise Location** – With trips, the heat transfer does not usually vary appreciably with streamwise location. The large decrease in heat transfer with increasing distance from the inlet measured in the model with smooth walls does occur with the trips. The exception occurs for flow downstream of turns with the skewed trips where the upstream vorticity has been convected to one side of the model and the flow readjusts in the new passage.
- **Trip Orientation** – The secondary flows produced by the trips can have a large effect on heat transfer. The skewed trips apparently caused secondary flow patterns which did not produce strong effects of density ratio. The normal trips apparently caused flow patterns which produced strong effects of density ratio.
- **Flow Direction** – The effects of flow direction were generally the same for the models with trips as for the models with smooth walls. The largest effects of flow direction occurred on the high pressure side of the coolant passage. For flow outward, a modest increase in heat transfer ratio occurred for the trailing surface. For flow inward, the heat transfer on the leading surface was essentially independent of rotation number and density ratio.

8.0 HEAT TRANSFER RESULTS FOR SIDE WALLS

Heat transfer from the side or rib walls is generally less critical to the thermal design of a blade than the heat transfer from the surfaces directly adjacent to the blade aerodynamic surfaces where the metal temperatures and temperature gradients are greater. However, the heat transfer relationships are of interest and will be discussed. Note that the side walls are smooth for both the models with skewed or normal trips on the leading and trailing surfaces in the straight passages. The heat transfer from the side walls for $\alpha = 0$ are not as sensitive to rotation and density ratio as the leading and trailing surfaces with trips. Therefore, representation of the results as variations of rotation number, density ratio and buoyancy does not appear to be warranted. The buoyancy parameter appeared to offer the best correlations for all the sidewall surfaces and was selected as the independent variable for this presentation of results. The variation of the heat transfer ratio with the rotational buoyancy parameter in the first and second passages of the models with the normal and skew trips are presented in Figures 8.1 and 8.2, respectively.

The heat transfer ratios (Figure 8.1a) from the model with normal trips are similar to those from the model with smooth walls for the first heat transfer segment in each passage (Heaters 2 and 20/Streamwise location B). The heat transfer ratios from wall segments downstream of the inlet in the first passage are higher than for zero rotation but approximately the same as the smooth wall, for values of the buoyancy parameters greater than 0.3.

The heat transfer ratios for the second passage (Figure 8.2a) of the model with the normal trips are also similar to those from the model with the smooth walls from the test segments near the inlet of the passage (Heaters 9 and 23/Streamwise location G). However, the heat transfer ratios are 20 to 50 percent greater for the model with normal trips than for the model with smooth walls at Streamwise locations H and I.

The heat transfer characteristics for the model with skewed trips are more complex than those for the models with normal trips or smooth walls because of the secondary flows caused by the skewed trip geometry. Note that the heat transfer from Heaters 2 to 4 of the model with skewed trips is 30 to 50 percent greater than that from Heaters 20 to 22 for Passage 1 (Figure 8.1b). Note also that the heat transfer ratios for Heaters 20 to 22 are well correlated by the buoyancy parameter whereas those for Heaters 2 to 4 deviate from the grouping for $R_o = 0.35$. Note also that small decreases in the heat transfer ratio with an increase in the buoyancy parameter occurred for both Heaters 4 and 22 at $X/d = 12.4$ (Streamwise location D). This decrease with rotation from the values for the stationary model did not occur for the models with smooth walls or with normal trips. These effects are attributed to the complex interactions between the secondary flows caused by the Coriolis forces, the buoyancy forces and the skewed trip geometry.

The heat transfer relationships for the second passage of the model with skewed trips also showed more complex relationships than occurred for the other two models. For Heaters 9 to 11, the heat transfer generally increases with increasing values of the buoyancy parameter. However, small (i.e., less than 10 percent) decreases were measured for $X/d = 1.9$ (Heater 9). The heat transfer ratios for Heaters 23 to 25 are more sensitive to rotation and inlet density ratio than the side walls with either normal trips or smooth walls. The heat transfer ratios for those three wall segments are also not well correlated by the buoyancy parameter. These heat transfer ratios apparently have first order effects from several flow and geometric factors and are not correlated by a single parameter (which would indicate a dominate force).

Symbol	○	◇	☆	△	D	□	△	▽
Rotation No.	0.00	0.006	0.05	0.12	0.18	0.25	0.35	0.50

Symbol Flag	$\Delta T_{in} / \Delta T_{OC}$ ($^{\circ}F$)
○	22.4 (40)
○-	44.4 (80)
○	66.7 (120)
○	88.9 (160)

Re = 25,000

$\alpha = 0$

$\bar{R}/d = 49$

Normal Trips - open symbols
Smooth Wall - solid symbols

HP - High Pressure
LP - Low Pressure

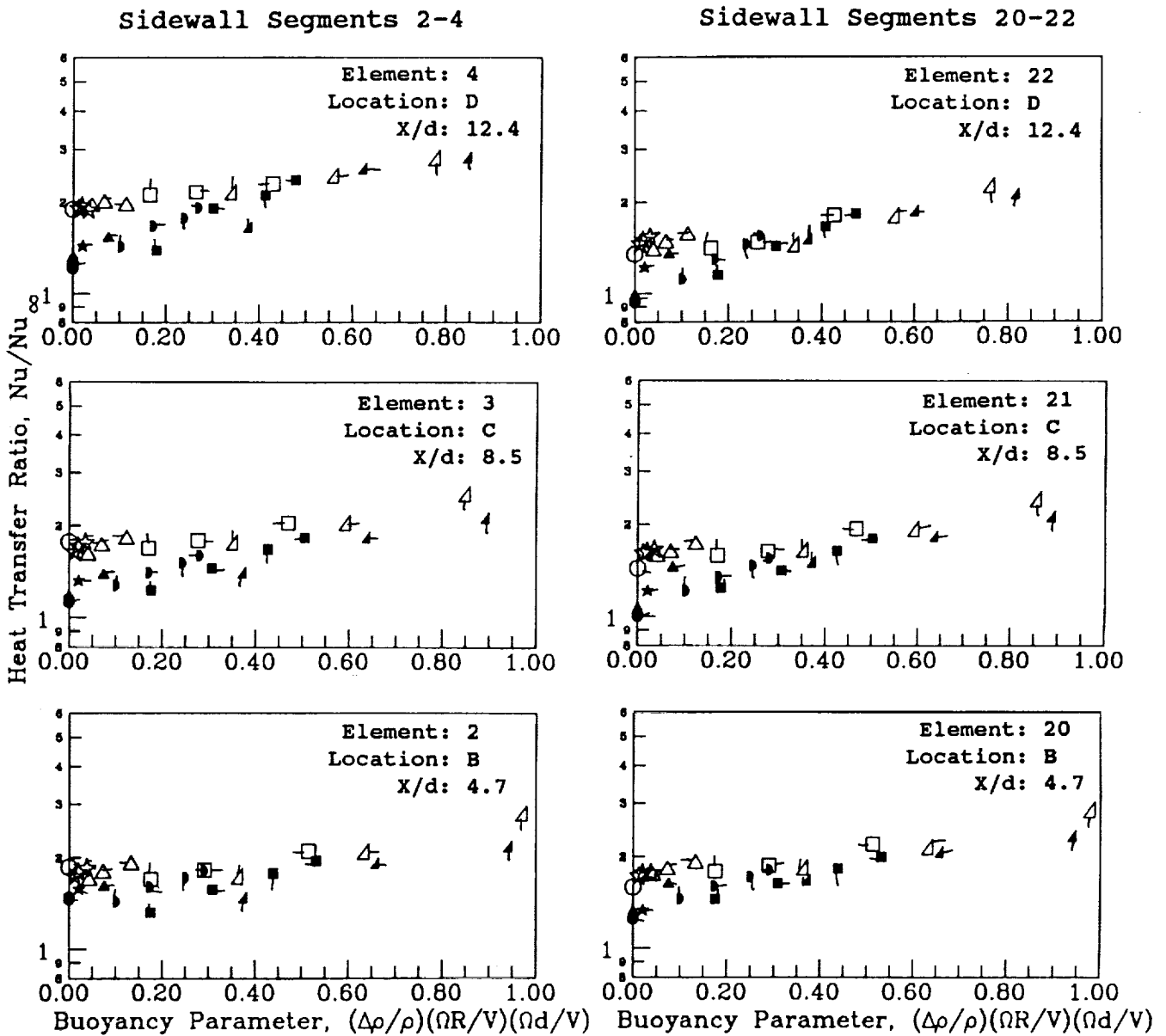


Figure 8.1a- Effect of Buoyancy Parameter on Heat Transfer Ratios in the First Passage.

Symbol	○	◇	☆	△	D	□	△	▽
Rotation No.	0.00	0.006	0.05	0.12	0.18	0.25	0.35	0.50

Symbol Flag	ΔT_{in} °C (°F)
○	22.4 (40)
○	44.4 (80)
○	66.7 (120)
○	88.9 (160)

Re = 25,000

$\alpha = 0$

$\bar{R}/d = 49$

Skewed Trips - open symbols
Smooth Wall - solid symbols

HP - High Pressure
LP - Low Pressure

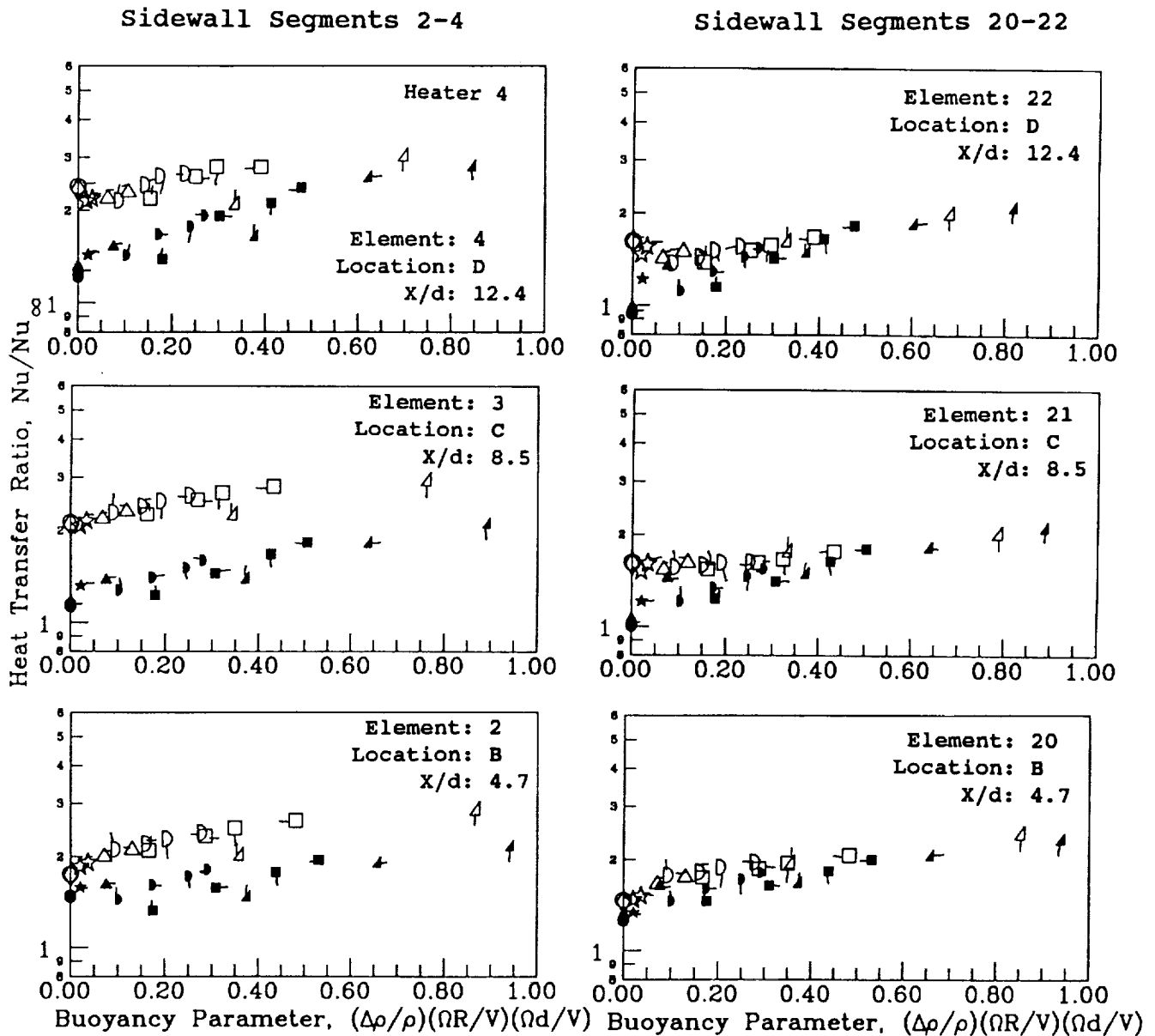


Figure 8.1b- Effect of Buoyancy Parameter on Heat Transfer Ratios in the First Passage.

Symbol	○	◇	☆	△	∅	□	▴	▽
Rotation No.	0.00	0.006	0.05	0.12	0.18	0.25	0.35	0.50

Symbol Flag	$\Delta T_{in_{OC}}$ ($^{\circ}F$)
○	22.4 (40)
○-	44.4 (80)
♀	66.7 (120)
○	88.9 (160)

Re = 25,000

$\alpha = 0$

$\bar{R}/d = 49$

Normal Trips - open symbols
Smooth Wall - solid symbols

HP - High Pressure
LP - Low Pressure

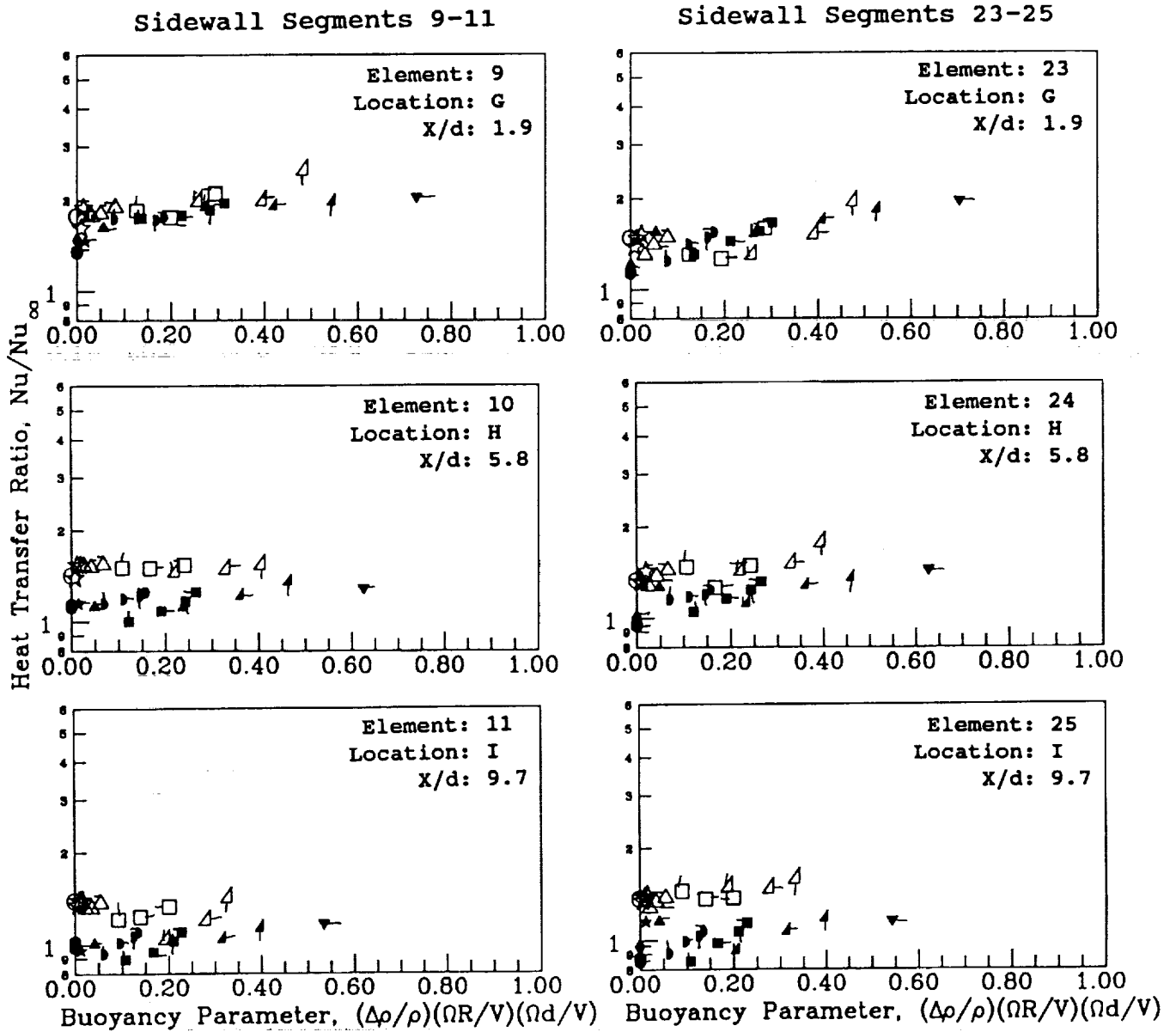


Figure 8.2a- Effect of Buoyancy Parameter on Heat Transfer Ratios in the Second Passage.

Symbol	○	◇	☆	△	∩	□	△	▽
Rotation No.	0.00	0.006	0.05	0.12	0.18	0.25	0.35	0.50

Symbol Flag	$\Delta T_{in,OC} (^{\circ}F)$
○	22.4 (40)
○	44.4 (80)
○	66.7 (120)
○	88.9 (160)

Re = 25,000

$\alpha = 0$

$\bar{R}/d = 49$

Skewed Trips - open symbols
Smooth Wall - solid symbols

HP - High Pressure
LP - Low Pressure

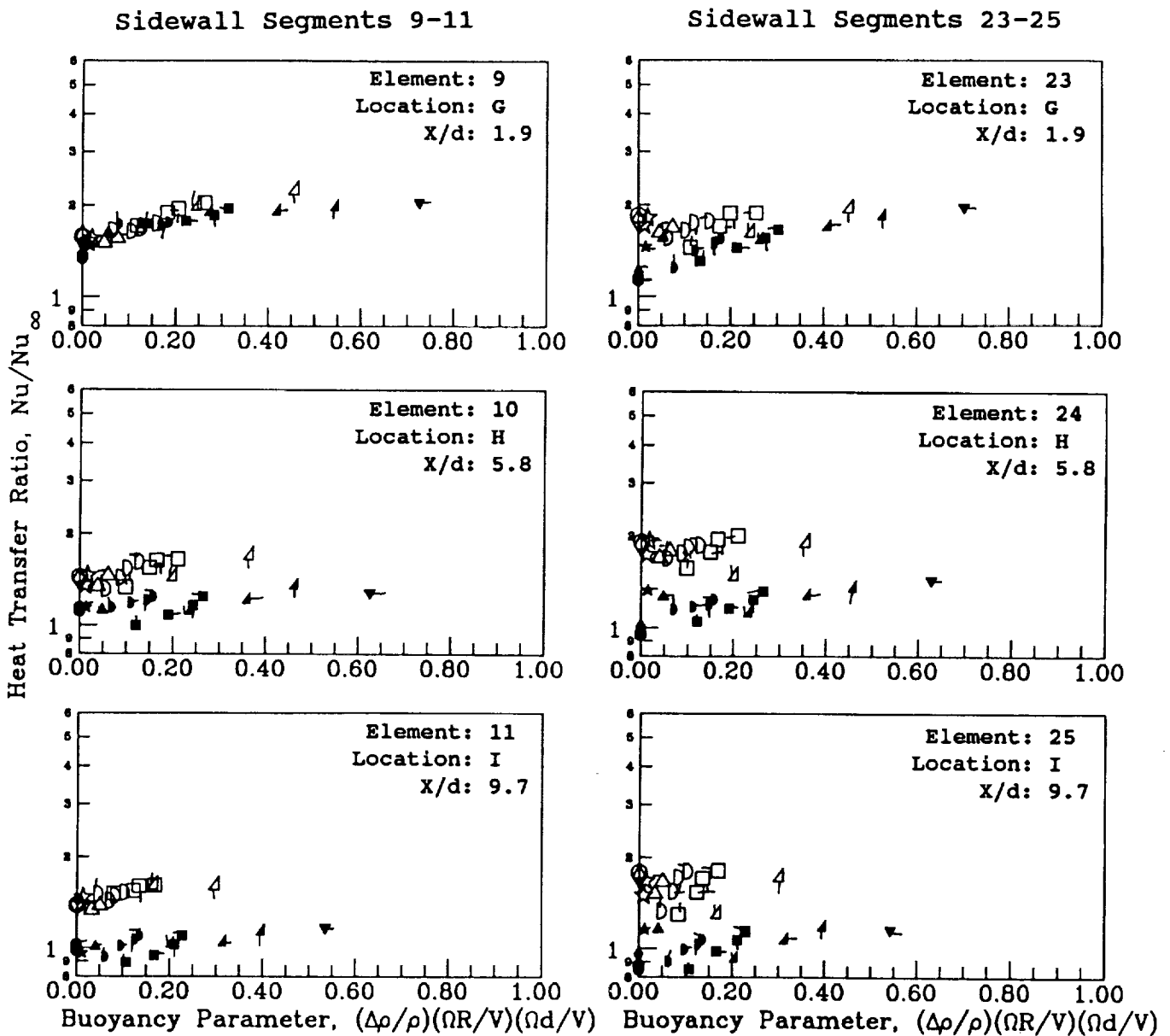


Figure 8.2b- Effect of Buoyancy Parameter on Heat Transfer Ratios in the Second Passage.

Although the heat transfer from the side walls is complex, the general tendency is for the heat transfer ratios to increase (or remain constant within 10 percent) with increasing rotation and inlet density ratio. The exception occurred for the second passage of the model with skewed trips where the heat transfer ratios decreased by as much as 35 percent from their value with the model stationary.

9.0 HEAT TRANSFER RESULTS FOR TURN REGIONS

The heat transfer in the tip and root turn regions of the serpentine passage results from the conservation of vorticity as the flow undergoes a 180 degree turn, the interaction of buoyancy forces, and the wall friction in the turn region. The vorticity at the entrance to the turn region is caused by Coriolis forces and secondary flows induced by the trips. Thus, the heat transfer in the turn regions can be expected to be a function of the upstream wall geometry (smooth, normal trip or skewed trip), the rotation number, the turn orientation (tip or root) and the density ratio. Exploratory numerical studies (Sturgess and Datta, 1987) of flow through rotating sharp 180 degree bends showed that the double vortices (formed at the end of the straight section with outward flow) coalesced into a single vortex at the exit of the turn region. The secondary flows due to the interaction Coriolis forces, velocity profiles in the straight passages due to wall friction and the secondary flows due to trip orientation are expected to be different at the entrance to each turn region. The buoyancy effects on both turns will tend to accelerate the heated flow near the wall radially inward. Thus, the buoyancy effects will interact in opposite manners with the vortex/vortices through the turn. The conclusion from this discussion is that the flow and hence heat transfer in the turn regions can be complex.

Although the numerical analysis of flows and heat transfer in rotating coolant passages is progressing rapidly, numerical results for the heat transfer of variable density flows in sharp 180 degree turns of rotating passages are not presently available. As previously discussed, the interaction can be complicated, therefore, the heat transfer results in the turns will be presented as functions of two buoyancy parameters. The first, denoted as "buoyancy term," $(\Delta\rho/\rho)(\Omega R/V)$, was found to provide a good correlating parameter for turns with the smooth walls (Volume 1). The second is the conventional (for this program) buoyancy parameter, $(\Delta\rho/\rho)(\Omega R/V)(\Omega d/V)$.

The Nusselt numbers and mean convective velocities for the turn region are based on the geometrical characteristics of the turn region. The average cross sectional flow areas and the average perimeter length are not the same as for the straight sections of the model. The local values for d (hydraulic diameter) and A_c (cross sectional area) are used in the calculation of the Nusselt number and in the determination of V (local average coolant passage velocity (Table 13.1)). The surfaces of all test section segments in the turn region are smooth. The references to models with normal and skewed trips and with smooth walls refer to the leading and trailing test surfaces in the straight section upstream and downstream of the turns.

9.1 Tip Turn

The variations of the heat transfer ratio with the buoyancy term and the buoyancy parameter for the first tip turn are presented in Figures 9.1 and 9.2. For the model with normal trips and at stationary condition (with both the buoyancy term or the buoyancy parameter equal zero), the heat transfer ratios are greater than or equal to the model with smooth walls (Figure 9.1a). For rotation numbers greater than 0.05, the heat transfer ratios with normal trips is less than or equal to the heat transfer ratios with smooth walls. With normal trips, the heat transfer ratio can decrease or increase with rotation in the first half of the turn and generally increases or remains constant with rotation in the last portion of the turn. The buoyancy term (Figure 9.1a) correlates the results for each heater segment better than the buoyancy parameter (Figure 9.2a).

For the model with skewed trips and at zero rotation, the heat transfer ratios are equal to or less than the heat transfer ratios for the smooth walls except for heater element 5 (Figure 9.1b). With rotation, the heat transfer ratios generally increase or remain constant

Symbol	○	◇	☆	△	▷	□	△	▽
Rotation No.	0.00	0.006	0.05	0.12	0.18	0.25	0.35	0.50

Symbol Flag	ΔT_{in} $^{\circ}C$ ($^{\circ}F$)
○	22.4 (40)
○	44.4 (80)
○	66.7 (120)
○	88.9 (160)

Re = 25,000

$\alpha = 0$

$\bar{R}/d = 49$

Normal Trips - open symbols
Smooth Wall - solid symbols

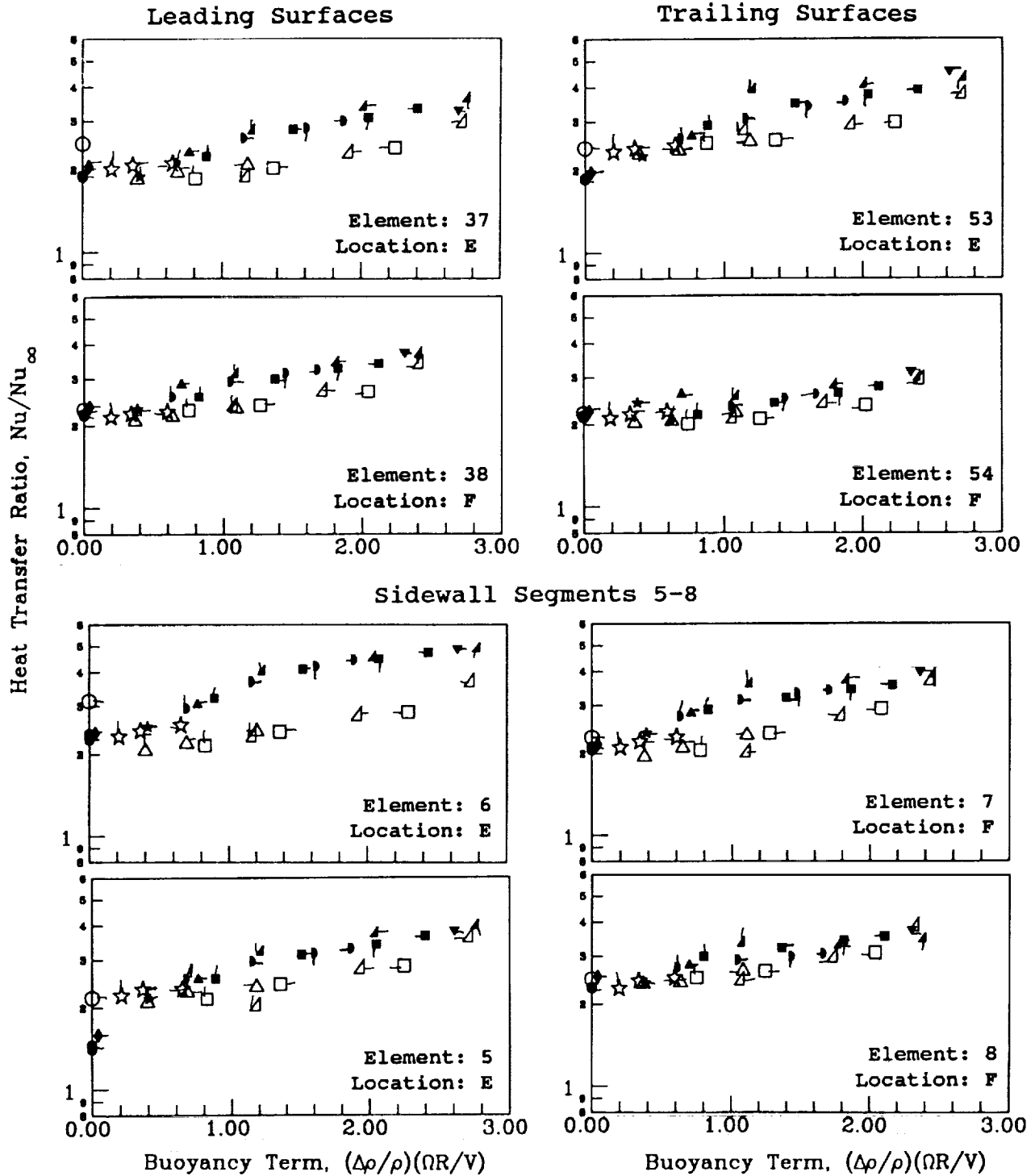


Figure 9.1a- Effect of Buoyancy Term on Heat Transfer Ratios in the First Turn.

Symbol	○	◇	☆	△	D	□	△	▽
Rotation No.	0.00	0.006	0.05	0.12	0.18	0.25	0.35	0.50

Symbol Flag	$\Delta T_{in} / \Delta T_{out} (OF)$
○	22.4 (40)
○	44.4 (80)
○	66.7 (120)
○	88.9 (160)

Re = 25,000 $\alpha = 0$ $\bar{R}/d = 49$

Skewed Trips - open symbols
Smooth Wall - solid symbols

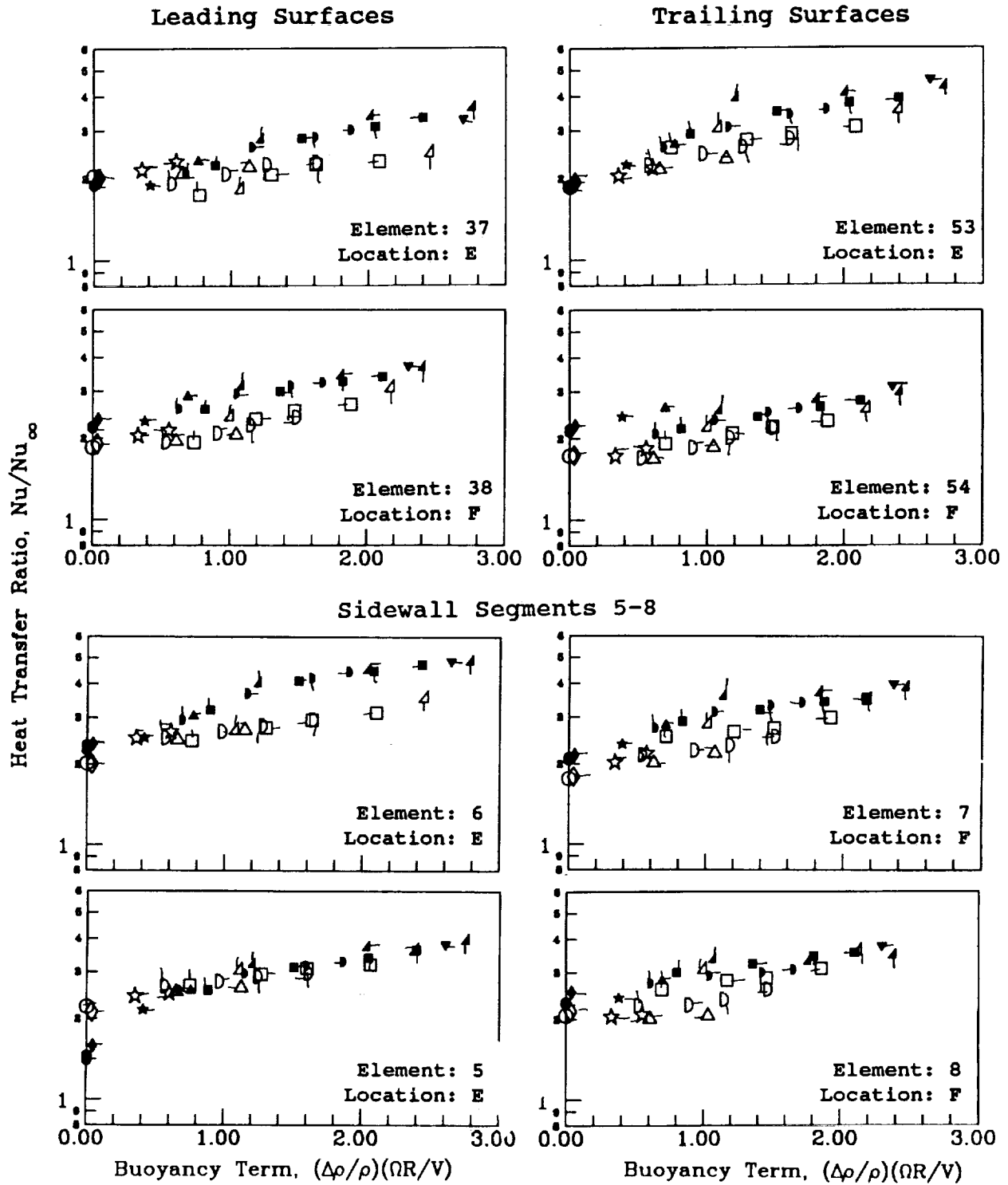


Figure 9.1b- Effect of Buoyancy Term on Heat Transfer Ratios in the First Turn.

Symbol	○	◇	☆	△	∩	□	▵	▽
Rotation No.	0.00	0.006	0.05	0.12	0.18	0.25	0.35	0.50

Symbol Flag	$\Delta T_{in}/\Delta T_{out}$ (°F)
○	22.4 (40)
○	44.4 (80)
◊	66.7 (120)
○	88.9 (160)

Re = 25,000 $\alpha = 0$ $\bar{R}/d = 49$

Normal Trips - open symbols
Smooth Wall - solid symbols

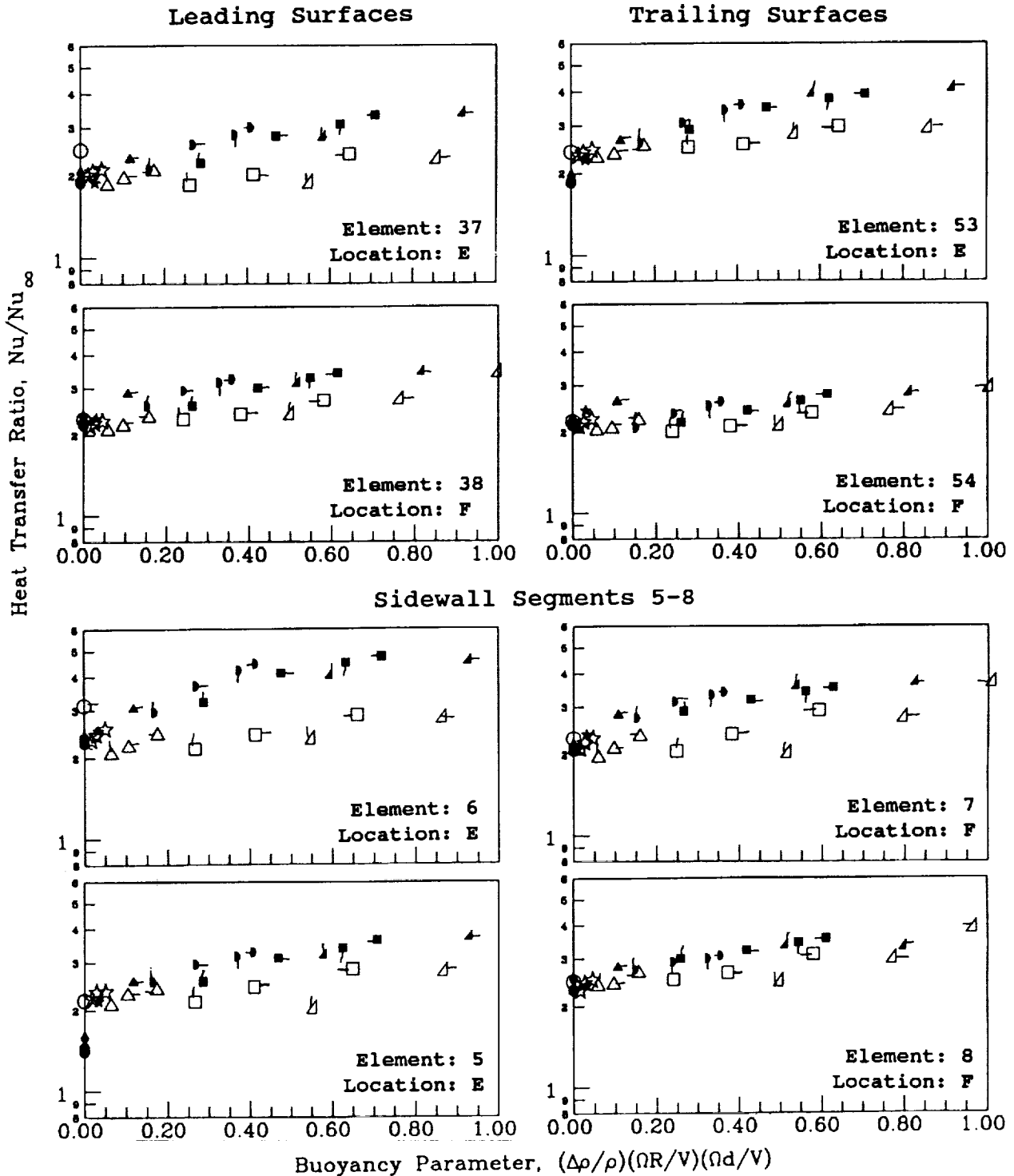


Figure 9.2a- Effect of Buoyancy Parameter on Heat Transfer Ratios in the First Turn.

Symbol	○	◇	☆	△	∩	□	▴	▽
Rotation No.	0.00	0.006	0.05	0.12	0.18	0.25	0.35	0.50

Symbol Flag	$\frac{\Delta T_{in}}{T_{OC}} ({}_{OF})$
○	22.4 (40)
○-	44.4 (80)
○	66.7 (120)
○-	88.9 (160)

Re = 25,000 $\alpha = 0$ $\bar{R}/d = 49$

Skewed Trips - open symbols
Smooth Wall - solid symbols

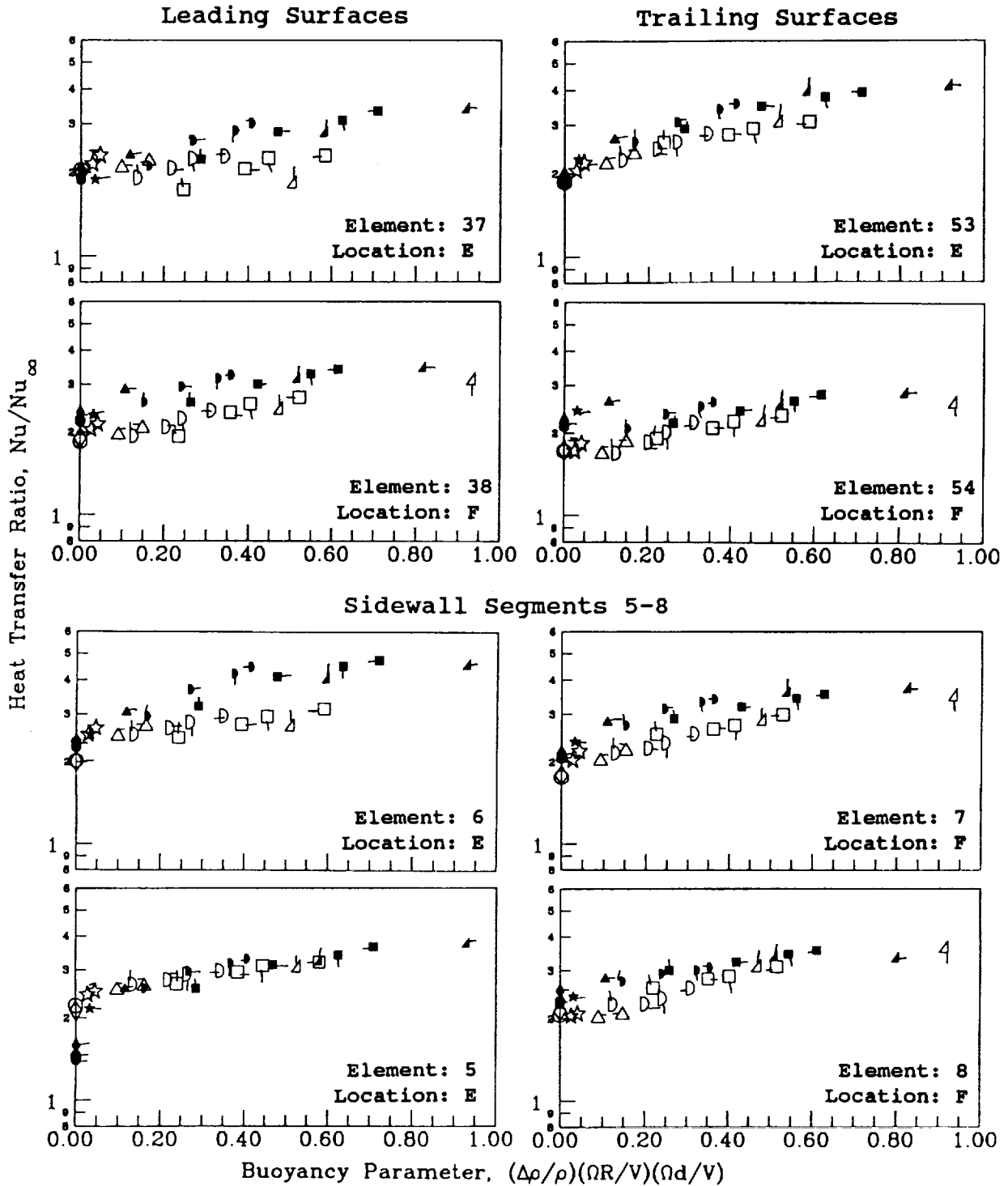


Figure 9.2b- Effect of Buoyancy Parameter on Heat Transfer Ratios in the First Turn.

Symbol	○	◇	☆	△	∩	□	▵	▽
Rotation No.	0.00	0.006	0.05	0.12	0.18	0.25	0.35	0.50

Symbol Flag	$\Delta T_{in} / \Delta T_{OC} (\circ F)$
○	22.4 (40)
○	44.4 (80)
○	66.7 (120)
○	88.9 (160)

Re = 25,000

$\alpha = 0$

$\bar{R}/d = 49$

Normal Trips - open symbols
Smooth Wall - solid symbols

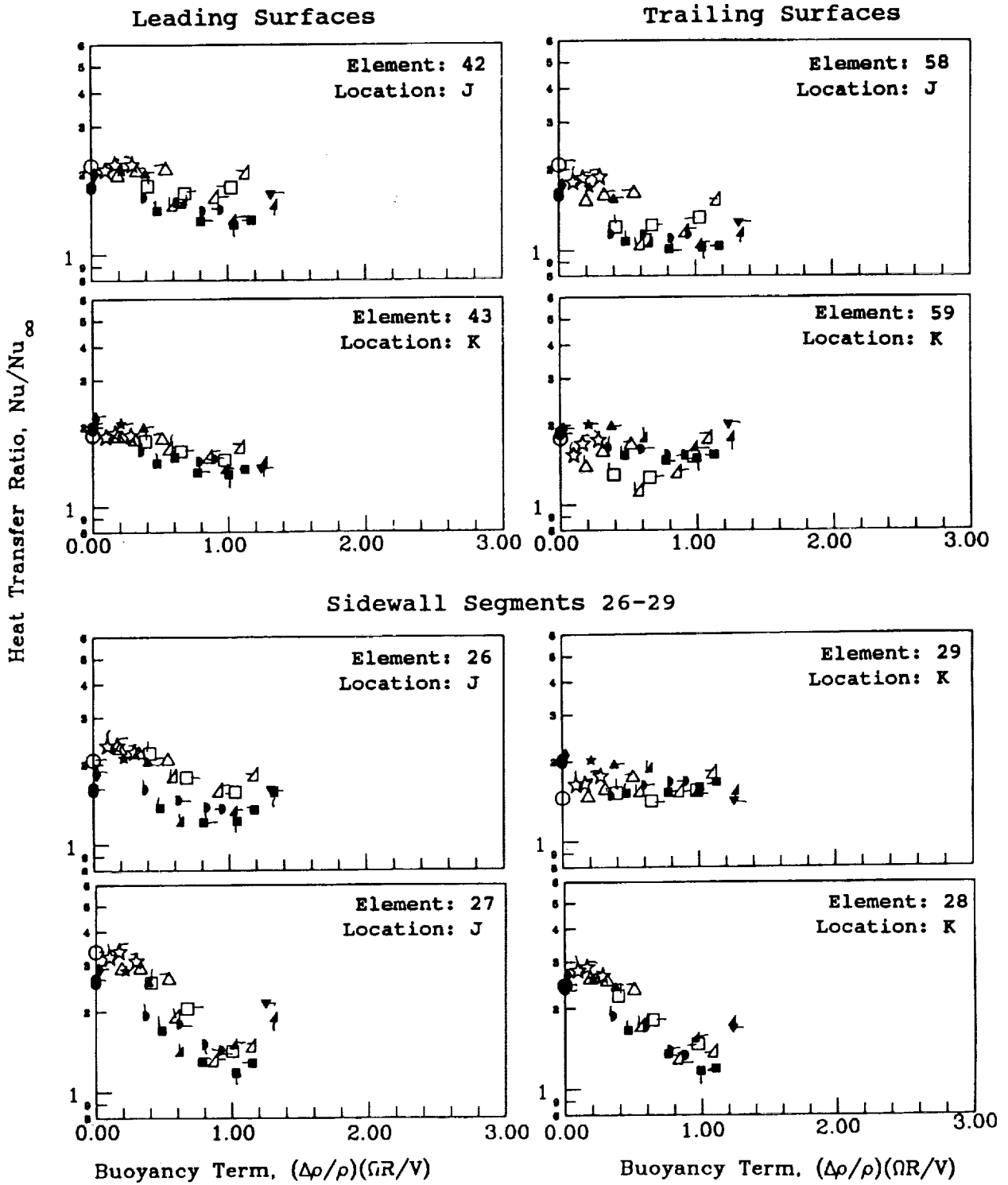


Figure 9.3a- Effect of Buoyancy Term on Heat Transfer Ratios in the Second Turn.

Symbol	○	◇	☆	△	∩	□	▴	▽
Rotation No.	0.00	0.006	0.05	0.12	0.18	0.25	0.35	0.50

Symbol Flag	$\Delta T_{in} / \Delta T_{OC} (OF)$
○	22.4 (40)
○	44.4 (80)
○	66.7 (120)
○	88.9 (160)

Re = 25,000 $\alpha = 0$ $\bar{R}/d = 49$

Skewed Trips - open symbols
Smooth Wall - solid symbols

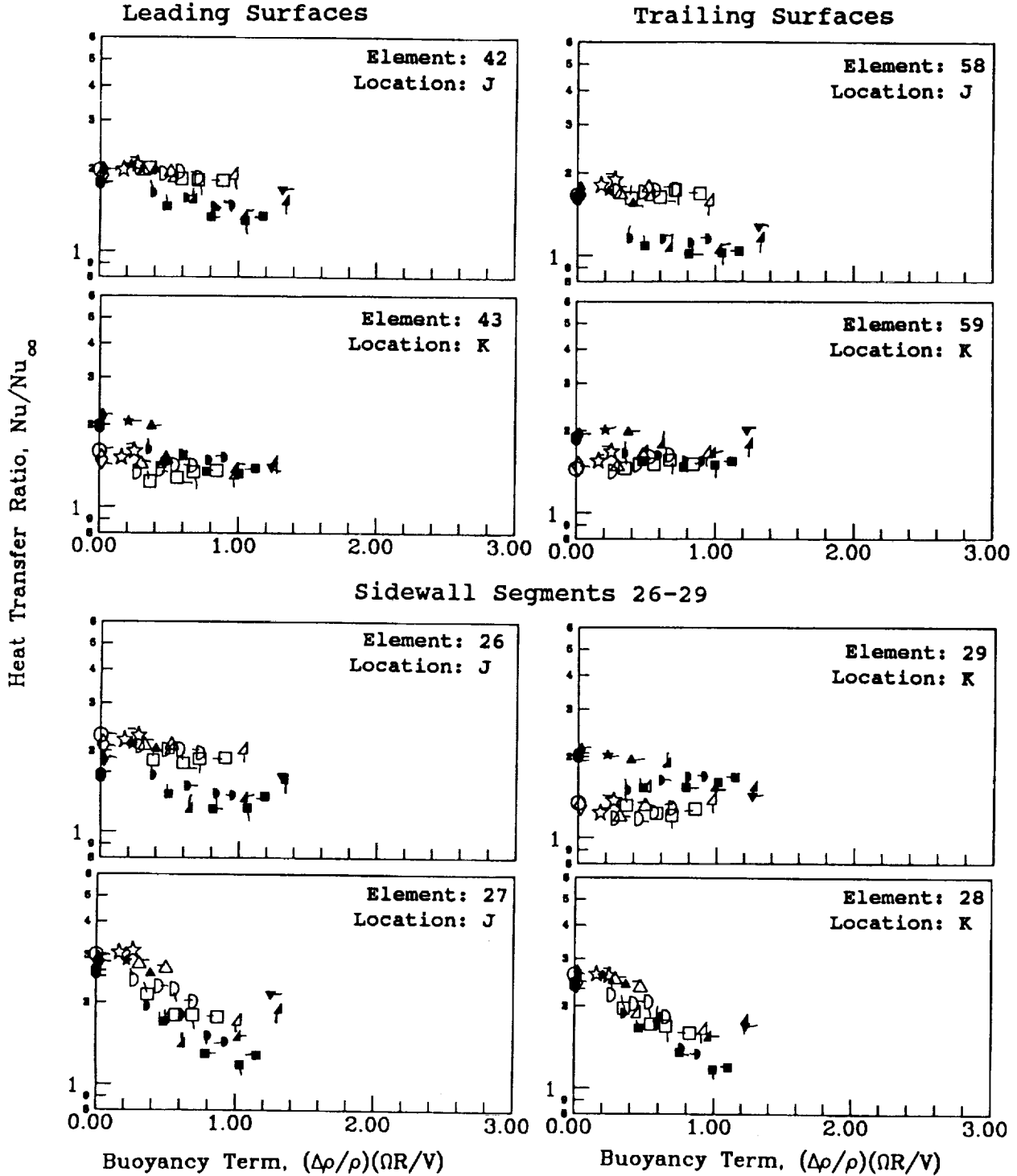


Figure 9.3b- Effect of Buoyancy Term on Heat Transfer Ratios in the Second Turn.

Symbol	○	◇	☆	△	∩	□	▵	▽
Rotation No.	0.00	0.006	0.05	0.12	0.18	0.25	0.35	0.50

Symbol Flag	$\Delta T_{in} / \Delta T_{out}$ (°F)
○	22.4 (40)
○-	44.4 (80)
○	66.7 (120)
○	88.9 (160)

Re = 25,000 $\alpha = 0$ $\bar{R}/d = 49$

Normal Trips - open symbols
Smooth Wall - solid symbols

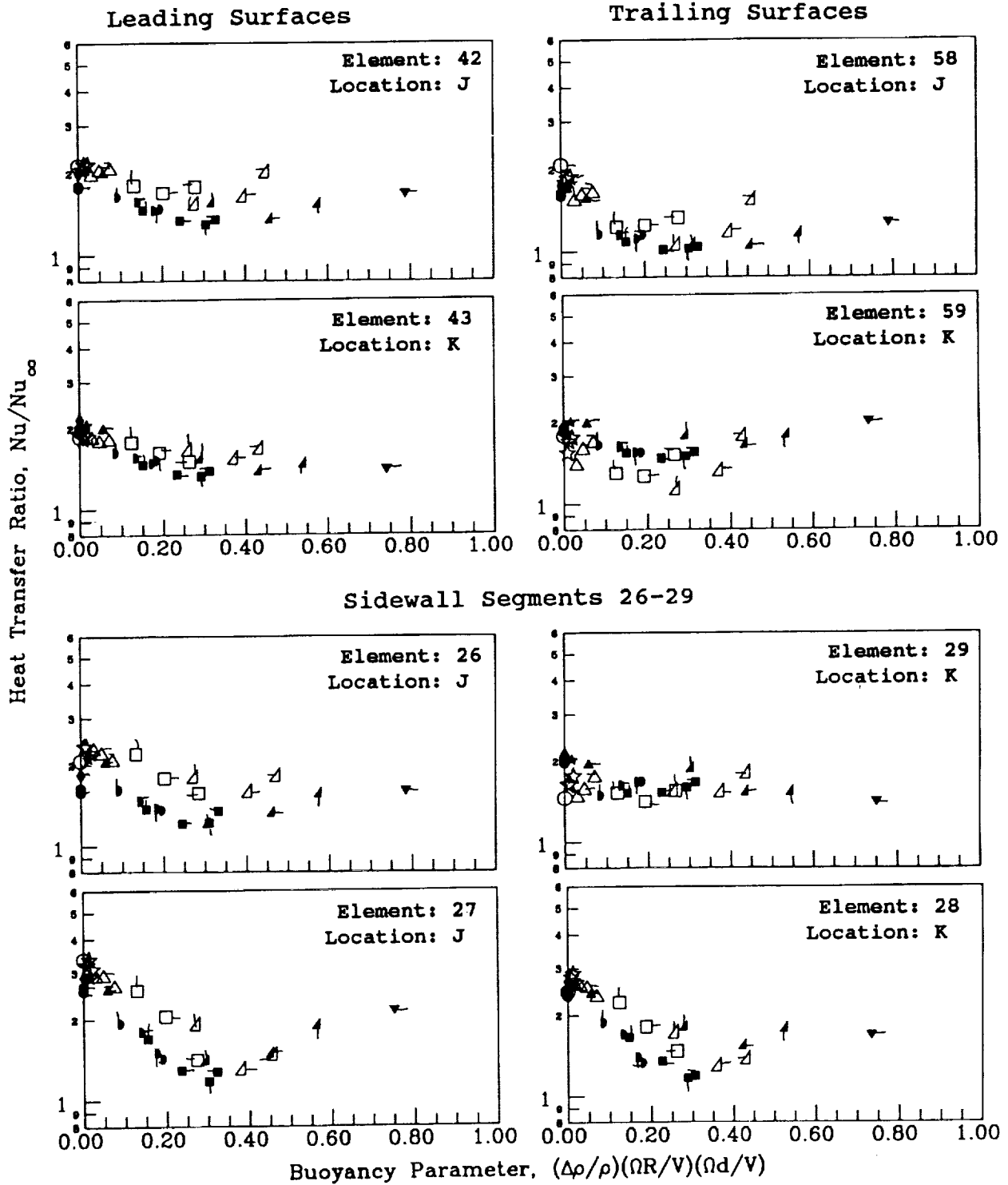


Figure 9.4a- Effect of Buoyancy Parameter on Heat Transfer Ratios in the Second Turn.

Symbol	○	◇	☆	△	D	□	▴	▽
Rotation No.	0.00	0.006	0.05	0.12	0.18	0.25	0.35	0.50

Symbol Flag	ΔT_{in} ΔT_{out} (°F)
○	22.4 (40)
○	44.4 (80)
○	66.7 (120)
○	88.9 (160)

Re = 25,000

$\alpha = 0$

$\bar{R}/d = 49$

Skewed Trips - open symbols

Smooth Wall - solid symbols

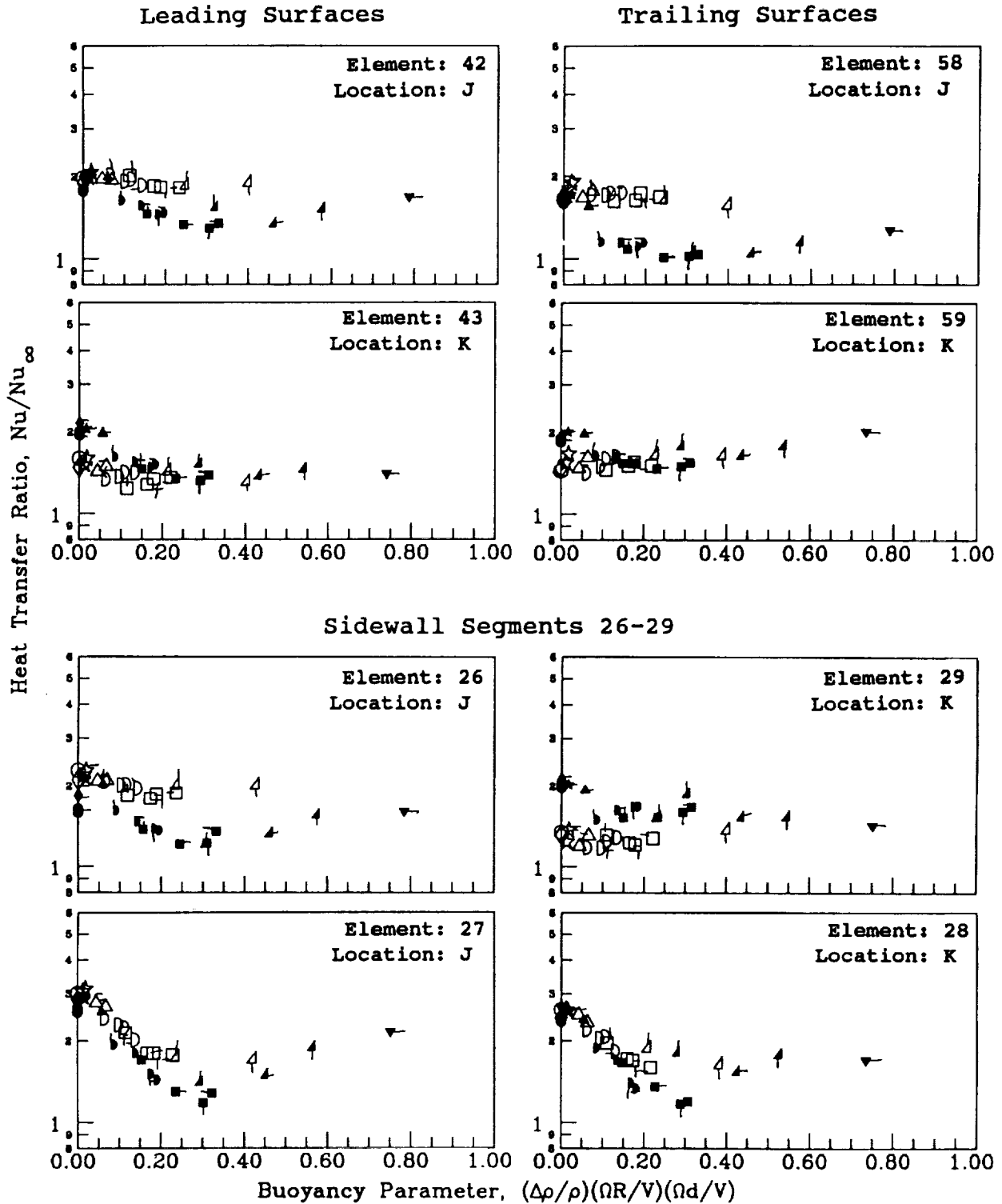


Figure 9.4b- Effect of Buoyancy Parameter on Heat Transfer Ratios in the Second Turn.

except for heater element 37 which is the first leading surface section downstream of the straight section. The heat transfer ratios for the leading surfaces (elements 37 & 38) and the first two side walls (5 & 6) of the model with skewed trips are correlated well by the buoyancy term. The heat transfer ratios for the trailing surfaces (Sections 53 and 54) and the downstream side walls (Sections 7 and 8) are well correlated by the buoyancy parameter.

The decrease in heat transfer ratio in the tip turn region, relative to the heat transfer for the model with smooth walls is attributed to the thicker viscous and thermal layers as the flow enters the turn region in models with trips. Numerical studies with constant density and buoyant flows will be required to sort out the complex relationships due to the conservation of vorticity and the buoyant forces in the turn regions.

9.2 Root Turn

The variation of heat transfer ratio with the buoyancy term and the buoyancy parameter for the root turn are presented in Figures 9.3 and 9.4. Note that for both models with trips and for the model with smooth walls, the heat transfer ratio generally decreases with rotation.

For the model with normal trips, the heat transfer ratio decreases as much as 60 percent of the value for the stationary model. When the heat transfer ratio decreases significantly with rotation, a minimum value was reached and further increase of rotation number or inlet density ratio resulted in an increase in the heat transfer ratio. The heat transfer ratio was well correlated by the buoyancy parameter for all the test sections for the model with normal trips.

The heat transfer ratios on the leading and trailing surfaces for the model with skewed trips were generally less sensitive to rotation than either the models with normal trips or with smooth walls. The largest decrease in heat transfer ratio on a leading surface due to rotation was to 62 percent of the stationary value for element 43. A minimum value was not apparently reached as had been obtained from the models with normal trips and with smooth walls. The lowest heat transfer ratio occurred for the value of the buoyancy parameter near where the minimums were obtained for the other models. The variation of the heat flux ratios for the root turn of the model with skewed trips was better correlated with the buoyancy parameter.

The decreases in the heat transfer in the root turn region are attributed to the migration of the slow warm fluid along the wall toward the center of rotation due to the radial pressure gradients. The colder fluid is caused to flow toward the unheated portion of the root turn region by Coriolis forces as well as the radial pressure gradient. Further insight into these complicated flow regions will be obtained from the numerical studies of flow and heat transfer in rotating coolant passages being conducted under other programs, concurrently with the preparation of this report.

10.0 COMPARISON WITH OTHER RESULTS

A limited number of rotating heat transfer experiments have been published with the passage and wall trip geometries, flow conditions and the heat transfer boundary condition (i.e. constant model wall temperature) employed in the present program. Following are comparisons and comments regarding heat transfer in stationary and rotating radial coolant passages presently available to the authors.

10.1 Stationary Experimental Results

The results from Test No. 301, the Stationary Baseline Flow Condition for the model with normal trips, are compared with results from Boyle (1984) and Han et al. (1986) in Figure 10.1. The present results in the region with trips, $3 < X/d < 14$, are almost identical with those from Boyle. The Boyle results were obtained for a constant heat flux boundary condition and sharp cornered trips which are modest variations from the present experiment. Heat transfer ratios from the surfaces with trips are generally consistent with the data band for Han's measurements. Note that the heat transfer results from the present program for $X/d < 3$ are from the smooth wall surfaces near the inlet of the first passage. However, in general, the levels of heat transfer augmentation due to the presence of the trips are consistent with those of Boyle and Han et al.

10.2 Rotating Analytical Results

At present, results from numerical studies for flow and heat transfer in rotating coolant passages with wall trip geometries (similar to the normal and skewed trip geometries of this study) are unavailable for comparison in this report. However, one numerical study, Taylor et al. (1991), has been conducted with a circular duct and square shaped ribs around the entire coolant passage. The ribs had a height to tube diameter ratio equal to 0.23. The numerical study was conducted with and without ribs for zero rotation and with $Ro = 0.0$ and 0.05 for ribs. The results from this study showed that the heat transfer was dominated by the rib geometry and was not significantly altered by rotation at $Ro = 0.05$. The present experiments had alternating trips on two walls with a local flow blockage of 10 percent. The referenced analysis had a local blockage at the rib inside diameter of 71 percent. Their calculations show an approximately 10 percent variation of the heat transfer coefficients, on the leading and trailing surfaces. The conclusion from their analysis is that the rib geometry dominates the average heat transfer for 71 percent blockage and $Ro = 0.05$. The present results in Figure 7.1a show that the heat transfer for the 10 percent blockage rib is increased by 150 percent due to the ribs. The heat transfer from the present model is also increased by 20 percent on the trailing surface and decreased by 20 percent on the leading surface due to rotation for $Ro = 0.05$.

10.3 Rotating Experimental Results

Results from this study have shown that rotational and buoyancy forces strongly influence turbulent heat transfer in rotating passages with trips normal to the flow for conditions found in gas turbine blades. The heat transfer results from stationary models with similar geometries agree quite well with the present work, i.e. Boyle (1984), Han et al. (1986) and Metzger et al. (1988). The heat transfer results from rotating models are more difficult to compare because of differences in the geometries and the boundary conditions. However, the heat transfer results of Clifford (1985) and Taslim et al. (1989) obtained with rotation will be related to the present results.

Clifford (1985) obtained heat transfer coefficients in a multi-pass model with trips normal to the flow using transient measurement techniques. Direct comparison with

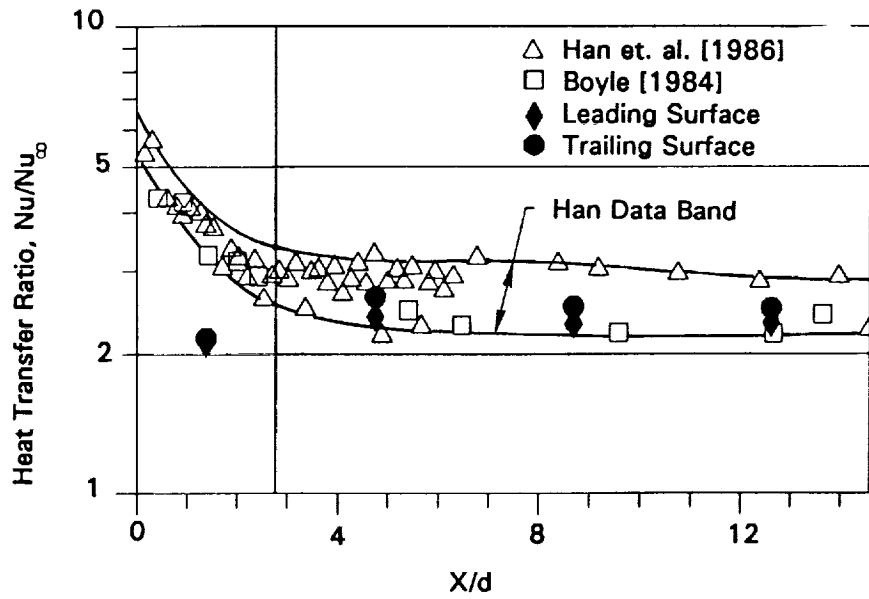


Figure 10.1- Comparison of Stationary Heat Transfer Results From Leading and Trailing Surfaces With Boyle (1984) and Han et. al. (1986).

Clifford's results is not possible due to the lack of specific model geometry and precise test conditions. Clifford observed increases in heat transfer of 36 percent on the pressure side of the model and decreases of 24 percent on the suction side of the first passage. Clifford's trends are in general agreement with the present results. However, the effects of rotation measured by Clifford are somewhat less than those measured in the present experiment. Clifford's heat transfer data from the second, inward flowing passage, was generally consistent with the present results.

Taslim et al. (1989) also obtained heat transfer results in a rotating square passage with trips normal to the flow for several trip heights. Trips were square-edged and were mounted on two opposing walls (one heated). The remaining smooth walls and one of the walls with trips were unheated. Although all of the heat transfer results with rotation measured by Taslim were greater than the stationary value for $Re_d = 24800$ and $e/D = 0.133$, the leading side heat transfer coefficients with rotation decreased with increasing rotation rate. This effect is similar to that observed by Clifford and in the present results. Taslim also measured increases in heat transfer, for most Reynolds numbers, on the trailing side of the model with increases in rotation rate for low values of rotation rate followed by relative decreases for further increases in rotation. The observations of Taslim on the trailing side of the passage are inconsistent with the present experiment where heat transfer was observed to increase with increases in rotation rate for a similar range of rotation number. The differences in the measured effects of rotation on the trailing side heat transfer are attributed to the differences in trip geometry ($e/D = 0.1$ and round trips for the present work and $e/D = 0.133$ and square trips for Taslim) and to the differences in the wall boundary conditions ($T_w = \text{constant}$ for the present work and $q_w = \text{constant}$ on one wall for Taslim). Additional work is necessary to determine the effects of model geometry and thermal boundary conditions with rotation.

11.0 CORRELATING PARAMETERS FOR ROTATING COOLANT PASSAGES

As discussed in the preceding sections, the distribution of heat transfer coefficients on the test surfaces is complex. For stationary cooling passages, the heat transfer is a function of flow rate, wall geometry, distance from the inlet and turns and location around the passage. As the rotation of the coolant passages are increased, Coriolis forces become important. Increasing the density ratio with rotation causes the buoyancy effects to increase.

Correlation equations for each of the flow regions were developed for the smooth wall model in Volume I. With the added complications of wall trips, correlating parameters are selected herein for each region based on the present experimental results. The recommended correlating parameters for rotating coolant passages are presented in Table 11.1.

The correlations presented herein are based on flow in coolant passages with aspect ratios of 1.0 and maximum X/d values of 15. The characteristic length scale was d , the hydraulic diameter of the almost square cross section passage. For this geometry the distance between the leading and trailing walls (12.7mm, 0.5 in.) is approximately the same as the hydraulic diameter (13.2mm, 0.518 in.). This characteristic is noted without recommending what characteristic length be used for coolant passages with aspect ratios other than 1.0.

The effects of rotation on the heat transfer from the low pressure surfaces of the coolant passages are somewhat independent of whether the surface is smooth or has trips with $e/d = 0.1$ and $P/e = 10$. The heat transfer will decrease (from the stationary values for each wall surface) with increasing rotation from the stationary value until a minimum value due to Coriolis effects is reached. The heat transfer may increase above the minimum value when buoyancy effects are appreciable. Therefore similar decreases in heat transfer on the low pressure can be expected for trips with smaller values of e/d . Large decreases in the heat transfer on the leading (low pressure) surface with flow outward have also been noted by other investigators.

The heat transfer from the test surfaces with skewed trips was less sensitive to density ratio than that with normal trips (e.g., see Figures 7.5a & b and 7.6a & b). The authors' recommendation is that skewed trips be employed to prevent the occurrence of buoyancy driven flow characteristics which apparently produce the large variation in the heat transfer coefficients.

The turn regions for the present model do not have turning vanes or wall trips used in several gas turbines. However, the results show the significant effects of turn location and buoyancy on heat transfer from the turn surfaces.

A set of tabulated data and results for the experiments with the models with skewed trips, normal trips and smooth walls is available on magnetic tape from Mr. Fred Yeh at NASA Lewis Research Center.

**TABLE 11.1 RECOMMENDED CORRELATION PARAMETERS
FOR ROTATING COOLANT PASSAGES**

- BP – Buoyancy Parameter – $(\Delta\rho/\rho)(\Omega R/V)(\Omega d/V)$
 BT – Buoyancy Term – $(\Delta\rho/\rho)(\Omega R/V)$
 * – See Chapter 12 Conclusion No. 10.

Wall Geometry	Flow Region	Surface	Recommended Correlation Parameter	Figure
Normal Trips	First Passage/ Flow Outward	Leading	R_o for $R_o \leq 0.24$ BP for $R_o > 0.24$	7.1a 7.7a
		Trailing	BP	7.7a
		Side	BP	8.1a
	Second Passage/ Flow Inward	Leading	R_o	7.2a
		Trailing	*	7.2a, 7.5a, 7.8c
		Side	BP	8.2a
	Third Passage/ Flow Outward	Leading	R_o for $R_o \leq 0.24$ BP for $R_o > 0.24$	7.3a 7.9a
		Trailing	*	7.3a, 7.6a, 7.9a
		Side	BP	8.1a
	Turn/Tip	Leading	BT	9.1a
		Trailing	BT	9.1a
		Side	BT	9.1a
	Turn/Root	Leading	BP	9.4a
		Trailing	BP	9.4a
		Side	BP	9.4a
Skewed Trips	First Passage/ Flow Outward	Leading	R_o for $R_o \leq 0.24$ BP for $R_o > 0.24$	7.1b 7.7b
		Trailing	BP	7.7b
		Side	BP	8.1b
	Second Passage/ Flow Inward	Leading	BP	7.8b
		Trailing	BP	7.8b
		Side	BP	8.2b
	Third Passage/ Flow Outward	Leading	R_o	7.3b
		Trailing	BP	7.9b
		Side	BP	8.1b
	Turn/Tip	Leading	BT	9.1b
		Trailing	BP	9.2b
		Side	(1st half turn) BT (2nd half turn) BP	9.1b, 9.2b
	Turn/Root	Leading	BP	9.4b
		Trailing	BP	9.4b
		Side	BP	9.4b

12.0 SUMMARY OF RESULTS AND CONCLUSIONS

This program has resulted in an extensive body of experimental data from heat transfer experiments in a rotating square passage with normal and skewed trips. It is believed that the large range of test parameters makes this data set unique. The extensive data base aided greatly in the data analysis and correlation and in developing physical models for the complex heat transfer characteristics. A summary of the major program results and, where possible, conclusions concerning the separate effects of forced convection, Coriolis, buoyancy and flow direction on heat transfer is presented in this section. A more detailed discussion of these conclusions and the authors' speculations regarding physical models for the cause and effect relationships, can be found in Sections 5.0 through 9.0 of this report.

Results from the present experiments with normal and skewed trips in rotating, radial, square coolant passages show that Coriolis forces and buoyancy effects can strongly influence heat transfer. The heat transfer coefficients on surfaces with normal trips were especially sensitive to rotation and buoyancy, decreasing as much as to one-third the stationary value due to rotation and increasing by a factor of 2.5 due to buoyancy. These effects were greater than measured previously for a smooth wall model. However, the maximum effects of buoyancy on surfaces with skewed trips was less than occurred on smooth surfaces. The author's conclusions from these observations that skewed trips provide higher heat transfer coefficients and less sensitivity to buoyancy effects and that skewed trips, rather than normal trips, should be employed for rotating coolant passages.

The comparison of results from the present experiments using normal and skewed trips with previous results for smooth wall models show that flow and heat transfer in rotating coolant passages can be complex, especially when no single flow mechanism dominates the heat transfer process. The present results were obtained for normal and skewed trips with values of trip streamwise pitch to trip height ($P/e = 10$) and trip height to coolant passage width ($e/D = 0.1$), typical of those used in coolant passages. These trip geometries generally produced heat transfer coefficients two to three times those obtained for smooth wall passages. The wide range of heat transfer coefficients obtained (0.65 to 5.0 times the values for fully developed flow in smooth passages) indicates that it is prudent to have a data base available for the design of specific coolant passages used in rotating turbine blades.

Following are observations regarding the effects of forced convection, Coriolis forces, buoyancy and flow direction on the heat transfer:

1. Heat transfer is strongly affected by rotation, causing increases in heat transfer up to 5 times fully developed, smooth tube levels on the first passage trailing surfaces and decreases to 65% of fully developed, smooth tube levels on the leading surfaces, depending upon trip geometry.
2. Increasing the density ratio with high rotation numbers generally caused an increase in heat transfer. However, the increase in heat transfer for the inward flowing passage was generally greater than that for outward flow.
3. The heat transfer ratio on the high pressure surfaces with the skewed trips was less significantly affected by flow direction than the surfaces with smooth walls.
4. The heat transfer ratio on the high pressure surfaces with normal trips was significantly affected by flow direction. The heat transfer was a strong function of the buoyancy parameter for the high pressure surfaces in the first and third passages with flow radially outward. However, the heat transfer was relatively unaffected by the buoyancy parameter for flow radially inward.

5. Increases in the density ratio caused the maximum increase in heat transfer in passages with normal trips to be greater than the maximum increases measured from the same model with smooth surfaces.
6. The heat transfer ratio is a complex function of buoyancy parameter and density ratio on the low pressure surfaces of the coolant passages, regardless of flow direction.
7. The decreases in heat transfer on the leading surfaces with increases in rotation number are attributed to the combined effects of stabilization of the near-wall flow and cross-stream flows which cause heated, near wall fluid from the trailing and sidewall surfaces to accumulate near the leading side of the coolant passage.
8. Heat transfer ratios from rotating passages with normal or skewed trips at the highest rotation numbers and buoyancy parameters were not significantly greater than the heat transfer ratios measured in the same model with smooth surfaces for the same parameters. The highest heat transfer ratios on the high pressure sides with flow outward were only 20 to 25 percent greater than the heat transfer ratios for the same locations and flow conditions with smooth walls. Ten and fifteen percent of this increase was attributed to the increased surface area for the test sections with the normal and skewed trips, respectively.
9. The effects of varying Reynolds number on heat transfer in the stationary or rotating models was reasonably well correlated by the heat transfer ratio Nu/Nu_{∞} , where Nu_{∞} is the correlation for fully developed, turbulent flow in a stationary rectangular passage.
10. The heat transfer ratios for the test elements in each model with trips were reviewed to determine a recommended correlation parameter for each element. The rotation number, buoyancy parameter or buoyancy term were found to be an adequate correlating parameter for all test elements except those test elements for the trailing surfaces with normal trips in the second and third passages.

13.0 APPENDIX

13.1 Error Analysis

An analysis to determine the estimated error in measured heat transfer was conducted using the method described in Abernathy and Thompson (1973). The error analysis was a summation of the estimated inaccuracies in the data used to calculate the heat transfer coefficient and Nusselt number as shown below. When comparative testing is done (as in this program), Abernathy and Thompson suggest that biasing errors may be ignored. Therefore, only the precision errors were determined.

$$(Nu)^2 = \sum_{i=1}^n [(dNu/df_i)^2 (f_i)^2] \quad 13.1$$

where f_i are the parameters used to determine the Nusselt number.

To do the error analysis, assumptions of the estimated inaccuracies had to be made. Generally, where information was read by eye from a device (i.e., flowmeter, pressure gauge, etc.), the estimated accuracy was assumed to be 1/4 of the smallest increment. Voltages read by the acquisition system were assumed to be accurate to the least significant digit, except for the thermocouple emfs which were assumed to be accurate to only 25 micro-volts. A summary of the estimated inaccuracies follows:

<u>Parameter, VD</u>	<u>Estimated Error (+)</u>	<u>Method</u>
VD	0.000025 Volt	T.C. wire repeatability
VC	0.000025 Volt	T.C. wire repeatability
VB	0.0001 Volt	least significant measurement
E	0.001 Volt	least significant measurement
I	0.001 Volt	least significant measurement
QALOSS	(0.05) QALOSS	5% accurate estimate
FMA	0.25	1/4 increase on flow meter
CFMA	(0.005)CFMA	0.5% flow meter reading
BFMA	(0.005)BFMA	0.5% flow meter reading
PMin	0.25	1/4 increase
TMin	0.5	1/2 resolution
h	(0.02)h at the inlet	2%
	(0.06)h at the exit	6%

Note: h was only used to estimate the error of determining the effective heat transfer surface area.

This analysis, applied to the case where the stationary test point Reynolds Number is 25,000, showed the error of determining heat transfer at the entrance of the model was $\pm 2\%$ and the error at the exit was $\pm 7\%$ of the local heat transfer rate. Of the estimated error, over 90% was due to the error in determining the temperature. Nine percent of the estimated error was due to the error in determining the backloss.

13.2 Pressure Loss Measurements

Measurements were obtained during all heat transfer tests to determine the pressure drop through the serpentine coolant passage (Figure 3.6). The measurements in all three models for a nonrotating flow condition at a lower-than-standard flow pressure showed that a large fraction of the pressure drop occurred in the three straight test section segments for the models with trips whereas the principle pressure drop for the smooth wall model occurred in the 180 deg turns. The uncertainty in the pressure measurements and the low dynamic head of the flow at the standard flow pressure $1.01325 \times 10^6 \text{N/m}^2$ (10 atm) precluded the acquisition of data which could yield "benchmark quality" results for both the rotating and nonrotating tests. Typical results from these data indicate a variation in the pressure distribution; however, the overall pressure drop from the inlet to the exit of the model indicated small effects of rotation. Following is a discussion of the instrumentation, estimated accuracy, data analysis and typical results from the pressure distribution tests.

Instrumentation

The pressure tap locations are located in 16 sidewall test surface elements as shown in Figure 3.6. The pressure measurements were obtained with a Scanivalve Model ZOC14 (zero, operate, calibrate) differential electronic pressure scanner. The pressure measurement equipment was located on the rotating arm at a radius of approximately 30.5 cm (12"). The pressure scanner was encased in a thermal control unit (Scanivalve Model ZOC TCU). The thermal control unit is specified to maintain a uniform temperature to $\pm 2\text{C}$ ($\pm 1\text{F}$) in a stationary environment. The differential pressure transducers were referenced to pressure tap #1 (Figure 3.6). The power to and the signals from the electronic pressure scanner and thermal control unit were transmitted through sliprings for the rotating tests.

Estimate of Pressure Measurement Accuracy

Although the ZOC14 electronic pressure scanner was rated to be accurate within $\pm 0.08\%$ of the 6895N/m^2 (1 psi) full scale value (i.e., $5.516 \text{N/m}^2 - (\pm 0.0008 \text{ psi})$), the uncertainties associated with the transducer temperature variation, the rotating environment and the slipring noise reduced the estimated accuracy and repeatability to approximately 1% full scale or 68.95N/m^2 (0.01 psi). This accuracy is compatible with previous UTRC experience for pressure measurements in rotating systems. The value of 68.95N/m^2 (0.01 psi) is also approximately $1.0 q_{in}$ for the baseline flow condition.

Data Analysis

The pressure drops measured in the rotating serpentine coolant passage model were referenced to the pressure drop in the nonrotating model by (1) subtracting the pressure increases due to work from model rotation on the coolant at locations radially outward from pressure tap #1 and (2) adding the pressure drop due to work from model rotation on the coolant at locations radially inward from pressure tap #1. In the four legged model (Figure 3.6), this pressure rise is of the order $(\Omega^2 r^2 \Delta\rho)/4$. The pressure increase due to a nominal 33C (60F) temperature increase in the coolant temperature is approximately 20N/m^2 (0.003 psi) or $0.4 q_{in}$ for the 550 rpm test condition.

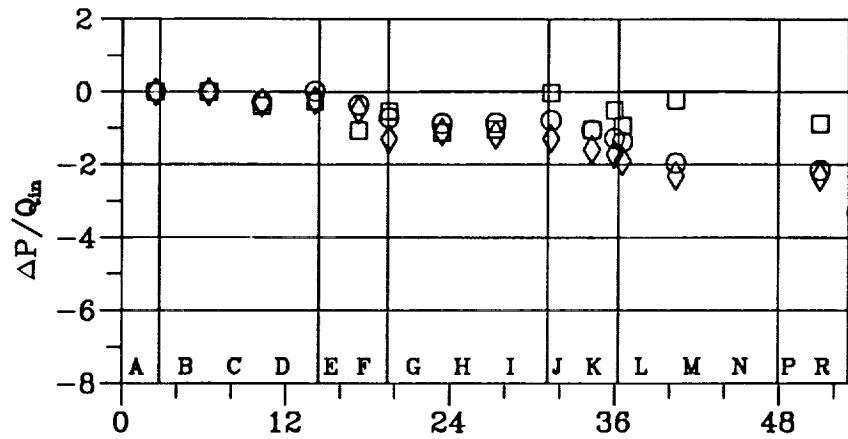
Results for Nonrotating Tests

Pressure drop ratios were measured in the nonrotating ($\Omega = 0$) models with trips for the operating flow conditions shown in Tables 4.1 and 4.2 along with comparable

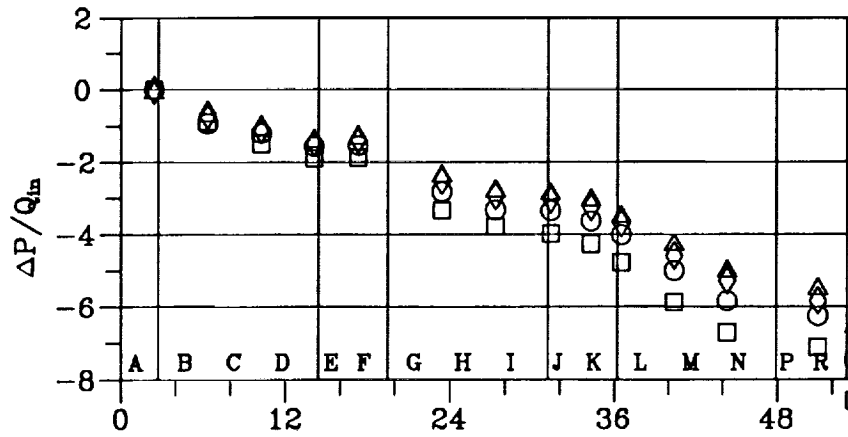
$\Omega = 0 \text{ rpm}$ $\Delta T \approx 44^\circ\text{C} (80^\circ\text{F})$

Symbol	□	○	◇	△
Re No.	12,500	25,000	50,000	75,000

a) Smooth Wall



b) Normal Trips



c) Skewed Trips

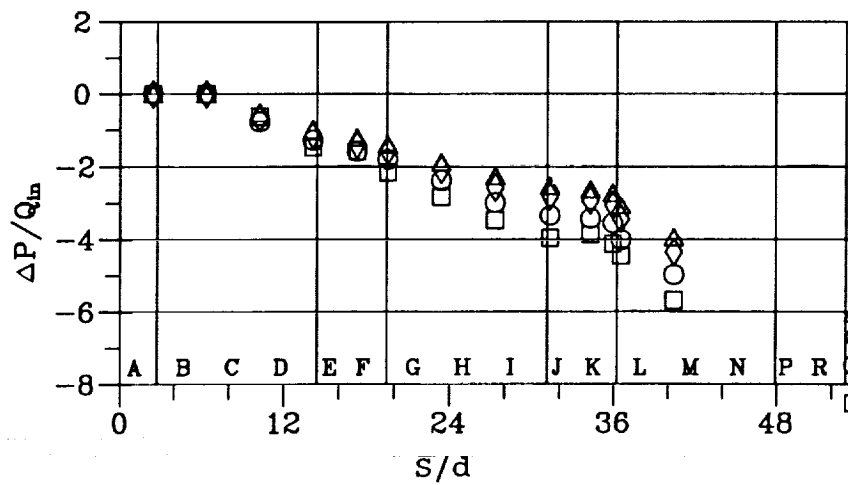
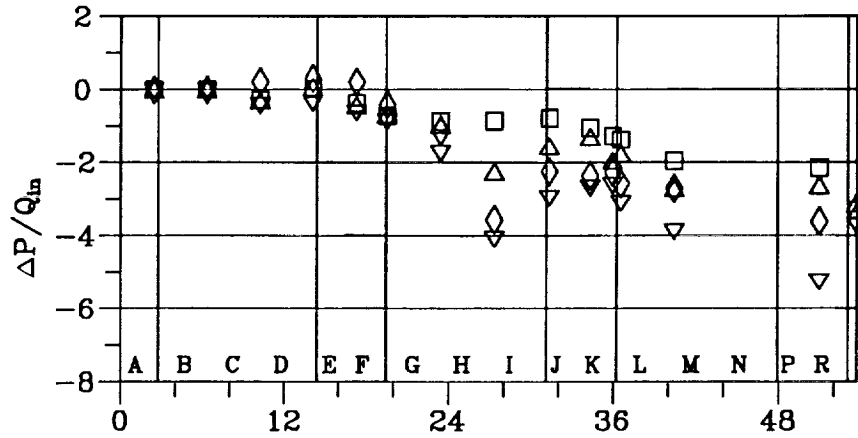


Figure 13.1- Effect of Reynolds Number on Dressure Drop in Model.

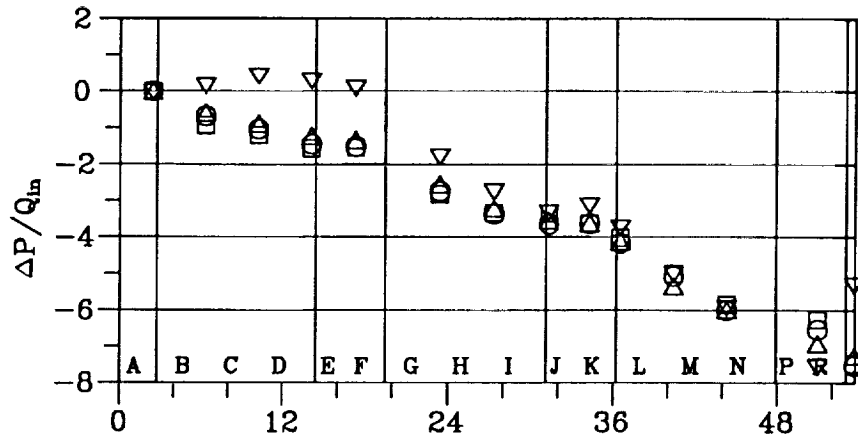
$\Delta T \approx 44^{\circ}\text{C}$ (80°F) $Re = 25,000$

Symbol	□	○	△	◇	▽
Speed (rpm)	0	145	275	412	550

a) Smooth Wall



b) Normal Trips



c) Skewed Trips

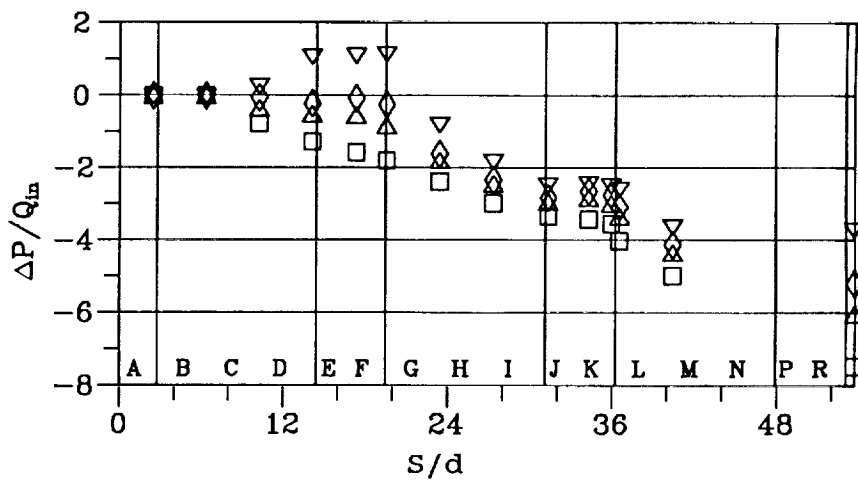


Figure 13.2- Effect of Rotation on Pressure Drop in Model.

smooth wall data. The pressure drop in the model with respect to the pressure at Tap No. 1 is shown in Figure 13.1. Note that the pressure drop ratios decrease with increasing Reynolds number (as expected). As noted previously, the uncertainty for the measurements for $Re = 25,000$ is $1.0 q_{in}$. This uncertainty decreases to $0.25 q_{in}$ with Re equal approximately 50,000 and increases to $4.0 q_{in}$ with Re equal approximately 12,500.

Results for Rotating Tests

Pressure drops were measured for rotating tests with Re approximately equal to 25,000 (Figure 13.2). The uncertainties in the measurements and the several assumptions required for data analysis make interpretation of the results difficult. However, the overall pressure drop measurements, from pressure taps located near the inlet and exit of the model, are expected to be the most accurate. Note that for the smooth wall and the normal trip models, the pressure drop ratio across the model is independent of rotation rate, except for the 550 rpm flow condition with the normal trip model. The pressure drop ratio across the normal trip model (Figure 13.2b) was more than twice the pressure drop across the smooth wall model (Figure 13.2a), i.e., $\Delta p/Q_{in}$ increased from 3.5 to 7.5. The pressure drop ratio for the normal trip model at 550 rpm was 5.5. This latter flow condition also showed a significant decrease in heat transfer ratio on several surfaces of the heat transfer model which was attributed to unattached flow regions. This anomalous pressure measurement may be related to the large variation in measured heat transfer; however, the uncertainties in the measurements preclude definitive conclusions without further measurements.

The overall pressure drop ratios for the flow in the model with skewed trips indicate a decrease in the pressure drop ratio with increasing rpm, i.e. rotation number, Ro . The consistency of the pressure drop relationship at all the streamwise locations lends credence to the measurements. The oblique flow guidance characteristics of the skewed trips and the similar heat transfer results from the skewed trip model at the highest rotation and buoyancy flow conditions are also in agreement with the measured result. However, the uncertainties in the measurements preclude definitive conclusions without further measurements with more sensitive pressure transducers.

13.3 Model Geometry Information

The test model heat transfer geometry information is tabulated in Table 13.1 as a function of the local test segment heater location (1-64). The test model pressure tap geometry information is tabulated in Table 13.2 as a function of pressure tap location (1-16). The variable names for each column are defined in the List of Symbols.

Table 13.1- Model Heat Transfer Geometry Information.

Heater Segment No.	d		A		CA		RADH		S		X	
	cm	(in.)	cm ²	(in. ²)	cm ²	(in. ²)	cm	(in.)	cm	(in.)	cm	(in.)
1	1.3155	0.5179	1.5923	0.2468	3.7258	0.5775	10.190	4.012	1.748	0.688	1.748	0.688
2	1.3155	0.5179	1.5923	0.2468	5.2484	0.8135	14.557	5.731	6.114	2.407	6.114	2.407
3	1.3155	0.5179	1.5923	0.2468	5.2484	0.8135	19.637	7.731	11.194	4.407	11.194	4.407
4	1.3155	0.5179	1.5923	0.2468	5.2484	0.8135	24.717	9.731	16.274	6.407	16.274	6.407
5	1.4323	0.5639	1.9555	0.3031	2.5116	0.3893	28.400	11.181	19.644	7.734	19.644	7.734
6	1.4323	0.5639	1.9555	0.3031	2.4277	0.3763	29.972	11.800	21.303	8.387	21.303	8.387
7	1.4323	0.5639	1.9555	0.3031	2.4277	0.3763	29.972	11.800	22.964	9.041	22.964	9.041
8	1.4323	0.5639	1.9555	0.3031	2.5166	0.3893	28.400	11.181	24.623	9.694	24.623	9.694
9	1.3155	0.5179	1.5923	0.2468	5.2484	0.8135	24.717	9.731	27.993	11.021	2.540	1.000
10	1.3155	0.5179	1.5923	0.2468	5.2484	0.8135	19.637	7.731	33.073	13.021	7.620	3.000
11	1.3155	0.5179	1.5923	0.2468	5.2484	0.8135	14.557	5.731	38.153	15.021	12.700	5.000
12	1.3155	0.5179	1.5923	0.2468	5.2484	0.8135	14.557	5.731	49.873	19.635	2.540	1.000
13	1.3155	0.5179	1.5923	0.2468	5.2484	0.8135	19.637	7.731	54.953	21.635	7.620	3.000
14	1.3155	0.5179	1.5923	0.2468	5.2484	0.8135	24.717	9.731	60.033	23.635	12.700	5.000
15	1.4323	0.5639	1.9555	0.3031	2.5116	0.3893	28.400	11.181	63.403	24.962	16.071	6.327
16	1.4323	0.5639	1.9555	0.3031	2.4277	0.3763	29.972	11.800	65.062	25.615	17.729	6.980
17	1.4323	0.5639	1.9555	0.3031	2.4277	0.3763	29.972	11.800	66.723	26.269	19.390	7.634
18	1.4323	0.5639	1.9555	0.3031	2.5116	0.3893	28.400	11.181	68.382	26.922	21.049	8.287
19	1.3155	0.5179	1.5923	0.2468	3.7258	0.5775	10.190	4.012	1.748	0.688	1.748	0.688
20	1.3155	0.5179	1.5923	0.2468	5.2484	0.8135	14.557	5.731	6.114	2.407	6.114	2.407
21	1.3155	0.5179	1.5923	0.2468	5.2484	0.8135	19.637	7.731	11.194	4.407	11.194	4.407
22	1.3155	0.5179	1.5923	0.2468	5.2484	0.8135	24.717	9.731	16.274	6.407	16.274	6.407
23	1.3155	0.5179	1.5923	0.2468	5.2484	0.8135	24.717	9.731	27.993	11.021	2.540	1.000
24	1.3155	0.5179	1.5923	0.2468	5.2484	0.8135	19.637	7.731	33.073	13.021	7.620	3.000
25	1.3155	0.5179	1.5923	0.2468	5.2484	0.8135	14.557	5.731	38.153	15.021	12.700	5.000
26	1.4323	0.5639	1.9555	0.3031	2.5116	0.3893	10.874	4.281	41.524	16.348	16.071	6.327
27	1.4323	0.5639	1.9555	0.3031	2.4277	0.3763	9.301	3.662	43.185	17.002	17.729	6.980
28	1.4323	0.5639	1.9555	0.3031	2.4277	0.3763	9.301	3.662	44.016	17.329	19.390	7.634
29	1.4323	0.5639	1.9555	0.3031	2.5116	0.3893	10.874	4.281	46.505	18.309	21.049	8.287
30	1.3155	0.5179	1.5923	0.2468	5.2484	0.8135	14.557	5.731	49.873	19.635	2.540	1.000
31	1.3155	0.5179	1.5923	0.2468	5.2484	0.8135	19.637	7.731	54.953	21.635	7.620	3.000
32	1.3155	0.5179	1.5923	0.2468	5.2484	0.8135	24.717	9.731	60.033	23.635	12.700	5.000
33	1.3155	0.5179	1.5923	0.2468	3.7258	0.5775	10.190	4.012	1.748	0.688	1.748	0.688
34	1.3155	0.5179	1.5923	0.2468	5.2484	0.8135	14.557	5.731	6.114	2.407	6.114	2.407
35	1.3155	0.5179	1.5923	0.2468	5.2484	0.8135	19.637	7.731	11.194	4.407	11.194	4.407
36	1.3155	0.5179	1.5923	0.2468	5.2484	0.8135	24.717	9.731	16.274	6.407	16.274	6.407
37	1.4323	0.5639	1.9555	0.3031	5.1877	0.8041	28.819	11.346	20.475	8.061	20.475	8.061
38	1.4323	0.5639	1.9555	0.3031	5.1877	0.8041	28.819	11.346	23.795	9.368	23.795	9.368
39	1.3155	0.5179	1.5923	0.2468	5.2484	0.8135	24.717	9.731	27.993	11.021	2.540	1.000
40	1.3155	0.5179	1.5923	0.2468	5.2484	0.8135	19.637	7.731	33.073	13.021	7.620	3.000
41	1.3155	0.5179	1.5923	0.2468	5.2484	0.8135	14.557	5.731	38.153	15.021	12.700	5.000
42	1.4323	0.5639	1.9555	0.3031	5.1877	0.8041	10.455	4.116	42.354	16.675	16.901	6.654
43	1.4323	0.5639	1.9555	0.3031	5.1877	0.8041	10.455	4.116	45.674	17.982	20.221	7.961
44	1.3155	0.5179	1.5923	0.2468	5.2484	0.8135	14.557	5.731	49.873	19.635	2.540	1.000
45	1.3155	0.5179	1.5923	0.2468	5.2484	0.8135	19.637	7.731	54.953	21.635	7.620	3.000
46	1.3155	0.5179	1.5923	0.2468	5.2484	0.8135	24.717	9.731	60.033	23.635	12.700	5.000
47	1.4323	0.5639	1.9555	0.3031	5.1877	0.8041	28.819	11.346	64.234	25.289	16.901	6.654
48	1.4323	0.5639	1.9555	0.3031	5.1877	0.8041	28.819	11.346	67.554	26.596	20.221	7.961
49	1.3155	0.5179	1.5923	0.2468	3.7258	0.5775	10.190	4.012	1.748	0.688	1.748	0.688
50	1.3155	0.5179	1.5923	0.2468	5.2484	0.8135	14.557	5.731	6.114	2.407	6.114	2.407
51	1.3155	0.5179	1.5923	0.2468	5.2484	0.8135	19.637	7.731	11.194	4.407	11.194	4.407
52	1.3155	0.5179	1.5923	0.2468	5.2484	0.8135	24.717	9.731	16.274	6.407	16.274	6.407
53	1.4323	0.5639	1.9555	0.3031	5.1877	0.8041	28.819	11.346	20.475	8.061	20.475	8.061
54	1.4323	0.5639	1.9555	0.3031	5.1877	0.8041	28.819	11.346	23.795	9.368	23.795	9.368
55	1.3155	0.5179	1.5923	0.2468	5.2484	0.8135	24.717	9.731	27.993	11.021	2.540	1.000
56	1.3155	0.5179	1.5923	0.2468	5.2484	0.8135	19.637	7.731	33.073	13.021	7.620	3.000
57	1.3155	0.5179	1.5923	0.2468	5.2484	0.8135	14.557	5.731	38.158	15.021	12.700	5.000
58	1.4323	0.5639	1.9555	0.3031	5.1877	0.8041	10.455	4.116	42.354	16.675	16.901	6.654
59	1.4323	0.5639	1.9555	0.3031	5.1877	0.8041	10.455	4.116	45.674	17.982	20.221	7.961
60	1.3155	0.5179	1.5923	0.2468	5.2484	0.8135	14.557	5.731	49.873	19.635	2.540	1.000
61	1.3155	0.5179	1.5923	0.2468	5.2484	0.8135	19.637	7.731	54.953	21.635	7.620	3.000
62	1.3155	0.5179	1.5923	0.2468	5.2484	0.8135	24.717	9.731	60.033	23.635	12.700	5.000
63	1.4323	0.5639	1.9555	0.3031	5.1877	0.8041	28.819	11.346	64.234	25.289	16.901	6.654
64	1.4323	0.5639	1.9555	0.3031	5.1877	0.8041	28.819	11.346	67.554	26.596	20.221	7.961

Table 13.2- Model Pressure Tap Geometry Information.

Smooth & Skewed Trips Pressure Tap No.	Normal Trips Pressure Tap No.	RADP		S		X	
		cm	(in.)	cm	(in.)	cm	(in.)
1	1	11.582	4.560	3.139	1.236	3.139	1.236
2	2	16.662	6.560	8.219	3.236	8.219	3.236
3	4	21.742	8.560	13.299	5.236	13.299	5.236
4	5	26.822	10.560	18.379	7.236	18.379	7.236
5	6	30.175	11.880	22.570	8.886	22.570	8.886
6	-	26.822	10.560	25.491	10.036	0.038	0.015
7	7	21.742	8.560	30.571	12.036	5.118	2.015
8	8	16.662	6.560	35.651	14.036	10.198	4.015
9	9	11.430	4.500	40.909	16.106	15.456	6.085
10	10	8.890	3.500	44.770	17.626	19.317	7.605
11	-	11.430	4.500	46.904	18.466	21.450	8.445
12	11	12.217	4.810	47.691	18.776	0.358	0.141
13	12	17.297	6.810	52.771	20.776	5.438	2.141
14	13	22.377	8.810	57.851	22.776	10.518	4.141
15	14	30.175	11.880	66.487	26.176	19.154	7.541
16	16	11.582	4.560	84.673	33.336	15.574	6.171

LIST OF SYMBOLS

A_c	Cross sectional area of the passage, cm^2 (in^2)
BFMA	Flow meter (B) reading, kg/sec (lbm/sec)
Cf	Skin friction coefficient, $\tau_w/(\rho V^2/2)$, dimensionless
CA	Local heated test surface segment (heater segment) surface area, cm^2 (in^2)
CFMA	Flow meter (C) reading, kg/sec (lbm/sec)
d	Local hydraulic diameter of the passage, cm (in)
e	Trip height
E	Heater element supply voltage, volts
FMA	Flow meter reading, kg/sec (lbm/sec)
Gr	Local rotational Grashof number based on hydraulic diameter, $(\Omega^2 R d^3)/(\rho_b - \rho_w)(\rho_b/\mu^2)$, dimensionless
Gr/Re ²	Local buoyancy parameter based on hydraulic diameter, $((\rho_b - \rho_w)/\rho_b)(\Omega R/V)(\Omega d/V)$, dimensionless
h	Local heat transfer coefficient, $Q_{\text{net}}/(CA(T_w - T_b))$, $W/(\text{m}^2\text{-C})$ ($\text{Btu}/(\text{hr-ft}^2\text{-F})$)
H	Coolant passage height, cm (in)
HP	High pressure surface
I	Heater segment current, amps
k	Thermal conductivity, $W/(\text{m-C})$ ($\text{Btu}/(\text{hr-ft-F})$)
LP	Low pressure surface
m	Mass flow rate, kg/sec (lbm/sec)
Nu	Local Nusselt number based on hydraulic diameter, hd/k , dimensionless
Nu _∞	Nusselt number for fully developed turbulent flow in a square duct $0.0176(\text{Re}^{0.8})$, dimensionless
P	Trip pitch (spacing)
P	Pressure
ΔP	Pressure difference between the local static pressure tap readings (corrected for pumping effects to the radius of model pressure tap #1) and the model pressure tap #1, N/m^2 (psi)

$\Delta P/Q_{in}$	Pressure difference between the local static pressure tap readings (corrected for pumping effects to the radius of model pressure tap #1) and the model pressure tap #1, normalized by the inlet dynamic pressure, dimensionless
Pr	Prandtl number, dimensionless
Q_{in}	Channel inlet dynamic pressure, N/m^2 (psi)
Q_{net}	Net heat rate input into the flow field from the heater segment, W (Btu/hr)
QALOSS	Heat flux loss from the heater elements, W/m^2 (Btu/(hr-ft ²))
R	Radial distance from the axis of rotation, RADH + RBASE for the heater segments, RADP + RBASE for the pressure tap locations. cm (in)
\bar{R}	Average model radius from the axis of rotation, cm (in)
R/d	Non-dimensional radial location
\bar{R}/d	Non-dimensional radial location based on the average model radius
RADH	Radial location to the center of a heater segment relative to the base of the model (RBASE). cm (in)
RADP	Radial location of wall pressure tap measured from the base of the model (RBASE). cm (in)
RBASE	Distance from the axis of rotation to the base of the model. The "base of the model" was an arbitrarily defined reference - point. RBASE equals 46.673 cm (18.375 in) for R/d = 49, and - RBASE equals 24.130 cm (9.50 in) for R/d = 33.
Re	Reynolds number based on hydraulic diameter, $md/A\mu$, dimensionless
Ro	Rotation number, $\Omega d/V$, dimensionless
S	Distance measured from the leading edge of the first channel heater segment. cm (in)
S/d	Non-dimensional distance measured from the leading edge of the first channel heater
STD	Standard rotating baseline flow conditions, Re = 25000, Ro = 0.24, $(\Delta\rho/\rho)_{in} = (\Delta T/T)_{in} = 0.13$, $\bar{R}/d = 49$, $\alpha = 0$, dimensionless
T_b	Local bulk temperature of the fluid. K (R)
T_w	Local wall temperature of the channel heater segment. K (R)
ΔT	Temperature difference, $(T_w - T_b)$. C (F)
$\Delta T/T$	Local temperature ratio, $(T_w - T_b)/T_w$, dimensionless
$(\Delta T/T)_{in}$	Temperature ratio, $(T_w - T_b)/T_w$, where T_b is evaluated at the inlet of the model, dimensionless. Note: $(\Delta T/T)_{in} = (\Delta\rho/\rho)_{in}$

V	Average coolant passage velocity at axial location, m/sec (ft/sec)
VB	Thermocouple voltage, volts
VC	Thermocouple voltage, volts
VD	Thermocouple voltage, volts
w	Coolant passage width
X	Distance measured from the leading edge of the first channel heater segment or the end of the last turn region, cm (in)
X/d	Non-dimensional distance measured from the leading edge of the first channel heater segment or end of the last turn region.
α	Model test section orientation angle with respect to the axis of rotation, deg
μ	Absolute viscosity, kg/m-sec (lbm/ft-sec)
ν	Kinematic viscosity, m^2/sec (ft^2/sec)
ρ_b	Local channel density based on local bulk temperature, kg/m^3 (lbm/ft ³)
ρ_w	Local channel density based on local wall surface temperature, kg/m^3 (lbm/ft ³)
$\Delta\rho/\rho$	Local density ratio, $(\rho_b - \rho_w)/\rho_b$, dimensionless
$(\Delta\rho/\rho)_{in}$	Density ratio, $(\rho_b - \rho_w)/\rho_b$, where ρ_b is evaluated at the inlet of the model, dimensionless. Note: $(\Delta\rho/\rho)^{in} = (\Delta T/T_{wall})_{in}$
Ω	Rotation rate, radian/sec
$(\Omega R/V)(\Delta\rho/\rho)$	Buoyancy term, dimensionless

Subscripts:

b	Bulk property
c	Cross section
in	Inlet to model
w	Wall surface property
x	Based on streamwise location X
∞	Fully developed turbulent smooth tube flow
0	Stationary (non-rotating) condition

Superscripts:

-	Vector quantity or average value
---	----------------------------------

REFERENCES

Abernathy, R. B., et al., and Thompson, J. W., Jr., Uncertainty in Gas Turbine Measurements, Arnold Engineering Development Center AEDC-TR-73-5, February 1973.

Aladyev, I. T., Experimental Determination of Local and Mean Coefficients of Heat Transfer for Turbulent Flow in Pipes. NACA TM 1356, 1954. (Translation from Russian).

Barua, S. N., Secondary Flow in a Rotating Pipe, Proc. R. Society A, Vol. 227, p. 133; 1954-55.

Bergles, A. E. and Webb R. L., Bibliography of Convective Heat and Mass Transfer List of References. Augmentation of Convective Heat and Mass Transfer, ed. Bergles, A. E. and Webb, R. L., ASME, New York, pp. 70-79, 1970.

Boelter, L. M. K., Young, G. and Iverson, H. W., NACA TN 1451, Washington, July 1948.

Boyle, R. J., 1984, Heat Transfer in Serpentine Passages with Turbulence Promoters. ASME Preprint 84-HT-24. Also issued as NASA Technical Memorandum 83614.

Brundrett, E. and Burroughs P. R., The Temperature Inner-Law and Heat Transfer for Turbulent Air Flow in a Vertical Square Duct. Int. J. Heat Mass Transfer, Vol. 10, pp. 1133-1142, 1967.

Burggraf, F., Experimental Heat Transfer and Pressure Drop with Two-Dimensional Turbulence Promoters Applied to Two Opposite Walls of a Square Tube. In Augmentation of Convective Heat and Mass Transfer., ed. Bergles, A.E. and Webb, R. L. ASME, New York, pp. 70-79; 1970.

Clifford, R. J., Rotating Heat Transfer Investigations on a Multipass Cooling Geometry, AGARD Conference Proceedings No. 390: Heat Transfer and Cooling in Gas Turbines, May 6-10, 1985.

Eckert, E. R. G., Diaguila, A. J. and Curren, A. N., Experiments on Mixed - Free and Forced-Convective Heat Transfer Connected with Turbulent Flow Through a Short Tube. NACA Technical Note 2974, 1953.

Eckert, E. R. G. and Diaguilla, A. J., Convective Heat Transfer for Mixed, Free and Forced Flow Through Tubes, Transactions ASME 76, p. 497-504 (1954).

Guidez, J., Study of the Convective Heat Transfer in Rotating Coolant Channel. ASME Paper 88-GT-33 presented in Amsterdam, The Netherlands. June. 1988.

Hajek, T. J., Wagner, J. H., Johnson, B. V., Higgins, A. W. and Steuber, G. D., Effects of Rotation on Coolant Passage Heat Transfer: Volume I - Coolant Passages with Smooth Walls. NASA Contractor Report 4396, Vol. I, September 1991.

Han, J. C., Park, J. S. and Ibrahim, M. Y., Measurement of Heat Transfer and Pressure Drop in Rectangular Channels With Turbulence Promoters, NASA Contractor Report 4015, 1986.

Han, J. C., Glicksman L. R. and Rohsenow, W. M., An Investigation of Heat Transfer and Friction for Rib-Roughened Surfaces. *Int. J. Heat Mass Transfer*, Vol. 21, pp. 1143-1156, 1978.

Hart, J. E., Instability and Secondary Motion in a Rotating Channel Flow. *J. Fluid Mech.*, Vol. 45, Part 2, pp. 341-351; 1971.

Iacovides, H., Launder, B. E., Parametric and Numerical Study of Fully-Developed Flow and Heat Transfer in Rotating Rectangular Ducts. ASME Paper 90-GT-24, 1990.

Iskakov, K. M. and Trushin, V. A., Influence of Rotation on Heat Transfer in a Turbine-Blade Radial Slot Channel. *Izvestiya VUZ. Aviatsionnaya Tekhnika*, Vol. 26, No. 1, pp. 97-99, 1983.

Iskakov, K. M. and Trushin, V. A., The Effect of Rotation on Heat Transfer in the Radial Cooling Channels of Turbine Blades, *Thermal Engineering*, Vol. 32, p. 93-96, 1985.

Ito, H., and Nanbu, K., Flow in Rotating Straight Pipes of Circular Cross Section. ASME Paper 70-WA/FE-13, 1970.

Johnson, B. V., Heat Transfer Experiments in Rotating Radial Passages with Supercritical Water. ASME Heat Transfer 1978 (Bound Publication of Proceedings from 1978 ASME Winter Annual Meetings).

Johnson, B. V., Wagner, J. H., Steuber, G.D. and Yeh, F. C., Heat Transfer in Rotating Serpentine Passages with Trips Skewed to the Flow. To be published in *ASME Journal of Turbomachinery*. (Also issued as ASME Preprint 92-GT-191 and NASA Technical Memorandum 105581, 1992).

Johnson, B. V., Wagner, J. H., Steuber, G. T. and Yeh, F. C., Heat Transfer in Rotating Serpentine Passages with Selected Model Orientations for Smooth or Skewed Trip Walls. To be published in *ASME Journal of Turbomachinery*. (Also issued as ASME Preprint 93-GT-305 and NASA Technical Memorandum 106126, 1993).

Johnston, J. P., The Effects of Rotation on Boundary Layers in Turbomachine Rotors, *Fluid Mechanics, Acoustics, and Design of Turbomachinery*, Part I, NASA SP-304, pp. 207-249, 1970.

Johnston, J. P., Halleen, R. M. and Lezius, D. K., Effects of Spanwise Rotation of the Structure of Two-Dimensional Fully Developed Turbulent Channel Flow. *J. Fluid Mech.*, Vol. 56, Part 3, pp. 533-557, 1972.

Kays, W. M. and Perkins, H. C., Forced Convection, Internal Flow in Ducts. From *Handbook of Heat Transferred* Rohsenow, W. M. and Hartnett, J. P., McGraw Hill. pp. 7-28 and 7-33, Copyright 1973.

Kays, W. M., *Convective Heat and Mass Transfer*. McGraw-Hill Book Company. 1966.

Kline, S. J. and McClintock, F. A., 1953, Describing Uncertainties in Single Sample Experiments, *Mechanical Engineering*, Vol. 75, pp. 3.

Lokai, V. I. and Gunchenko, E. I., Heat Transfer Over the Initial Section of Turbine Blade Cooling Channels Under Conditions of Rotation. *Therm. Enging.*, Vol. 26, pp. 93-95, 1979.

Metais, B. and Eckert, E. R. G., Forced, Mixed, and Free Convection Regimes. *J. Heat Transfer*, pp. 295-296, 1964.

Metzger, D. E., Fan, C. S. and Plevich, C. W., Effects of Transverse Rib Roughness on Heat Transfer and Pressure Losses in Rectangular Ducts with Sharp 180 Degree Turns, AIAA Paper 88-0166, 1988.

Moore, J., Effects of Coriolis on Turbulent Flow in Rotating Rectangular Channels. M.I.T. Gas Turbine Laboratory Report No. 89; 1967.

Mori, U., Fukada, T. and Nakayama, W., Convective Heat Transfer in a Rotating Radial Circular Pipe (2nd Report). *Int. J. Heat Mass Transfer*, Vol. 14, pp. 1807-1824, 1971.

Morris, W. D. and Ayhan, T., Observations on the Influence of Rotation on Heat Transfer in the Coolant Channels of Gas Turbine Rotor Blades. *Proc. Instn. Mech. Engrs.*, Vol. 193, pp. 303-311, 1979.

Morris, W. D., Heat Transfer and Fluid Flow in Rotating Coolant Channels. Research Studies Press, Copyright 1981.

Rothe, P. H. and Johnston, J. P., Free Shear Layer Behavior in Rotating Systems. *J. Fluids Engineering*, Vol. 101, pp. 117-120; 1979.

Schlichting, H., Boundary-Layer Theory, McGraw-Hill Book Company, New York, 6th Edition, pp. 575, 1968.

Sturgess, G. J. and Datta, P., Calculation of Flow Development in Rotating Passages for Cooled Gas Turbine Blades, Proc. 1987 ASME International Computers in Engineering Conference and Exhibition, New York, New York, Edit. R. Raghaven & T. J. Cokonis, pp. 145-158, August 9-13, 1987.

Suo, M., Turbine Cooling in the Aerothermodynamics of Aircraft Gas Turbines, ed. Oates, G., Air Force Aero Propulsion Lab., AFAPL TR 78-52, 1978.

Suo, M., Unpublished Notes, United Technologies Research Center, 1980.

Taslim, M. E., Rahman, A. and Spring, S. D., An Experimental Investigation of Heat Transfer Coefficients in a Spanwise Rotating Channel with Two Opposite Rib-Roughened Walls, ASME Paper 89-GT-150, 1989 .

Taylor, C., Xia, J. Y. Medwell, J. O., and Morris, W. D., Numerical Simulation of the Three Dimensional Turbulent Flow and Heat Transfer within A Multi-Ribbed Cylindrical Duct. ASME Paper 91-GT-8.

Taylor, J. R., Heat Transfer Phenomena in Gas Turbines. ASME Paper No. 80-GT-172, 1980.

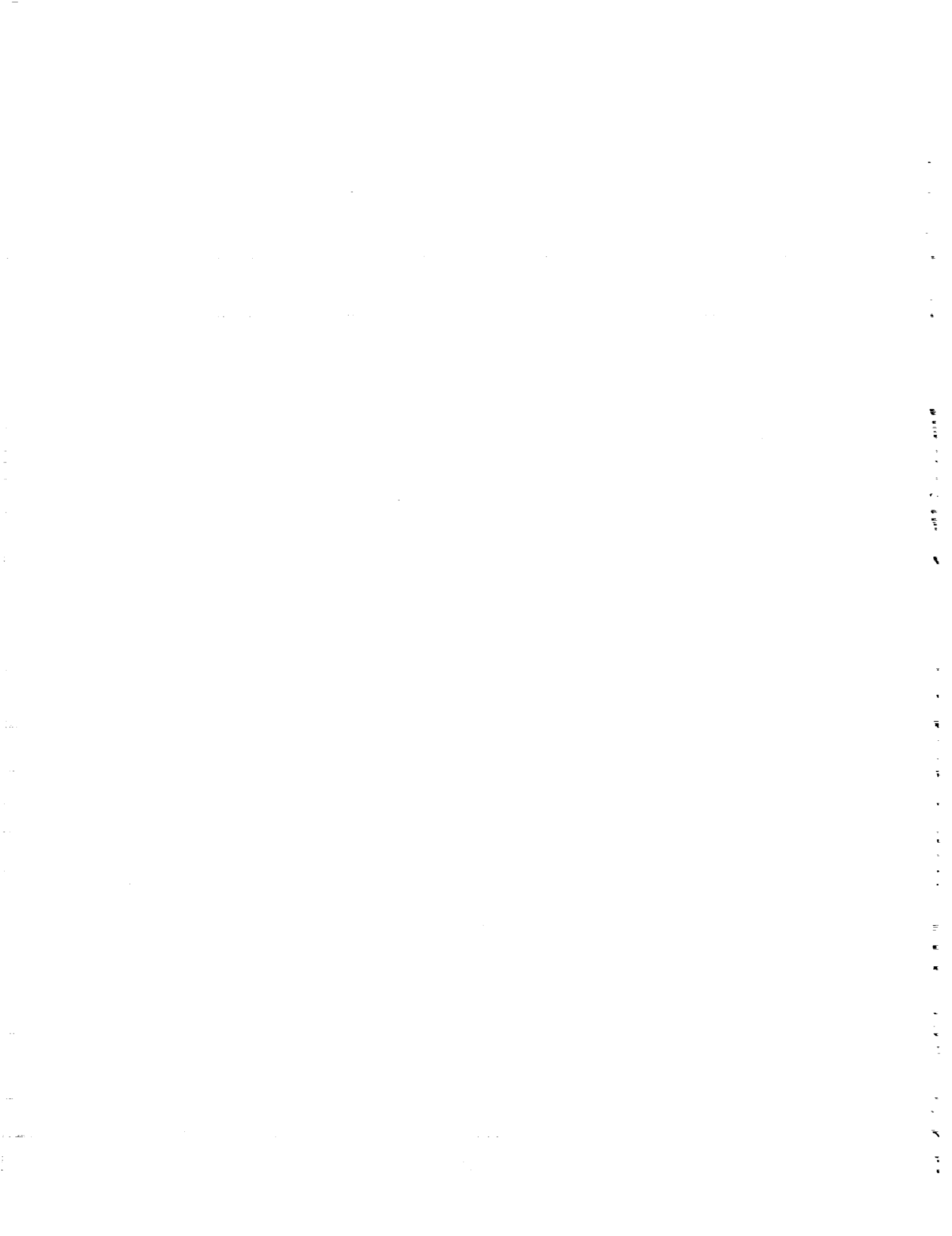
Wagner, J. H., Johnson, B. V., and Hajek, T. J., Heat Transfer in Rotating Passages with Smooth Walls and Radial Outward Flow. *ASME Journal of Turbomachinery*, Vol. 113, pp. 42-51, January 1991 (first presented as ASME Paper 89-GT-272, 1989).

Wagner, J. H., Johnson, B. V., Graziani, P. A. and Yeh, F. C., Heat Transfer in Rotating Serpentine Passages with Trips Normal to the Flow, ASME Journal of Turbomachinery, Vol. 114, pp 847-857, 1992. (Also issued as NASA TM 103758 and ASME Paper 91-GT-265)

Wagner, J. H., Johnson, B. V., and Kopper, F. C., Heat Transfer in Rotating Serpentine Passages with Smooth Walls. ASME Journal of Turbomachinery, Vol. 113, p 321-330, 1991. (Also issued as ASME Paper 90-GT-331, 1990).

Wagner, R. E. and Velkoff, H. R., Measurements of Secondary Flows in a Rotating Duct. J. Eng. for Power, ASME Paper 72-GT-17, 1972.

Webb R. L., Eckert, E. R. G. and Goldstein R. J., Heat Transfer and Friction in Tubes with Repeated Rib Roughness. Int. J. Heat Mass Transfer, Vol. 14. pp. 601-617. 1971.



REPORT DOCUMENTATION PAGE			Form Approved OMB No. 0704-0188	
Public reporting burden for this collection of information is estimated to average 1 hour per response, including the time for reviewing instructions, searching existing data sources, gathering and maintaining the data needed, and completing and reviewing the collection of information. Send comments regarding this burden estimate or any other aspect of this collection of information, including suggestions for reducing this burden, to Washington Headquarters Services, Directorate for Information Operations and Reports, 1215 Jefferson Davis Highway, Suite 1204, Arlington, VA 22202-4302, and to the Office of Management and Budget, Paperwork Reduction Project (0704-0188), Washington, DC 20503.				
1. AGENCY USE ONLY (Leave blank)	2. REPORT DATE October 1993	3. REPORT TYPE AND DATES COVERED Final Contractor Report		
4. TITLE AND SUBTITLE Effects of Rotation on Coolant Passage Heat Transfer Volume II - Coolant Passages With Trips Normal and Skewed to the Flow			5. FUNDING NUMBERS WU-505-62-61 C-NAS3-23691	
6. AUTHOR(S) B. V. Johnson, J. H. Wagner, and G. D. Steuber				
7. PERFORMING ORGANIZATION NAME(S) AND ADDRESS(ES) Pratt & Whitney 400 Main Street East Hartford, Connecticut 06108			8. PERFORMING ORGANIZATION REPORT NUMBER E-6470-1	
9. SPONSORING/MONITORING AGENCY NAME(S) AND ADDRESS(ES) National Aeronautics and Space Administration Lewis Research Center Cleveland, Ohio 44135-3191			10. SPONSORING/MONITORING AGENCY REPORT NUMBER NASA CR-4396, Vol. II	
11. SUPPLEMENTARY NOTES Project Manager, Frederick C. Yeh, Internal Fluid Mechanics Division, NASA Lewis Research Center, (216) 433-5872.				
12a. DISTRIBUTION/AVAILABILITY STATEMENT Unclassified - Unlimited Subject Category 34			12b. DISTRIBUTION CODE	
13. ABSTRACT (Maximum 200 words) An experimental program was conducted to investigate heat transfer and pressure loss characteristics of rotating multipass passages, for configurations and dimensions typical of modern turbine blades. This experimental program is one part of the NASA Hot Section Technology (HOST) Initiative, which has as its overall objective "the development and verification of improved analysis methods that will form the basis for a design system that will produce turbine components with improved durability." The objective of this program was the generation of a data base of heat transfer and pressure loss data required to develop heat transfer correlations and to assess computational fluid dynamic techniques for rotating coolant passages. The experimental work was broken down into two phases. Phase I consists of experiments conducted in a smooth wall large scale heat transfer model. A detailed discussion of these results was presented in volume I of a NASA Report. In phase II the large scale model was modified to investigate the effects of skewed and normal passage turbulators. The results of phase II along with comparison to phase I is the subject of this volume II NASA Report.				
14. SUBJECT TERMS Heat transfer, Rotation; Turbomachinery			15. NUMBER OF PAGES 128	
			16. PRICE CODE A06	
17. SECURITY CLASSIFICATION OF REPORT Unclassified	18. SECURITY CLASSIFICATION OF THIS PAGE Unclassified	19. SECURITY CLASSIFICATION OF ABSTRACT Unclassified	20. LIMITATION OF ABSTRACT	

